ON LOAN
RETURN TO:
NUCLEAR ENGINEERING LIBRARY
138 ALBANY STREET
CAMBRIDGE, MASS. 02139

COO-2245-12 Topical-Report
MITNE-165

NUCLEAR ENGINEERING
READING ROOM - M.I.T.

ANALYSIS OF MIXING DATA RELEVANT TO WIRE WRAPPED FUEL ASSEMBLY THERMAL-HYDRAULIC DESIGN

E. U. Khan

N. E. Todreas

W. M. Rohsenow

A. A. Sonin

September 1974

Departments of Mechanical Engineering and Nuclear Engineering
Massachusetts Institute of Technology
Cambridge, Massachusetts 02139

AEC Research and Development
Contract AT(11-1)-2245
U.S. Atomic Energy Commission

NUCLEAR ENGINEERING
READING ROOM - M.I.T.

ANALYSIS OF MIXING DATA RELEVANT TO WIRE-WRAPPED FUEL ASSEMBLY THERMAL-HYDRAULIC DESIGN

by

E. U. Khan
N. E. Todreas
W. M. Rohsenow
A. A. Sonin

Massachusetts Institute of Technology
Cambridge, Massachusetts

TABLE OF CONTENTS

ABSTRACT

In this report analysis of recent experimental data is presented using the ENERGY code. A comparison of the accuracy of three types of experiments is also presented along with a discussion of uncertainties in utilizing this data for various code calibration purposes. The existence of internal swirl is discussed. The two empirical coefficients in ENERGY are determined from the data within a certain range of accuracy. This range is dictated to a large extent by the accuracy of the experiments and to a smaller extent by the ability of the code to utilize all sets of data in each experiment.

The effect of geometry and bundle size on mixing and swirl flow is discussed. A realistic estimate of the degree of accuracy within which we can predict temperature distribution within the bundle and along the duct of a 217-pin wire wrapped fuel assembly of an LMFBR is presented.

Gaps in data which need to be filled in to enhance our confidence in predicting coolant temperature distributions in a 217-pin LMFBR fuel bundle, are given. A brief description of two experiments that would fill these data gaps is presented. A novel experiment which

would be very useful for both fuel and poison assembly mixing studies is described. Conclusions drawn from this study are believed to be quite general in nature.

Acknowledgement

The authors are grateful to Dr. L. Wolf for discussions and for bringing to our notice [redacted] reports from Karlshrue. We also would like to thank Mr. Y. Chen, Mr. A. Hanson and Mr. T. Eaton for their comments in reviewing this report. In addition we would like to thank Dr. J. J. Lorenz of Argonne National Laboratory for several useful discussions

1. INTRODUCTION

In the design of a wire wrapped Liquid Metal Fast Breeder Reactor (LMFBR) fuel assembly,coolant mixing caused by wire wraps is the most significant mode of energy redistribution[1,2]*. At the high Reynolds number range of steady state operation of a typical LMFBR energy transport by conduction plays a secondary role only to energy transport by wire wrap mixing.

The maximum burnup (Mwd/T) for current LMFBR designs is very sensitive to the peak coolant temperature in the hot channel[3], which in turn could depend, to a large extent, on interchannel mixing rates. In addition, the fuel assembly housing bowing is also of special concern. Bowing of the hexagonal housing is caused by differential thermal expansion. It is greatly enhanced by radiation induced stainless steel swelling in a fast spectrum and the temperature dependence of this induced swelling. Thus realistic predictions of assembly temperature distribution could have important effects on the flow housing design considerations. At present a purely theoretical analysis is not adequate to establish the extent of mixing caused by wire wraps in LMFBR assemblies. In order to reduce the uncertainty in predicting mixing rates caused by wire wraps (also known as flow sweeping - see Section 7.2 and Ref. 2 for a detailed description of various other modes

* superscripts refer to references cited

of energy transport) many different types of experiments have been performed. Some of these experiments, in addition to providing data from which mixing-coefficients can be determined for use in computer programs, provide useful information on flow and pressure distribution in the rod bundle.

The three types of experiments that are most frequently used for determining wire-wrap mixing in a rod bundle can be classified according to their boundary conditions.

1) Continuous injection of an electrolyte salt solution at a point in the bundle. Electrical conductivity measurements at various points in the rod bundle can give an estimate of the amount of salt transported by mixing. From this a mixing coefficient can be derived.

2) Continuous local injection of heated coolant. Temperature measurement in the three dimensional bundle matrix will yield a mixing coefficient with appropriate data analysis.

3) Employment of one, several, or a complete array of heated pins. By measuring temperature distributions in the bundle, one can derive a mixing coefficient.

The mixing coefficient one would like to derive from these experiments should solely represent the contribution of wire-wraps in promoting energy transport from one point to another within the bundle. However, as indicated in Ref. 2,

other modes of energy transport co-exist (e.g. diversion cross-flow, flow scattering, energy transfer by turbulence) although their magnitudes may be considerably smaller than the wire wrap sweeping effect. It is often not possible to separate (except for thermal conduction) the individual contributions of the mixing mechanisms, from these experiments, to a good degree of accuracy. This is one of the reasons why computer programs like ENERGY[1] combine all the mixing mechanisms into one lumped mixing coefficient which is empirically determined. Other computer programs make an effort to determine the individual contributions of the wire-wrap, sweeping, diversion cross-flow and turbulence energy exchange and linearly add them. Linear addition of these effects is questionable. However, since the flow sweeping by wire wraps so completely dominates the mixing process, errors in either neglecting or linearly adding the effect of other mixing mechanisms are expected to be small. In addition to the experiments mentioned before, experimenters have used several techniques to measure axial and circumferential velocities in wire wrapped rod bundles. One of these is the use of Laser Doppler Velocimeter to determine velocity and turbulent intensity.

In this respect analysis of recent experimental data is presented using the ENERGY code. A comparison of the accuracy of three types of experiments is also presented along with a discussion of uncertainties in utilizing this data for

various code calibration purposes. The existence of internal swirl is discussed. The two empirical coefficients in ENERGY are determined from the data within a certain range of accuracy. This range is dictated to a large extent by the accuracy of the experiments and to a smaller extent by the ability of the code to utilize all sets of data in each experiment. The effect of geometry and bundle size on mixing and swirl flow is discussed. A realistic estimate of the degree of accuracy within which we can predict temperature distribution within the bundle and along the duct of a 217-pin wire wrapped fuel assembly of an LMFBR is presented. Gaps in data, which need to be filled in, to enhance our confidence in predicting coolant temperature distributions in a 217-pin LMFBR fuel bundle, are given. A brief description of two experiments that would fill these data gaps is presented. A novel idea for an experiment which would be very useful for both fuel and poison assemblies mixing studies is described.

It is necessary to point out that the conclusions drawn from this study regarding flow distributions within the fuel assembly, internal swirl, bundle size effects, effect of geometry on mixing and swirl are quite general in nature. The code used to obtain these conclusions is the ENERGY code. However, the results and conclusions are expected to be independent of the tool used to obtain them.

2. Theoretical Background

The ENERGY[1] computer program models the periodic sweep flow through rod gaps as an enhanced effective eddy diffusivity. The model subdivides the fuel assembly into two predominant regions. In the central region the enhanced effective eddy diffusivity is responsible for energy transport in the transverse directions. Near the duct wall, flow is unidirectional and parallel to the duct wall. Energy transport can occur both by diffusion and by convection, although it has been found that the energy transport by convection (swirl flow) predominates[1]. ENERGY models the heat generation in the fuel rods as a volumetric heat source in the fluid. Until more data is available ENERGY uses two options for flow split. 1) Hydraulic diameter flow split, 2) uniform velocity in the entire bundle. Each set of data was analyzed by taking two splits into consideration. The available data yields some useful information on this flow split, as is shown later.

The ENERGY code requires as input two empirical constants $\overline{\varepsilon_H^*}$ and C_1. All the mixing effects (e.g. turbulent exchange, diversion cross-flow, flow sweep due to wire wraps) are lumped into $\overline{\varepsilon_H^*} = [\overline{\varepsilon_H}/(Vde)]$. It should however be noted that the effect of wire wrap for the current fuel assembly design almost completely dominates other effects included in $\overline{\varepsilon_H^*}$. C_1 represents the swirl flow in the wall region and is defined as the ratio of the velocity in the gap between rod

and wall to the average axial bundle velocity ($C_1 = \bar{V}g/\bar{V}$). It is necessary to note that C_1 is assumed to be uniform around the bundle and represents the average circumferential swirl velocity in the gap between rod and wall. The three types of experiments, namely, electrolyte salt injection, hot water injection experiment, and heated pins, are used to determine $\overline{\varepsilon_H^*}$ and C_1. Based on physical insight and inspection of the fundamental energy balance equation we can determine that $\overline{\varepsilon_H^*}$ and C_1 are dependent on the following parameters,

$$\overline{\varepsilon_H^*} = f(h/d,\ p/d,\ Re,\ Pr) \qquad (1)$$

$$C_1 = f(h/d,\ p/d,\ Re,\ Pr) \qquad (2)$$

Since these experiments have been performed for fuel assemblies of different geometries and at various Reynolds numbers it is possible to determine these functional relationships for $\overline{\varepsilon_H^*}$ and C_1.

The heated pin experiments provide a boundary condition which represents the actual LMFBR fuel assembly assembly heat transfer boundary condition. The parameters $\overline{\varepsilon_H^*}$ and C_1 in ENERGY are varied until coolant temperatures predicted by the code match the experimentally measured temperatures.It was found that $\overline{\varepsilon_H^*}$ and C_1 can be found independently by matching the central region and wall region temperature maps respectively. Apparently, swirl flow effects, fortunately, do not appear to penetrate significantly within the fuel assembly. Thus $\overline{\varepsilon_H^*}$ can

be determined from the data in the inner region and C_1 from the data on the wall region.

In order to show that both the salt injection and hot water injection experiments would also yield a mixing coefficient which can directly be used in the ENERGY code for LMFBR fuel assembly temperature calculations, it is necessary to realize that $\overline{\varepsilon_H^*}$ predominantly represents the wire sweep flow mixing effect. Thus the mixing coefficients determined from equations (3) and (4) below need not be modified (as is normally done in literature when mass eddy diffusivities are converted to heat eddy diffusivities or vice versa) in any manner for use in ENERGY.

The equations governing salt diffusion in salt injection experiments and heat diffusion in hot water injection experiments along with injection boundary conditions are given below (note: we may only concern ourselves with the steady state equation),

$$\underline{\text{Hot Water Injection}}: \quad \frac{DT^*}{Dt} = \frac{1}{Re}\left(\frac{\varepsilon_H^*}{\gamma} + \frac{1}{Pr}\right)\nabla^2 T^* \qquad (3)$$

when $z = 0$, $T^* = 1$ where $T^* = \dfrac{T - T_{COLD}}{T_{HOT} - T_{COLD}}$

Water is generally used as the working fluid. One finds $\dfrac{\varepsilon_H^*}{\gamma} >> \dfrac{1}{Pr}$.

$$\underline{\text{Salt Injection}}: \quad \frac{DC^*}{Dt} = \frac{1}{Re}\left(\frac{\varepsilon_D^*}{\gamma} + \frac{1}{Sc}\right)\nabla^2 C^* \qquad (4)$$

when $z = 0$, $C^* = 1$ where $C^* = \dfrac{C}{C_o}$ and C_o = inlet concentration

For all tracers utilized in wire wrap studies independent of the particular tracer $\frac{\varepsilon_D^*}{\gamma} >> \frac{1}{Sc}$. For reasons discussed before one expects $\varepsilon_D^* = \varepsilon_H^*$.

3. RESULTS OF DATA ANALYSIS AND ENERGY CALIBRATION

3.1 Overview

Fig. 3.1 shows a comparison of the theoretical (hydraulic diameter including the effect of wire-wrap presence) flow split[7] and experimentally observed flow split for the wall channels of wire-wrap bundles ranging in size from 7 to 217 pins. The theoretical flow split was obtained by (a) completely neglecting geometrical tolerance, and (b) allowing for geometrical tolerance. In reality, geometrical tolerance effect exists and must be taken into account. Following the method given by Hanson in Ref. 4 (appendix) if T is the diametrical tolerance across the flats of a bundle, a fraction F of this would be accomodated within the bundle and a fraction (1 - F) in the wall region. Then the pitch, P, of the wire wrapped bundle must be increased by ΔP due to the "looseness" caused by geometrical tolerance, where

$$\Delta P = TF/(\sqrt{3}.N_{RINGS})$$

The gap between the wire and the wall is given by

$$\Delta R = \frac{T}{2}(1 - F)$$

The two extreme cases for tolerance distribution are

Case I: $F = 0$ $\Delta P = 0$ $\Delta R = T/2$

Case II: $F = 1$ $\Delta P = T/(\sqrt{3}.N_{RINGS})$ $\Delta R = 0$

The effect of these two extreme cases on flow split in the wall channel are shown in Fig. 3.1 for the MIT 61-pin

bundle which has a diametrical tolerance of 0.0195 inches in a duct with a distance across the hexagonal flats of 2.560 in.

In most bundles it is expected that Case II will exist where all the tolerance is accomodated within the bundle. Observation of the (Ref. 4) M.I.T. bundle agrees with this suggestion as the pins were observed to contact the duct faces when the bundle was assembled. This was also observed in the AI 217 pin bundle (Ref. 30). Wherever there is a doubt as to which of the two limiting cases exists within a bundle, we have shown the two limits of flow splits for wall channel corresponding to the two cases.

It is interesting to note that for the 7-pin bundle it was possible to predict both the wall channel and inner channel flow splits (see Section 7) accurately. As the bundle size increased there appears to be a divergence between the theoretical predictions and experimentally observed data on a similar geometry. Allowing for the experimental predictions to have an associated error bar, it still appears that the theoretical flow split predicts higher axial velocities in the wall channels (and lower axial velocities in central and corner channels) than experimentally observed. If the divergence in the theoretical and experimental curves is in fact real then a correction factor on hydraulic diameter alone would not bring the two curves together. A bundle size effect exists in that case. If a bundle size effect exists it could be only due to a change in the basic flow field in going from a 7-pin to a 217-pin bundle.

Until this is fully resolved one needs to take into account the flow split effect while analyzing other data and in predicting temperatures for the full size bundle at power conditions. The ENERGY analysis of data (Section 7) takes into account a flow split effect in calibrating the two constants $\overline{\varepsilon_H^*}$ and C_1.

A thorough analysis of each set of data described in Section 7 was made using the ENERGY code. It was necessary to completely understand the experimental techniques used to obtain the specific set of data including tolerance on geometry, accuracy of measurements and the fraction of total data, in any one experiment, that is useful for calibration purposes. In addition the ENERGY code has certain inherent assumptions built into it. Our ability to analyze a certain set of experimental data was superimposed upon the expected accuracy of the data to determine a realistic error bar on $\overline{\varepsilon_H^*}$ and C_1. For example, for the FFTF geometry the HEDL tests yield an $\overline{\varepsilon_H^*}$ from 0.015 to 0.03, whereas the O.R.N.L. tests give an $\overline{\varepsilon_H^*}$ from 0.028 to 0.048. Considering the fact that the HEDL data could only be used after the first twelve inches from the inlet;that mass balances changed continuously from inlet to exit; that there appeared to be an effect of injection concentration; that two point measurements in the same channel gave results up to 50% different; that the boundary condition of salt injection is not a prototype boundary condition; one would tend to have more confidence in the O.R.N.L. 19 pin

heated data. However, the O.R.N.L. experiments were on a much smaller bundle and rod bowing and bundle helixing at large power input rates were observed. Since ENERGY could predict many sets of data for various power skews with almost a single value of $\overline{\varepsilon_H^*}$ it was decided to put more confidence on O.R.N.L. 19 pin experiments. Therefore the range of $\overline{\varepsilon_H^*}$ recommended (for $p/d \sim 1.24$, $h/d \sim 48 - 52$, $d \sim 0.23$ in.) is from 0.025 to 0.048 with a weighted mean around 0.04. As will be seen later (Section 4) such a large range in $\overline{\varepsilon_H^*}$ only slightly affects the exit temperature distribution and the maximum exit temperature of a 217 pin FFTF bundle at full power.

Tables 3.1 and 3.2 show the fuel-assembly data analyzed. Table 3.1 lists the data based on bundle size and experimental techniques and Table 3.2 based on the significant geometrical characteristics. Only data relevant to fuel assembly calculations was considered for analysis and only the data for which all required details were available was analyzed. Although the standard fuel assembly geometry is $d \sim 1/4"$, $h/d \sim 50$, $p/d \sim 1.25$, the data analyzed covers a reasonably wide range about the standard fuel assembly design in order to permit thermal-hydraulic optimization studies. No data on poison and blanket assemblies was analyzed as this is not the present goal.

Fig. 3.2 shows that the variation of $\overline{\varepsilon_H^*}$ vs $1/(h/d)$ is linear in the range of interest. As the wire wrap pitch is increased ($d/h \to 0$ or $h/d \to \infty$) the $\overline{\varepsilon_H^*}$ vs d/h plot is expected to curve and tend to an asymptotic value for the case of no

wire-wrap. Only the natural turbulence effect would be contributing to $\overline{\varepsilon_H^*}$ in that case. Fig. 3.3 is a cross-plot of Fig. 3.2. It shows that the $\overline{\varepsilon_H^*}$ vs p/d curve has a maxima in between p/d of 1.2 and 1.3. Fig. 3.4 shows the variation of C_1 ($= \bar{v}_g/\bar{V}$) vs d/h. There seems to be better agreement in data at d/h $\sim$ 0.02 (h/d $\sim$ 50) than at larger values of d/h. The only available data for large values of d/h (d/h > 0.02) are the SKOK (Ref. 8) and M.I.T (3) data.

For practical use the recommended value of $\overline{\varepsilon_H^*}$ is the value read from Figs. 3.2 or 3.3 with approximately a $\pm$30% (of $\overline{\varepsilon_H^*}$) error bar. At d/h $\sim$ 0.02 p/d $\sim$ 1.24, the range shown in Fig. 3.2 is 0.025 to 0.048. Wherever the range is not shown the above mentioned range in $\overline{\varepsilon_H^*}$ may be used. For C_1 the range shown in Fig. 3.4 must be used.

The analysis of data of Ref. 8 is described in Section 7 and Table III. Since only data over one axial wire wrap pitch is given in Ref.8, our confidence level in analyzing it is not good. The values of C_1 obtained from the data of Ref. 8 required many assumptions. It appeared that C_1 so obtained was underestimated. Thus the SKOK data is shown as a lower limit on C_1. The M.I.T. results on the other hand appear to overpredict C_1. This is because only one value of transverse velocity in the gap between rod and wall was measured. If the flow field is turbulent, the average gap velocity could be as much as 20% lower than the point velocity measured. Superimposed upon this velocity profile effect is an independent error bar in the range 12 to 14%. The value of C_1 lies between the limits shown in Fig. 3.4.

The value of C_1 for the FFTF geometry lies somewhere between 0.07 from the HEDL[23] data to 0.12 from O.R.N.L.[9] and M.I.T.[3] data. Discussions of bundle size effect are delayed until later. However the effect of this range of C_1 on the duct temperature gradient (Section 4) does not appear to be very significant.

The calibration of ENERGY described above should hold for the p/d and h/d ratios considered. In addition all of the data (except SKOK data for which ENERGY calibration is not expected to be good) used was for rod diameters close to 0.25 in. Rod diameters in a range close to this should present no significant effect on $\overline{\varepsilon_H^*}$. This limitation is imposed as a precautionary measure (see Ref. 26; calibration of THI-3D also imposes this limitation) since data with other rod diameters have not been analyzed.

3.2 Comparison of Heated Pin, Hot Water Injection and Salt Injection Experiments

Our analysis of the various types of data showed that the heated pin experiments are probably the most reliable, provided care is taken in designing the temperature sensors and the heated rods. The discussion to follow compares heated pin experiments with non-heated pin experiments (salt and hot water injection included). The Laser Doppler Velocimeter experiments are not discussed since they can at present only be used for wall channels where they can supplement the results of any of the above experiments.

The major problem with the two non-heated experiments (apart from a different boundary condition than the prototype) is that an injector must be introduced into the main flow stream. Local perturbations of the bulk flow can affect the measurements many inches downstream of the injection point. Three factors that are extremely important in obtaining reliable reproducible results with any injection device are the injector design, injector position and injection flow rate[12,19]. Considerable effort has been devoted by Lorenz[19] and Pederson[12] in testing various injector designs. Their results show a centrally located injector with injection velocities close to the local mainstream velocity should give reliable results for wall channels. An extension of a similar detailed study [24] for centrally located injector is required for central channels. The HEDL[23] inlet perturbation effects were found to last from 6 in to 9 in. The flow drift of two channels (see Section 7) has been interpreted by investigators as an internal swirl flow. ENERGY analysis shows that this drift is an inlet perturbation effect. A similar inlet perturbation effect was found by examining, level by level, the GE-127 pin[22] hot water injection data. The inlet perturbation in this case is an extremely small internal swirl flow which dies off after about 12-18 in.

Every size of bundle tested needs to have a detailed injection study made similar to that in Refs. 12 and 19, especially for wall channels. The state of our understanding of the hydraulics of the wire wrapped bundle is such at present

that an injection scheme tested for a small bundle cannot be used for a large bundle with a great deal of confidence. Thus until a complete knowledge of the local flow fields within subchannels of a wire wrapped bundle is available each bundle would require related injector development work.

The tracer detection by wall thermocouples (for hot water injection) and wall conductivity probes is a localized point measurement not suitable for lumped subchannel analysis computer programs. The isokinetic sampling technique[6], however, along with conductivity probes (or thermocouples) located near or at the center of the subchannel[9,13] can yield more useful results. Although wall thermocouples can be designed[22] carefully, a steep temperature gradient between wall and the center of the subchannels could give misleading results. The M.I.T. experiments[27] use a variable injection position and fixed detection probes at the outlet of the bundle. These probes are located at the center of the subchannels. The tracer detection in non-heated experiments can, therefore, be carefully designed to give reliable results. The mass balance (in salt-injection experiments) and energy balance (in hot water injection experiments) should be as good as the energy balance in heated pin experiments[9]. To date poor mass balances[23] and energy balance[12] for central injection have been obtained. Heated pin experiments (Refs. 9, 15) have yielded energy balance within 3-5% as compared to 13-35%[23] for non-heated pin experiments.

The isokinetic sampling technique does not appear to suffer from the same major drawbacks as the others but a possible source of error in this technique is discussed below. Using the isokinetic sampling technique the differential static pressure between a subchannel and another reference subchannel at the exit plane to the test section is measured under the undisturbed conditions. Then an extraction device is placed at the measuring plane and flow withdrawn until the previous $\Delta P_{ref.}$ between the subchannel and the reference subchannel is obtained. It is then assumed that the original flow split is re-established and the "proper flow" flow split is being sampled[6]. The problem with the technique is that re-establishing the previous $\Delta P_{ref.}$ between the subchannel and reference subchannel is necessary but not sufficient to ensure that the original flow split is established. This is because the pressure difference between the subchannel in question and subchannels other than the reference may not be the same as before even though $\Delta P_{ref.}$ has been re-established. Fig. 3.5 shows a comparison of isokinetic sampling data on nearly similar geometries in a 7-pin[6] and in a 91-pin[19] experiment. Although wire orientations are different for the two cases the difference in results cannot be explained by wire-orientation effect alone since wire orientation C lies in between A and B but the corresponding curve for C/C_o does not.

It could possibly be a bundle size effect. If the latter is ruled out (at present the latter cannot be ruled out) then the reliability of the technique can be questioned. More

experiments are required to test fully the reliability of the isokinetic sampling method.

The most useful portion of the data generated by salt and hot water injection experiments is produced in the first twelve to fifteen inches axially. Codes like CϕTEC[11] and THI-3D[10] use the first few inches for sweep flow calibration. As discussed in subsection X of Section 7, as one goes downstream very small errors in tracer concentration yield a large range for $\overline{\varepsilon_H^*}$ (the calculated salt concentration vs $\overline{\varepsilon_H^*}$ curves become flatter with distance downstream. A small error bar on data superimposed upon this could give a very wide range of $\overline{\varepsilon_H^*}$.). Moreover for ENERGY purposes the injection channel data was found to give the least errors in calibration (see Fig. 8 of Appendix) for the reasons mentioned in Section 7.1. If inlet perturbation effects continue for a few inches downstream of the injection plane, the most useful portion of the data is lost. It is more difficult to develop data free of inlet perturbations for central injection than for wall injection due to lack of maneuverability (bundle must be disassembled every time) and accessibility. In heated pin experiments any rod in the bundle can be easily heated by external control. Whereas concentrations in the injection and neighboring channels continuously decrease in the tracer injection experiment, the temperatures of the channel near the heated rod or rods in a heated pin experiment (line source) continuously increase. Heated pin experiments can be designed

more easily to give accurate reliable axial temperature variations by changing the length of the pin heated and using the same exit (see Section 5A) thermocouples. The data from Refs. 9, 15 and 16 has generally shown a greater degree of accuracy and reliability than for tracer injection experiments.

One of the most important features of tracer injection experiments (that can again be achieved by heated pin experiments in which heat is generated only over a small axial length) was found in Ref. 12. Tracer injection into an inner (No. 12) channel adjacent to the wall channel (see Fig. 33 of Ref. 12) shows that most of the fluid is transferred to an adjacent inner channel 11 by diversion cross-flow[2] (due to the presence of wire in channel 12 its hydraulic diameter decreases) and very little to adjacent channel 3. One would have expected at least an equal amount to be transferred to both channels due to diversion cross-flow plus an additional amount to channel 3 by sweep flow as the wire crosses the gap between rods 2 and 3. It is not correct to assume that interaction between wall and inner region is small based on this evidence. There is some evidence that (Section 7) mixing is uniform in the bundle[15]. However, a knowledge of these local hydraulic interactions between subchannels can be very useful in trying to assess the relative importance of sweep and diversion cross-flow in codes that linearly add these two effects. It is believed by the present authors that no code, as yet, can predict this type of a local flow redistribution with any degree of confidence. This is one reason that simpler codes like ENERGY prefer to lump

these modes of energy transfer. However as more sophistication is built into the hydraulic models of the more advanced codes like THI-3D and COBRA, this type of data will be most useful.

Only two sets of heated pin experiments are available for the fuel-assembly geometry. These are the ORNL[9] 19 pin and the German[16] 61 pin experiments. Although several sets of useful data are available from these experiments a number of important issues still remain unclear. The German[16] 2 heated pin experiments show (Fig. 1.8) that the effect of wall swirl flow penetrates at least 3-4 channels radially inwards, almost to the center. This effect is not due to conduction because conduction effects have been found to be an order of magnitude smaller than the wire wrap mixing effects for Re > 10000. If internal swirl exists (which we do not believe, based on our analysis of the 217 pin bundle. However an additional set of data could put the matter to rest) for the 61 pin bundle its effect cannot be separated out due to penetration of wall effects. However, if a 217-pin experiment were performed using water with single or two heated pins strategically located it would be possible to confirm our belief, based on analysis of HEDL experiments, that no internal swirl exists. By locating heated pins near the wall the swirl flow (C_1) can be determined and further confirmed by laser measurements. In addition the existence of bundle size effects can be checked. The need for such an experiment (for a large range of h/d, p/d, d) exists and is described in Section 5.

3.3 Reynolds Number Effect

Both $\overline{\varepsilon_H^*}$ and C_1 were found to be independent of Reynolds number for Re > 10000. This result is not unexpected and needs no further discussion.

3.4 Bundle Size Effect

A question that must be resolved is whether the swirl flow and mixing coefficient (or sweep flow) remain constant as the size of the bundle is increased (more pins) for the same geometrical characteristics (p/d, h/d). There is every reason to expect a smaller bundle ($\sim$ 61-91 pins) to be able to model a larger (217 pin) bundle well if h/d and p/d remain the same. If a bundle size effect actually exists it should be more obvious in going from a 19 pin to a 91 pin bundle than in going from a 91 to a 217 pin bundle, based on ratio of interior to wall channels. However, our analysis has shown that C_1 remains almost constant in going from a 19 to a 91 pin bundle. Yet the HEDL[23] analysis shows that $C_1 \sim .07$, almost half of the swirl velocity in the small bundles (Fig. 3.6). The $\overline{\varepsilon_H^*}$ obtained from the HEDL[23] analysis is also considerably smaller than that obtained from the ORNL[9] heated pin experiments. At this stage, with the available data, one cannot determine with any degree of certainty whether this is a bundle size effect or if it is an instrumentation and injection effect.

The flow split (Fig. 3.1) shows a bundle size effect. Our analysis of the available data shows that internal swirl may be prevalent for smaller bundles (although its magnitude is

so small so as not to effect the results) but as the bundle size increases the internal swirl decreases. The ORNL[9] 19-pin experiments show an asymmetry in radial temperature distribution for the centrally heated pin. This could be due to rod bowing or internal swirl. The Japanese[13] experiments (Fig. 14 of appendix) show an asymmetry in tracer concentration at the exit of the bundle. This could be due to internal swirl. However, analysis of the HEDL[23] experiments shows that no internal swirl exists.

In addition Fig. 3.5 shows that the difference in concentration decay rates for wall injection into two bundles of different sizes (7 and 91 pins) but similar geometry is quite large. Is this a bundle size effect?

Does the basic hydraulics change within a bundle in going to a large bundle? If so, data obtained on smaller bundles should not be used for large bundle predictions. This open question can only be resolved with more experimentation.

Given below is more evidence of the difficulty one faces in trying to determine if the observed differences in local flow field is due to a bundle size effect or due to different experimental techniques. In Ref. 12 Pederson has experimentally observed that subchannels near the downstream corner of a face (in the swirl flow direction) have a higher swirl flow. Based on this observation an explanation for the decrease in swirl flow with increasing bundle size is available.

Fig. 3.7 shows the velocity ratio $\bar{v}_g/\bar{V}$ ($=C_1$) for these adjacent rod gaps near the downstream corner of a face, as a function of axial distance. These were measured by a Laser Doppler Velocimeter and are expected to be quite accurate ($\pm$ 15%) (Ref. 4). No significant change in swirl velocity is observed for any position of the wire wrap, unlike that observed by Pederson[12] for a 91 pin bundle. It is difficult to imagine a significant bundle size effect of this type can exist in going from 61 to 91 pins for similar geometries.

4. Application of ENERGY calculations to a 217-pin FFTF Bundle

The callibrations of the ENERGY code is described in section 7. The values of the two empirical constants $\overline{\epsilon^*_H}$ and C_1 were determined from several sets of data on geometry similar to the FFTF dimensions. The value of $\overline{\epsilon^*_H}$ obtained was in a range 0.025 (HEDL) to 0.048 (O.R.N.L.) and C_1 was in a range from 0.07 (HEDL) to 0.12 (O.R.N.L., M.I.T.). Moreover there is a considerable uncertainty in flow split which must be taken into account. In order to see the effect of this wide range in the coefficients, on our ability to predict the coolant temperature distributions in a prototype FFTF 217-pin bundle a parametric study was run using the following base parameters.

1). The mean temperature rise across the bundle of 300°F.

2). Axial power skew (peak/avg.) of 1.23 and

3). Radial power (linear) skew (max/min) of 1.50.

4). Inlet temperature of the coolant of 600°F.

The maximum duct wall temperature difference at the exit of the core was investigated for various size bundles. The base case conditions were maintained for bundles of all sizes. Fig. 4.1 shows that whereas mixing (finite $\overline{\epsilon^*_H}$) reduces (ΔTmax) duct for small bundles it increases it for bundles containing more than 91 pins. Thus an increased value of $\overline{\epsilon^*_H}$ is conducive to reducing the maximum $(\Delta\text{Tmax.})_{ax.}$ temperature within the bundle but increases the duct wall temperature difference. The swirl flow (finite C_1) on the other hand has been found to reduce the (ΔTmax) duct without any appreciable effect on $(\Delta\text{Tmax})_{axial}$ since $(\Delta\text{Tmax})_{axial}$ occurs inside region I which is unaffected by C_1.

Fig. 4.2 shows the maximum dimensionless axial temperature rise in the

$[\frac{(\Delta Tmax)_{ax}}{\overline{\Delta T}}]$ bundle and the maximum dimensionless duct wall remperature difference $[\frac{(\Delta Tmax)_{duct}}{\overline{\Delta T}}]$ at the core exit as a function of $\overline{\varepsilon_H}^*$ and C_1. Fig. 4.2 was plotted for the theoretical flow split case (see Fig. 1). By superimposing the $\overline{\varepsilon_H}^*$ range from 0.025 to 0.048 on figure 4.2 one obtains the following range of predictions:

$$1.286 \leq \left(\frac{\Delta Tmax}{\overline{\Delta T}}\right)_{axial} \leq 1.307$$

$$0.273 < \left(\frac{\Delta Tmax}{\overline{\Delta T}}\right)_{duct} \leq 0.301 \qquad 4.1$$

A range similar to equation 4.1 above can be obtained for the case where uniform velocity is maintained within the bundle. The following range of predictions results:

$$1.250 \leq \left(\frac{\Delta Tmax}{\overline{\Delta T}}\right)_{axial} \leq 1.27$$

$$0.291 \leq \left(\frac{\Delta Tmax}{\overline{\Delta T}}\right)_{duct} \leq 0.318 \qquad 4.2$$

Based on the limits specified by equations 4.1 and 4.2 the following limit on predictions of the maximum temperature within the bundle, Tmax, and $(\Delta T_{max})_{duct}$ is formed.

$$977°F \leq Tmax \leq 993°F$$

$$82° \leq (\Delta Tmax)_{\substack{duct \\ core\ exit}} \leq 95°F \qquad 4.3$$

The limits on Tmax are clearly shown in Fig. 4.5 where temperatures along a cross-section A-B of the bundle exit (exit of core) are shown. As $\overline{\varepsilon_H}^*$ is decreased, the maximum exit temperature increases and occurs at a position closer to the duct wall.

A large range of $\overline{\varepsilon_H}^*$ and C_1, do not significantly effect Tmax and $(\Delta T_{max})_{duct}$. Tmax can be predicted to within ± 8°F and $(\Delta Tmax)_{duct}$ at the core exit to within ± 6.5° F. It is interesting to note that most of the predictions by other codes lie very close to this range (Table 4.1 and Fig. 4.5).

It is necessary to indicate that the range of ± 8° F on a ΔT_{axial} of 285° F (or 885°F for Tmax at exit) may be deceptively small especially since hot channel factors have not been inluded in the calculations. With the inclusion of H.C.F's the temperature range within which we can predict Tmax with great degree of confidence is expected to increase.

Fig. 4.6 shows the variation of $(\Delta Tmax)_{duct}$ with axial distance for two values of C_1. The axial distance is measured from the inlet of the core (active-fuel) and extends to the exit of the fuel-assembly. Fig. 4.7 shows a cross plot of Fig. 4.6 for the nominal $\overline{\varepsilon_H}^* = 0.04$. It is seen that the effect of lowering C_1 from 0.12 to 0.07 is to raise the spatial average value of $(\Delta Tmax)_{duct}$ from 36 in. to 84 in. by approximately 10°F. Duct structural designers must specify if this difference in $(\Delta Tmax)_{duct}$ is significant.

The peak temperature in the duct wall at the 84 in elevation occurs at the midpoint of face C (see Fig. 4.4) for $C_1 = 0.12$. However if $C_1 = 0.070$ the peak temperature occurs on face A very close to the corner between faces A and C. The rotation of the peak temperature in the duct wall appears to be relatively insensitive to C_1. This should be useful for core design restraint purposes.

5.1 Proposed Experiments

Based on the data analysis (Section 7), discussions (Section 3) and application of the code ENERGY to a 217-pin prototype bundle at full power (Section 4) we have come to the conclusion that further experimentation is required if reduction of the range of $\pm$ 8°F on T_{max} and $\pm$ 6.5°F on $(\Delta T_{MAX})_{DUCT}$ is desired. The reduction in the space-averaged $(\Delta T_{max})_{duct}$ was about 10°F when C_1 was increased from 0.07 to 0.12. Since each degree F reduction in T_{max} could mean an increase in max. burnup by up to 500 Mwd/T **(3)** it is imperative that a better understanding of the flow field and bundle size effects be obtained from more carefully designed experiments. Two different experiments will be briefly described. The first experiment is similar to the heated pin experiments described in Ref. 15. The second experiment has not been used before for LMFBR mixing studies and is strongly recommended. It may even be possible to combine the two types of experiment in an optimum fashion into a single setup. Before describing the experiment design let us again briefly examine the need for these experiments.

(1) Each °F reduction in T_{max} could mean up to 500 Mwd/T increase in burnup. Decrease in $(\Delta T_{max})_{duct}$ also means an increase in burnup.

(2) Tables 3.1 and 3.2 show that certain data gaps exist before a thermal-hydraulic optimization study on LMFBR fuel assembly design can be made. Very little

reliable data exists for swirl flow and $\overline{\varepsilon_H^*}$ at low values of h/d (h/d < 48). The only complete set of data available below h/d < 24 is SKOK[8] hot water injection data on 7-pin bundles. More data is required on larger bundles for low h/d and p/d and different rod diameters.

(3) Although several sets of experiments have been performed on FFTF bundle geometry, yet there is a great deal of speculation with regards to the flow field in bundles of various sizes. For example, is the bundle size effect observed real or is it due to faulty instrumentation and errors in measurement? Is the flow split a function of bundle size? A knowledge of the correct flow split could significantly reduce errors in predicting temperature distributions. If internal swirl flow exists for smaller bundles and reduces to zero as the bundle size increased to a 217 pin bundle, then the internal swirl flow must affect the flow field in these smaller bundles. Therefore experimental data observed on bundles smaller than the full size bundle could lead to erroneous results. Ref. 12 has found that the mixing coefficient between wall and the interior channel is low. Conflicting evidence exists on this. It must be resolved.

None of the experiments on heated pin measure fluid temperatures in the axial direction. Point measurements of temperatures by the wire and wall thermocouples cannot be easily used by existing subchannel analysis codes. The experiment proposed will permit measurement of axial fluid temperature distribution with as much accuracy as the exit fluid temperature distribution by varying the heated length of the pin but keeping the same exit where the exit rake thermocouples measure the fluid temperature.

5.2 Experiment I

A 217 pin experiment is proposed below with single or two heated pins strategically located in the manner suggested in Ref. 16. A wide range of d, h/d and p/d should be covered for two bundle sizes (91 and 217 pin). A 217 pin bundle is shown in Fig. 5.1. Fig. 5.1 also shows the location of the thermocouples in the subchannels. These thermocouples are placed in an exit rake similar in design to the O.R.N.L. exit rake. Water is used as the coolant. The use of water as coolant is justified for fuel assemblies where buoyancy effects are unimportant at high Reynolds number and also (since $\overline{\varepsilon_H} >> \alpha$) thermal conduction is unimportant both for sodium and water. Initially only rod 1 is heated. Fig. 5.2 shows the temperature rise as a function of the radial distance for three different Reynolds numbers. The rod power for the experiment in Fig. 5.2 is 10Kw/ft. Since $\overline{\varepsilon_H^*}$ is not expected to be a function of Reynolds number, the same value of $\overline{\varepsilon_H^*}$ ($\overline{\varepsilon_H^*} = 0.04$) was used to obtain curves I, II

and III. Fig. 5.3 shows the temperature distribution vs radial distance when the rod power is changed to 5 and 15 kw/ft but Reynolds number is maintained at 10000. One would ideally like to use a rod with the maximum power rating. But rod bowing at high linear power rating (i.e. 8 kw/ft) has been observed[9] in a 19 pin experiment. Here the power to flow ratio is much smaller than in Ref. 9 and it is expected that bowing and related problems should diminish considerably in severity. In order to cover a wide Reynolds number range ($5 \times 10^3 - 15 \times 10^3$) and yet produce accurate data with the lowest power rating of the rod it is recommended that the 10 kw/ft rod be used for the experiments. As the h/d is reduced the mixing rate $\overline{\varepsilon_H^*}$ increases and the maximum temperatures in Fig. 5.2 would reduce. The thermocouples can be designed to measure temperatures to within $\pm$ 1/2°F. Since only one thermocouple (located at the subchannel centroid) is used in each subchannel in these experiments it is expected that the temperature measured by it may be slightly different from the subchannel average temperature. However, the temperature gradients are small in the transverse direction and the difference in the thermocouple reading and the subchannel average temperature is expected to be small. In order to take such errors into account for determining a realistic estimate of the reduction in the range of $\overline{\varepsilon_H^*}$ and C_1 from the proposed experiment a large error bar of $\pm$ 1°F is applied to the thermocouple precision. Fig. 5.4 shows the calculated variation of the temperature rise recorded by thermocouple L vs $\overline{\varepsilon_H^*}$. On superimposing a $\pm$ 1°F error bar on these curves one finds that $\overline{\varepsilon_H^*}$ can be determined accurately.

As the power to flow ratio decreases (in going from curve I to III in Fig. 5.4) the precision with which $\overline{\varepsilon_H^*}$ can be determined decreases. For this reason curve III in Fig. 5.4 shows a much larger $\overline{\varepsilon_H^*}$ range than curves I and II. Therefore for the 10 kw/ft experiment only curves I and II (at Reynolds number of 5000 and 10000) should be used to determine $\overline{\varepsilon_H^*}$. A third set of data, if desired, could be obtained at a Reynolds number of 7500. The range within which one can determine $\overline{\varepsilon_H^*}$ (assuming a nominal value of $\overline{\varepsilon_H^*}$ of 0.041) is 0.038 to 0.044.

Fig. 5.5 shows the radial temperature distribution for two rods heated one at the center and one at the wall (Fig. 5.1). Both rods have the same power. It is seen that the swirl flow affects the temperature gradients significantly only near the wall. The wall thermocouples F_1 and F_2 show a large effect of variation of C_1. This is also seen in Figs 5.6 and 5.7 where the circumferential temperature profile is plotted.

As the swirl velocity ratio C_1 is varied, calculations show that the temperature profile in the circumferential direction changes significantly. Fig. 5.8 shows the calculated sensitivity of the temperature of thermocouple F_2 to variations in C_1. It is obvious that C_1 can be determined to a high degree of accuracy. An independent set of measurements using the Laser Doppler Velocimeter (LDV) can be used to verify the value of C_1 so obtained. The experience at M.I.T. with the LDV has shown that C_1 can be obtained within an accuracy of 12 to 15%. ENERGY analysis of the ORNL 19 pin experiment[9] showed that

C_1 lies in the range 0.12 - 0.14[1]. Much later it was verified[4] by Laser Measurements that for a 61 pin bundle of a similar geometry $C_1 = 0.13 \pm .015$. It is thus assumed that C_1 can be determined (if the nominal value is 0.12) within a range 0.11 to 0.13. The LDV should also be able to give valuable information on the flow split. Assuming the flow split is known and that $\overline{\varepsilon_H^*}$ is determined to be in the range 0.038 to 0.044 and C_1 is within the range 0.11 to 0.13, one can show, using Fig. 4.3 (or Fig. 4.2), that the maximum core exit temperature, T_{max}, can be predicted to within $\pm$ 2°F and the $(\Delta T_{max})_{DUCT}$ can be predicted at the core exit to within $\pm$ 2.5°F. Even if these limits were arbitrarily doubled, the precision with which the temperature distribution can be determined from the proposed experiments would be far better than the present day accuracy and confidence of these predictions.

The axial temperature distribution can also be determined from the proposed experiment by using different heated rod lengths (linear power rating, Reynolds number etc. should be left unchanged) and measuring the temperatures at the exit of the bundle. Thus by varying the active heated length (measured from the exit of the bundle) the axial temperature distribution can be obtained.

5.3 Experiment II

This experiment is an integral part of experiment I and provides information that can be input into the first experiment.

The motivations for this experiment are as follows. There is a considerable concern and some experimental evidence (Ref. 12) that the hydraulic interaction between the wall and the first row of inner channels is smaller than the hydraulic interaction between inner channels. In terms of ENERGY nomenclature, there appears to be evidence that $\overline{\varepsilon_H^*}$ is smaller at the boundary of the central and wall regions than its value in the inner region. This must be resolved.

Another motivation which is, perhaps, even more important than the first is as follows. While calibrating computer programs like COTEC[11] and ENERGY[1] a certain velocity profile is assumed in the bundle. Codes like THI-3D[10] calculate this velocity profile. While some small amount of data is available on flow splits there is not a single set of reliable data that can give the cross-sectional distribution of subchannel average velocities in the bundle. If the codes[1,11] assume a 3-dimensional velocity profile or if THI-3D[10] calculates a velocity profile different from the 'correct'velocity profile there will be errors made in calibration of mixing coefficients. Moreover the velocity profile may vary axially due to changes in coolant properties with temperature. Thus substituting a known velocity field into the energy equation and then determining a $\overline{\varepsilon_H^*}$ (or a coefficient for sweep flow as was done for THI-3D when using ORNL data(Ref.26)) by matching temperature fields is not strictly correct.

The experiment described below does not use the fluid within the bundle as a heat sink and so the velocity and temperature profiles remain constant axially. For such a system with

no internal heat generation the energy equation becomes

$$\frac{\partial}{\partial r}\left[r(\rho C_p \varepsilon_H(r) + k)\frac{\partial T}{\partial r}\right] = 0 \qquad (5.1)$$

At high Re for water (also for sodium) as coolant in the presence of wire wrap $\rho C_p \varepsilon_H >> k$, then

$$\frac{\partial}{\partial r}\left[r\rho C_p \varepsilon_H \frac{\partial T}{\partial r}\right] = 0 \qquad (5.2)$$

If the total heat transferred in a length L is Q(Btu/hr) then using this as a boundary condition

$$\varepsilon_H(r) = - \frac{Q}{2\pi r L(\rho C_p)\left(\frac{\partial T}{\partial r}\right)}$$

whence

$$\varepsilon_H^*(r) = - \frac{Q/(\bar{V}de)}{2\pi r(\rho C_p L)\left(\frac{\partial T}{\partial r}\right)_{r=r}} \qquad (5.3)$$

$\bar{V}$ = bundle average velocity

This type of experiment was originally designed by Yagi and Kunii (Ref. 29) for studying heat transfer near wall surface in packed beds. If Q is known then by measuring the temperature gradient $\left(\frac{\partial T}{\partial r}\right)_{r=r}$ at the radial position 'r' one can calculate the radial distribution of $\varepsilon_H^*(r)$. Thus, if the mixing coefficient near the duct wall decreased, it should be reflected by a change of slope of the T vs r curve. With such a system, therefore, the velocity data need not enter the calculation of $\overline{\varepsilon_H^*}$ and consequently the possible error in determining $\overline{\varepsilon_H^*}$ is reduced.

Figs. 5.9 and 5.10 show the cross-section of the experimental setup. The details, such as flow rates within the bundle and the coolant flow rate outside the bundle, can be calculated easily and are not given. The thermocouple locations are also not shown in the figure.

Since the fluid phase is not a heat sink a steady temperature profile (a single heated rod is located at the center of the bundle) distribution will be established after a developing length which could be as long as 8-9 ft. It would be possible to reduce considerably the axial distance required to achieve steady temperature profiles provided preheated fluid with a similar temperature distribution as the steady state distribution could be supplied at the inlet of the bundle. Obviously one does not know the steady temperature profile 'a priori'. So to start the experiment, preheat the inlet coolant to give a radial inlet temperature distribution (in practice several concentric zones) which is similar to a calculated steady temperature profile. Then by a trial and error procedure it should be fairly straightforward to preheat the inlet fluid in a manner such that steady temperature profile is established within 12 to 18 in.

It is necessary to note that a one-dimensional energy transport is assumed in the formulation of equation (5.3). Consideration must be given to the fact that a swirl velocity exists near the wall.

However, for the centrally heated rod it is difficult to imagine the existence of a circumferential temperature gradient. The German experiments[15,16,17] do not report a temperature gradient in the circumferential direction for the case when the central pin was heated. These tests were carried out very carefully, at low power rating of the centrally heated

pin. The O.R.N.L. 19 pin experiments report a circumferential temperature gradient for the centrally heated pin. It is believed that this is due to rod bowing since the pin was operated at 10 kw/ft. and bowing was observed at power ratings above 8 kw/ft. Even if a very small fraction of the total energy is transported circumferentially (which we believe will not occur after 12-24 in.) the results should not be affected to any large extent.

The sequence in which the two experiments should be conducted is as follows:

1) Perform the single centrally heated pin portion of Experiment I and determine if circumferential temperature gradients exist.

2) Perform the two heated pin portion of Experiment I - get swirl flow data. (For this case uniform $\overline{\varepsilon_H^*}$ is assumed throughout the bundle.)

3) For the pin-array of Experiment I - get swirl flow data from Laser Doppler Velocimeter.

4) If in step 1 it is found that for the centrally heated pin circumferential gradients exist, Experiment II cannot yield $\varepsilon_H^*(r)$. If however circumferential gradients are found to be very small or non-existent then conduct Experiment II to determine $\overline{\varepsilon_H^*}(r)$. The bundle array of Experiment I could be modified by adding a circumferential cooling jacket.

5) It is expected that $\overline{\varepsilon_H^*}$ is not a function of radius. However, if it is found to be a function of the radial position in

step 4, step 2 must be repeated and in calibration of C_1 the swirl velocity ratio, the correct local $\overline{\varepsilon_H^*}$ should be used.

Titles For Illustrations

TABLE 3.1

REF. \ NO. OF PINS	7	19	37	61	91	127	217
ANL - RAS ANL - CT ANL - CT	①(b)				⑧(a) ⑨(b)		
ORNL		④(c)					
MIT				⑤(d)			
BATELLE	②(d)						
JAPANESE				⑥(b)			
HEDL							⑪(b)
GE						⑩(a)	
KARLSRUHE				⑦(c)			
CADARACHE	③(a)						

LEGEND ① 1,2,---11 NUMBER ASSIGNED TO EACH EXPERIMENT FOR USE IN TABLE 3.2
② TYPE OF EXPERIMENT (a) HOT WATER INJECTION (b) SALT INJECTION
(c) HEATED PIN (d) LASER

TABLE 3.2 DATA ANALYSED

p/d \ h/d	14	17	19	21	24	26.5	28	34	43	48	50	52	55
1.065			3*										
1.1													
1.14	3			3			3						
1.20									6	1 8			
1.24										9		4 11	
1.25					5					5			
1.28					10								2
1.315		7						7			7		
1.355						3							

* NUMBERS REFER TO TABLE - I

Table 4.1 [19]

Comparison of Predicted Maximum Subchannel Temperatures at the Core Exit for a 217-pin FFTF Assembly With a 1.2 Power Skew and 300 Core ΔT.

	Max. Coolant Temperatures
SIMPLE [28]	1000 °F
THI-3D [10]	992 °F
Cϕ TEC [11]	988 °F
ENERGY	985 °F $\pm$ 8 °F
Fϕ RCMX [20]	972 °F

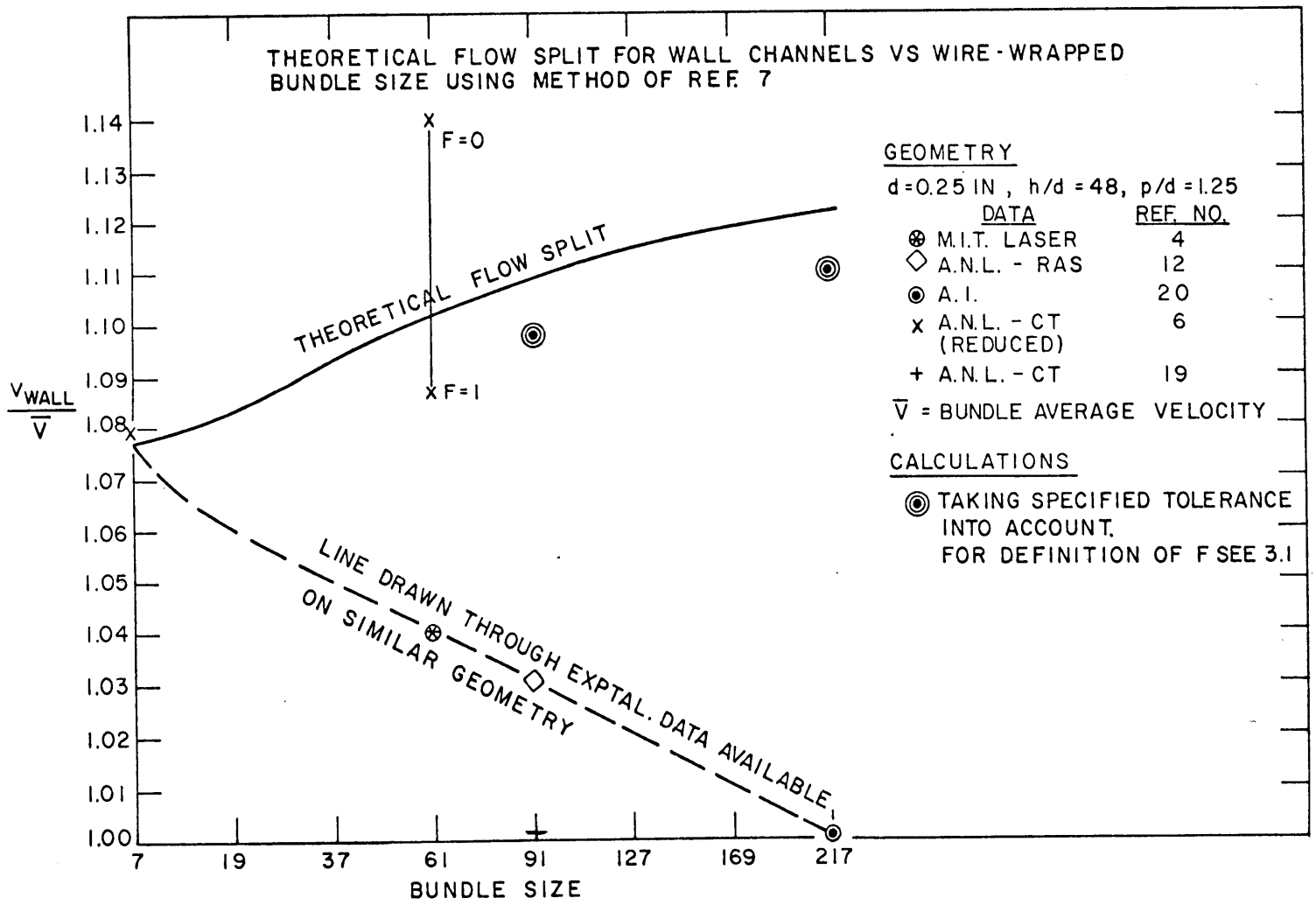
THEORETICAL FLOW SPLIT FOR WALL CHANNELS VS WIRE-WRAPPED BUNDLE SIZE USING METHOD OF REF. 7
$\frac{V_{WALL}}{\overline{V}}$
1.14
1.13
1.12
1.11
1.10
1.09
1.08
1.07
1.06
1.05
1.04
1.03
1.02
1.01
1.00
F=0
F=1
THEORETICAL FLOW SPLIT
LINE DRAWN THROUGH EXPTAL. DATA AVAILABLE ON SIMILAR GEOMETRY
7
19
37
61
91
127
169
217
BUNDLE SIZE
GEOMETRY
d=0.25 IN , h/d = 48, p/d = 1.25
DATA
REF. NO.
M.I.T. LASER 4
A.N.L. - RAS 12
A.I. 20
A.N.L. - CT (REDUCED) 6
A.N.L. - CT 19
$\overline{V}$ = BUNDLE AVERAGE VELOCITY
CALCULATIONS
TAKING SPECIFIED TOLERANCE INTO ACCOUNT.
FOR DEFINITION OF F SEE 3.1

FIG. 3.1

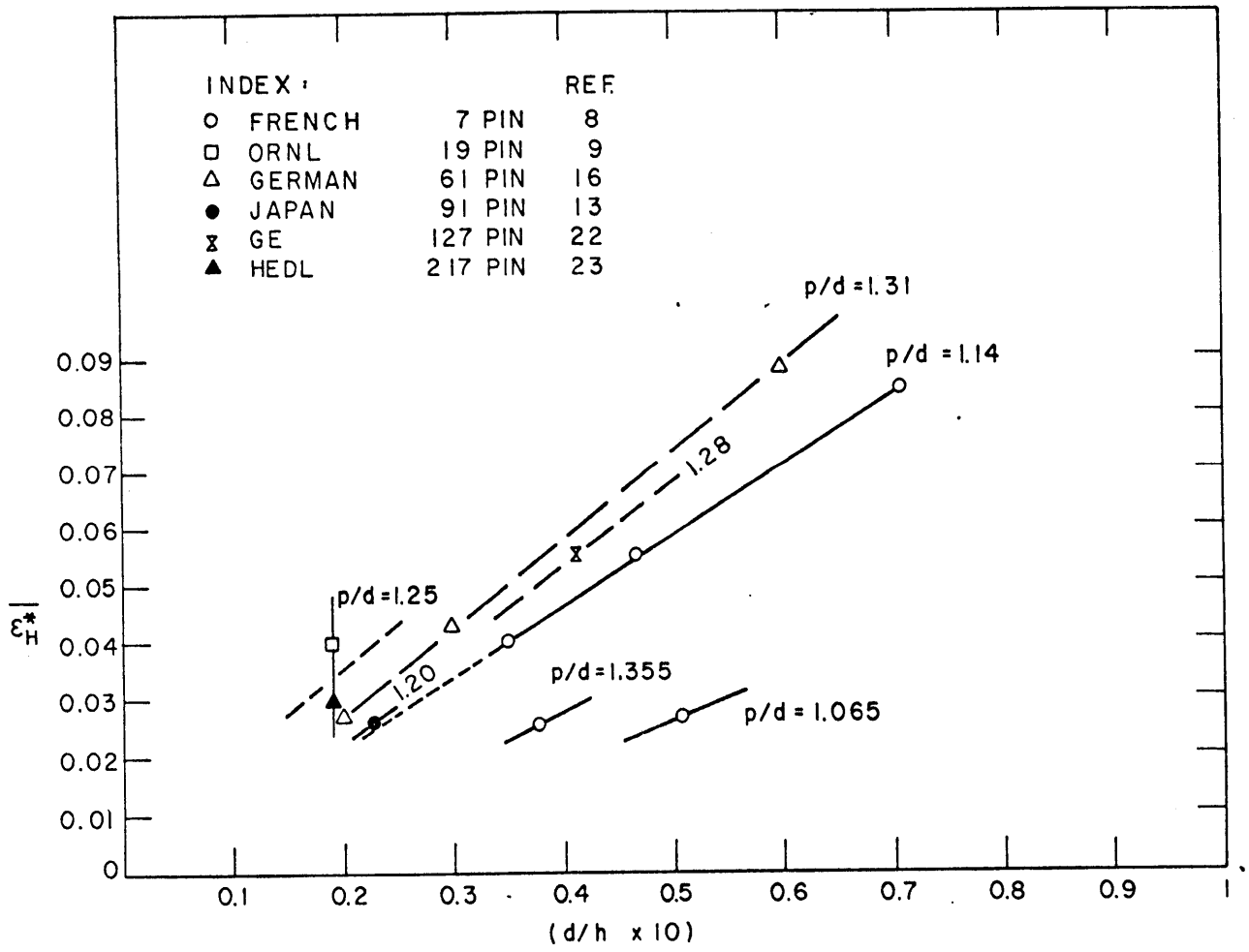
INDEX :
REF.
FRENCH 7 PIN 8
ORNL 19 PIN 9
GERMAN 61 PIN 16
JAPAN 91 PIN 13
GE 127 PIN 22
HEDL 217 PIN 23
p/d = 1.31
p/d = 1.14
1.28
1.20
p/d = 1.25
p/d = 1.355
p/d = 1.065
$\overline{\varepsilon_H^*}$
0.09
0.08
0.07
0.06
0.05
0.04
0.03
0.02
0.01
0
0.1
0.2
0.3
0.4
0.5
0.6
0.7
0.8
0.9
1
(d/h x 10)

FIG. 3.2

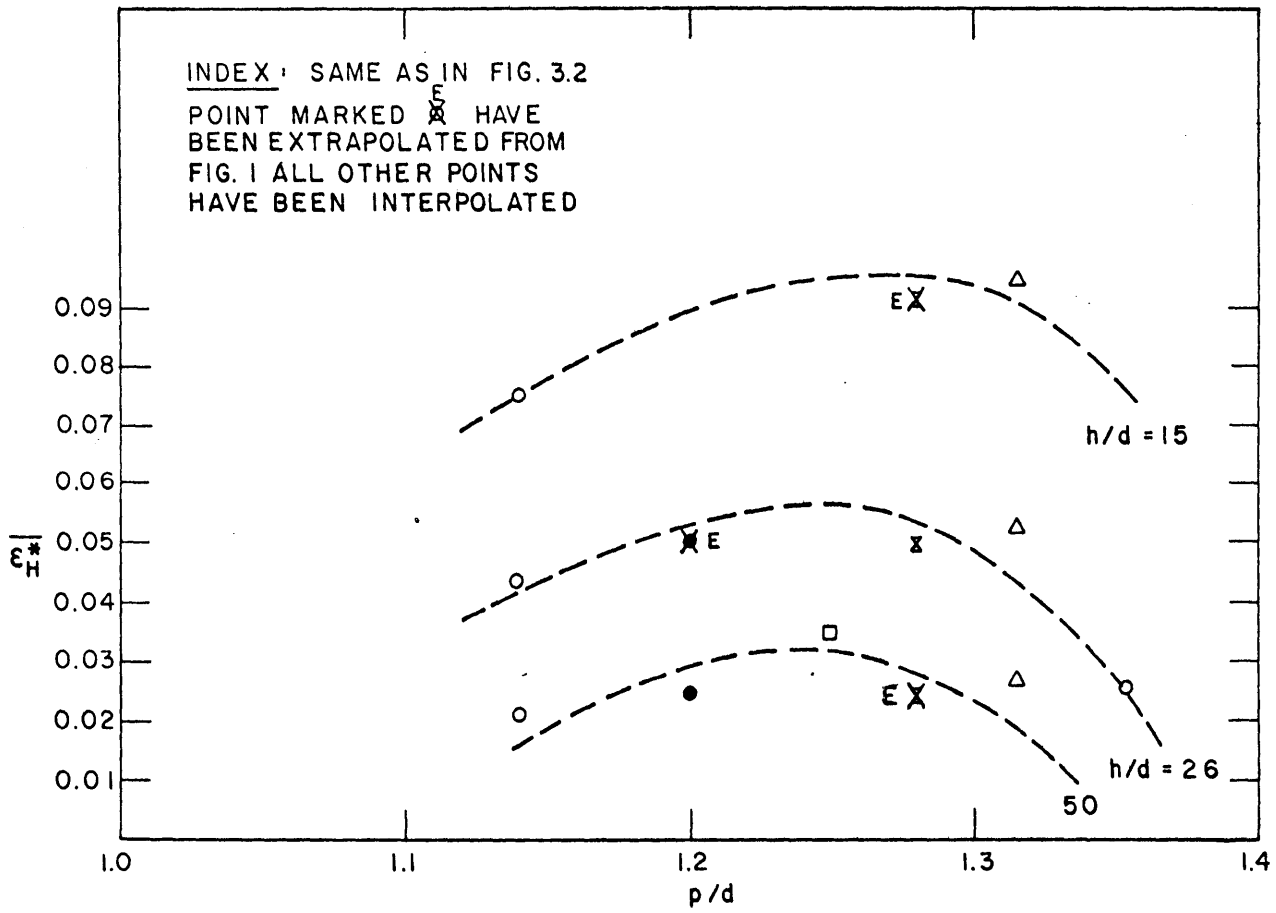
INDEX : SAME AS IN FIG. 3.2
POINT MARKED E HAVE BEEN EXTRAPOLATED FROM FIG. 1 ALL OTHER POINTS HAVE BEEN INTERPOLATED
0.09
0.08
0.07
0.06
0.05
0.04
0.03
0.02
0.01
$\overline{\varepsilon_H^*}$
h/d = 15
h/d = 26
50
E
1.0
1.1
1.2
1.3
1.4
p/d

FIG. 3.3

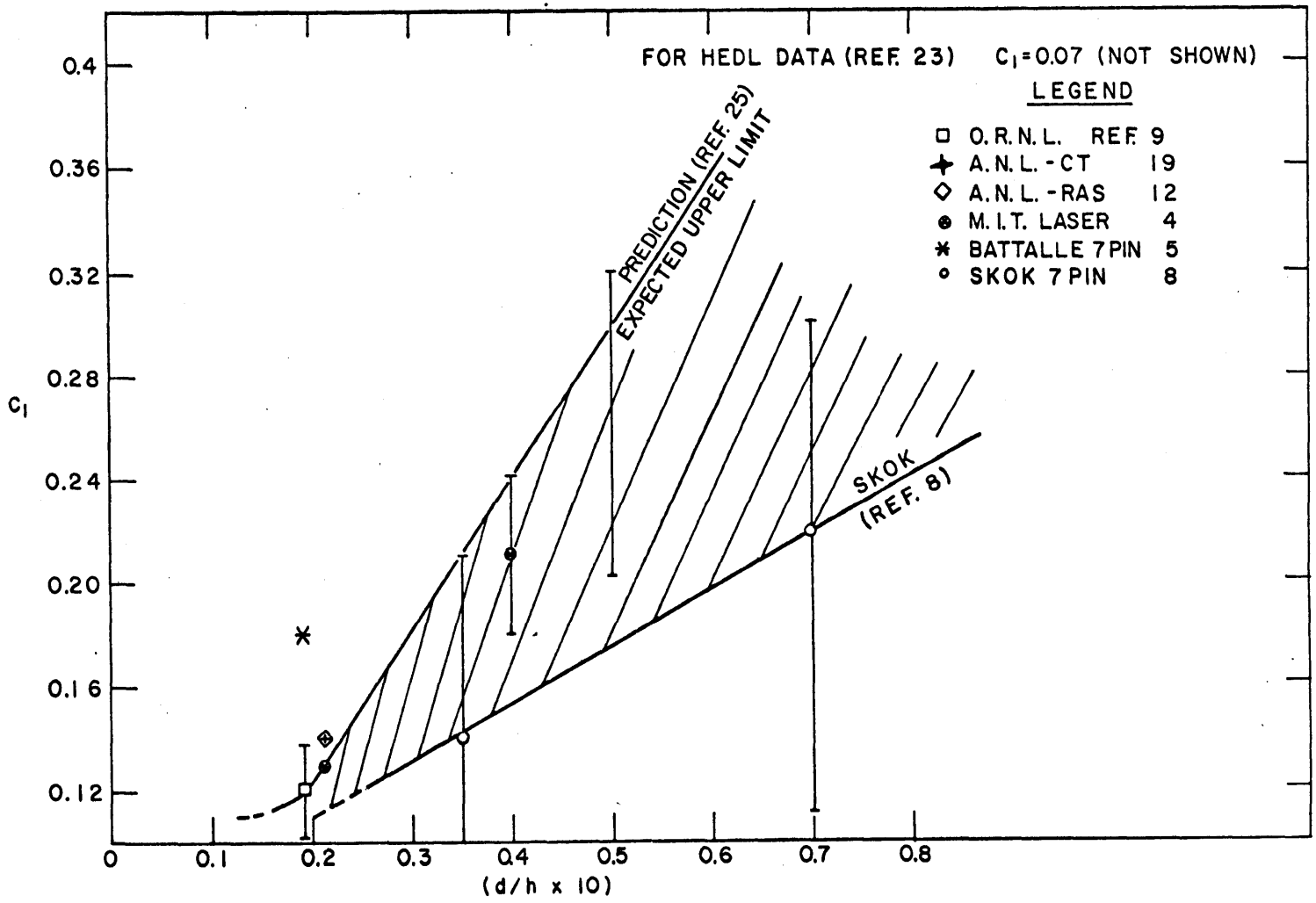
FOR HEDL DATA (REF. 23) C_1=0.07 (NOT SHOWN)
LEGEND
O. R. N. L. REF. 9
A. N. L. - CT 19
A. N. L. - RAS 12
M. I. T. LASER 4
BATTALLE 7 PIN 5
SKOK 7 PIN 8
PREDICTION (REF. 25)
EXPECTED UPPER LIMIT
SKOK
(REF. 8)
C_1
0.4
0.36
0.32
0.28
0.24
0.20
0.16
0.12
0
0.1
0.2
0.3
0.4
0.5
0.6
0.7
0.8
(d/h x 10)

FIG. 3.4

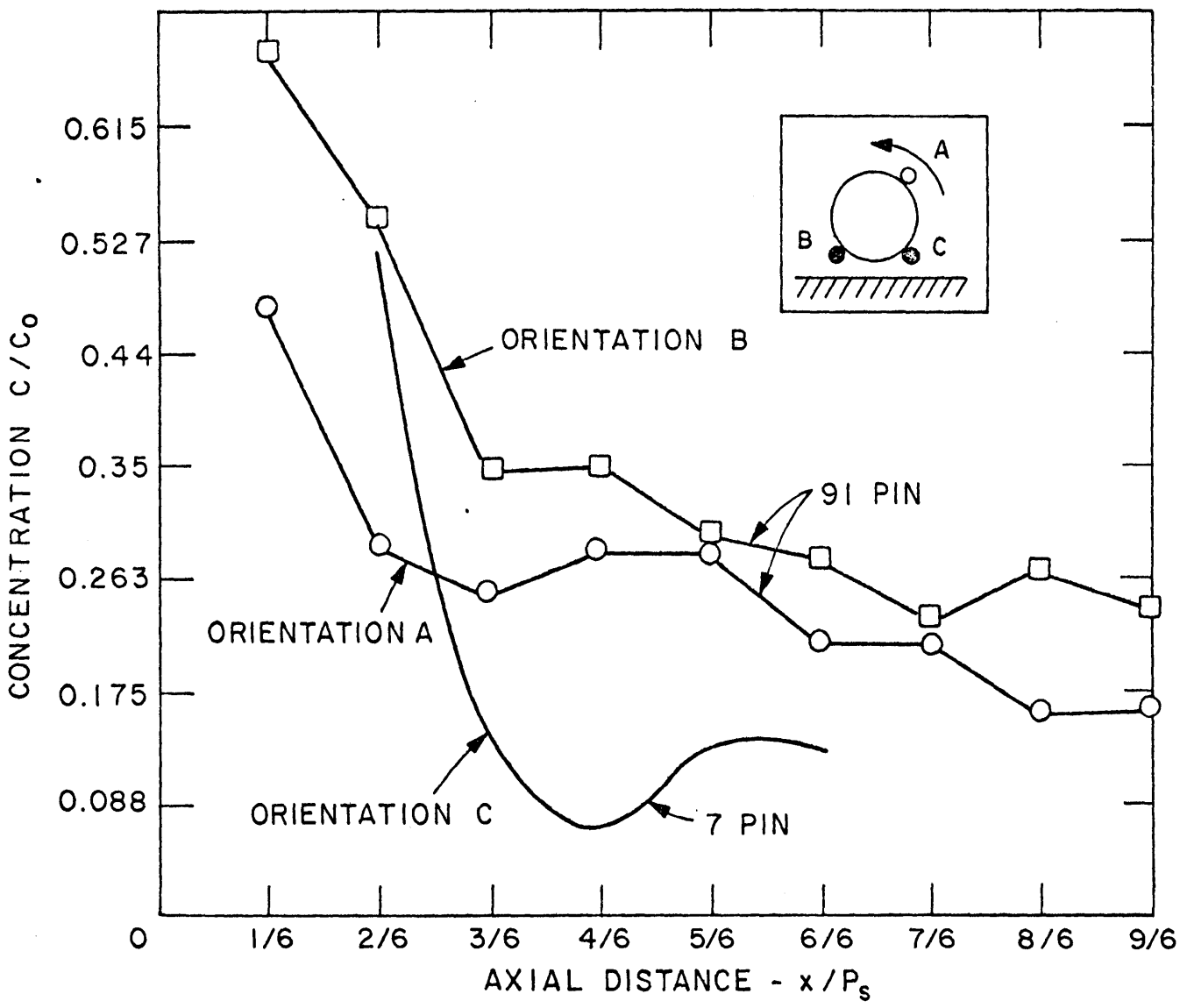
0.615
0.527
0.44
0.35
0.263
0.175
0.088
0
1/6
2/6
3/6
4/6
5/6
6/6
7/6
8/6
9/6
CONCENTRATION C/C0
AXIAL DISTANCE - x/Ps
ORIENTATION B
ORIENTATION A
ORIENTATION C
91 PIN
7 PIN
A
B
C

FIG. 3.5

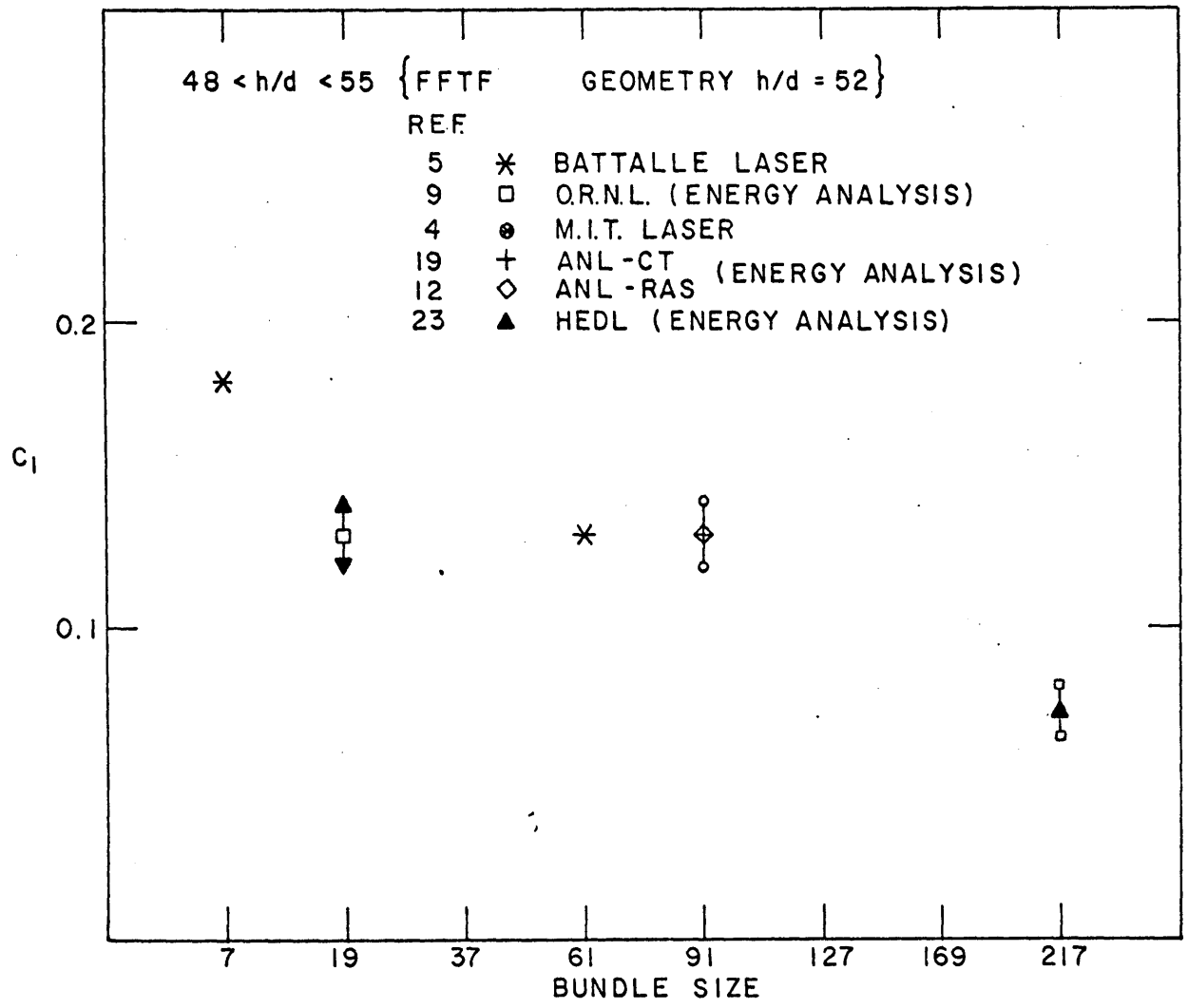
48 < h/d < 55 {FFTF GEOMETRY h/d = 52}
REF.
5 BATTALLE LASER
9 O.R.N.L. (ENERGY ANALYSIS)
4 M.I.T. LASER
19 ANL-CT (ENERGY ANALYSIS)
12 ANL-RAS
23 HEDL (ENERGY ANALYSIS)
0.2
0.1
C_l
7
19
37
61
91
127
169
217
BUNDLE SIZE

FIG. 3.6

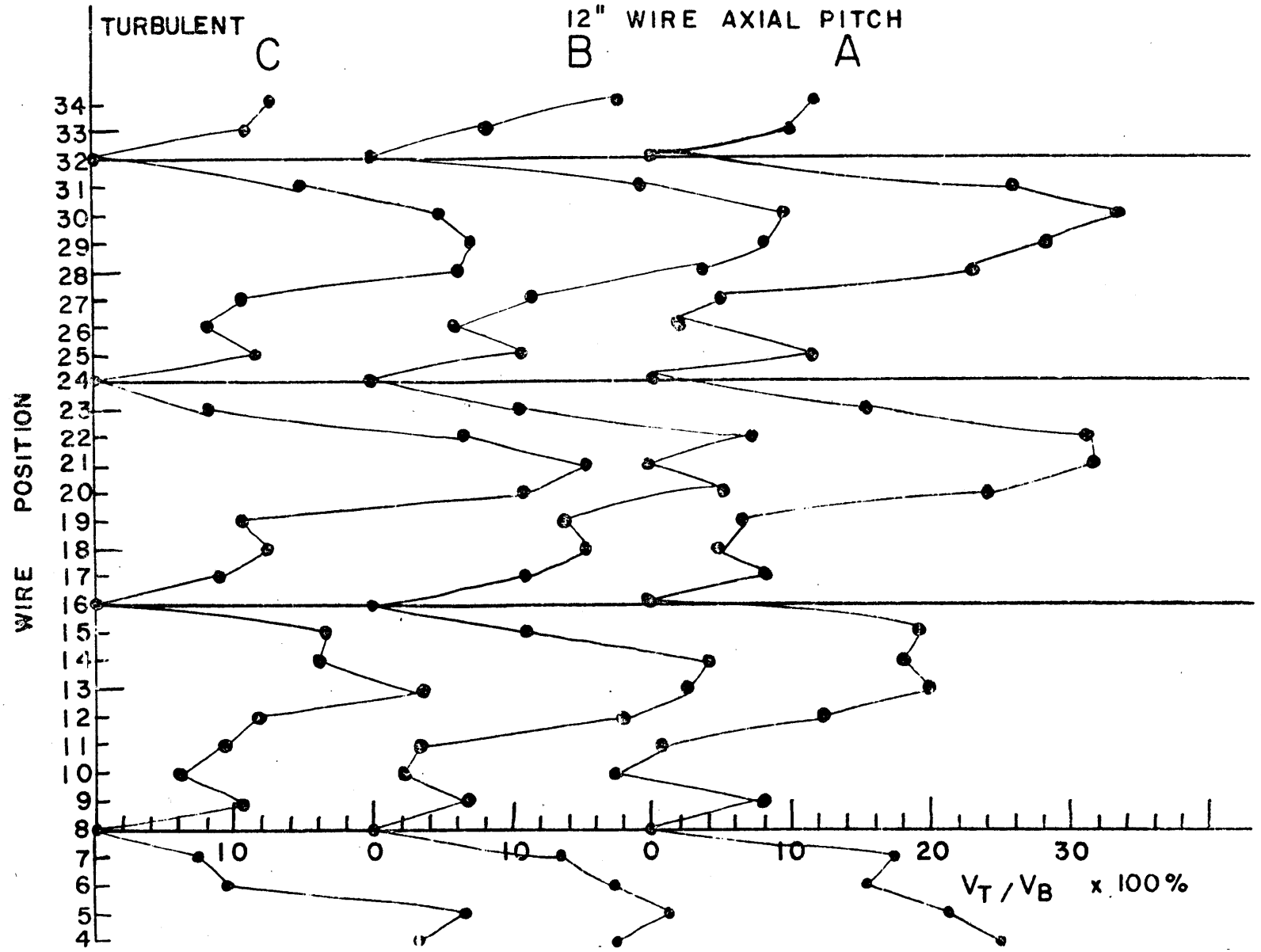
TURBULENT
12" WIRE AXIAL PITCH
C
B
A
WIRE POSITION
34
33
32
31
30
29
28
27
26
25
24
23
22
21
20
19
18
17
16
15
14
13
12
11
10
9
8
7
6
5
4
10
0
10
0
10
20
30
V_T / V_B x 100%

FIG. 3.7

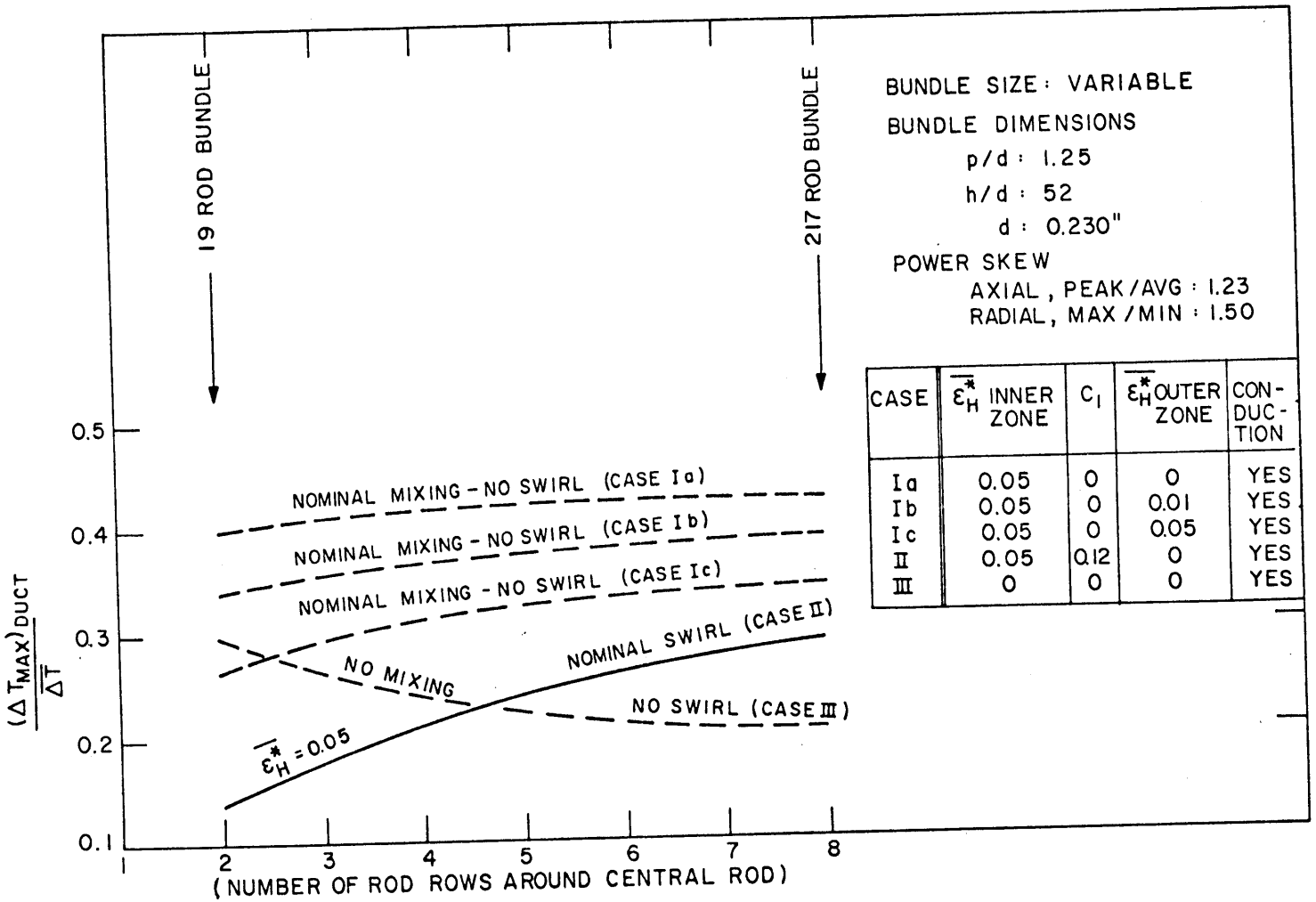
19 ROD BUNDLE
217 ROD BUNDLE
BUNDLE SIZE: VARIABLE
BUNDLE DIMENSIONS
p/d : 1.25
h/d : 52
d : 0.230"
POWER SKEW
AXIAL, PEAK/AVG : 1.23
RADIAL, MAX/MIN : 1.50
CASE | $\overline{\varepsilon_H^*}$ INNER ZONE | C_1 | $\overline{\varepsilon_H^*}$ OUTER ZONE | CONDUCTION
Ia | 0.05 | 0 | 0 | YES
Ib | 0.05 | 0 | 0.01 | YES
Ic | 0.05 | 0 | 0.05 | YES
II | 0.05 | 0.12 | 0 | YES
III | 0 | 0 | 0 | YES
NOMINAL MIXING - NO SWIRL (CASE Ia)
NOMINAL MIXING - NO SWIRL (CASE Ib)
NOMINAL MIXING - NO SWIRL (CASE Ic)
NO MIXING
NOMINAL SWIRL (CASE II)
NO SWIRL (CASE III)
$\overline{\varepsilon_H^*} = 0.05$
$\frac{(\Delta T_{MAX})_{DUCT}}{\Delta \bar{T}}$
0.5
0.4
0.3
0.2
0.1
1
2
3
4
5
6
7
8
(NUMBER OF ROD ROWS AROUND CENTRAL ROD)

FIG. 4.1

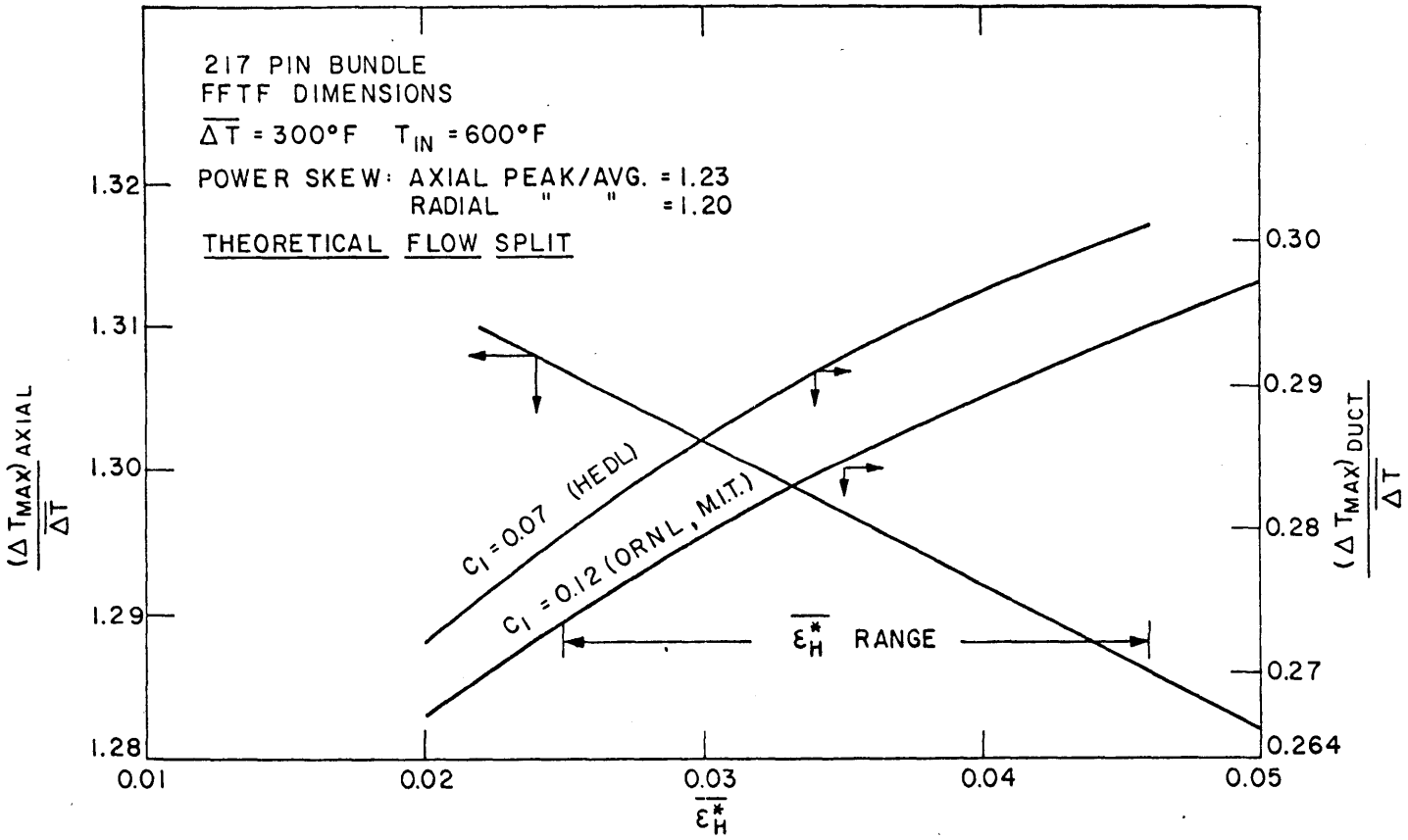
217 PIN BUNDLE
FFTF DIMENSIONS
$\overline{\Delta T}$ = 300°F T_{IN} = 600°F
POWER SKEW: AXIAL PEAK/AVG. = 1.23
RADIAL " " = 1.20
THEORETICAL FLOW SPLIT
C_1 = 0.07 (HEDL)
C_1 = 0.12 (ORNL, M.I.T.)
$\overline{\varepsilon_H^*}$ RANGE
$\frac{(\Delta T_{MAX})_{AXIAL}}{\overline{\Delta T}}$
$\frac{(\Delta T_{MAX})_{DUCT}}{\overline{\Delta T}}$
1.32
1.31
1.30
1.29
1.28
0.30
0.29
0.28
0.27
0.264
0.01
0.02
0.03
0.04
0.05
$\overline{\varepsilon_H^*}$

FIG. 4.2

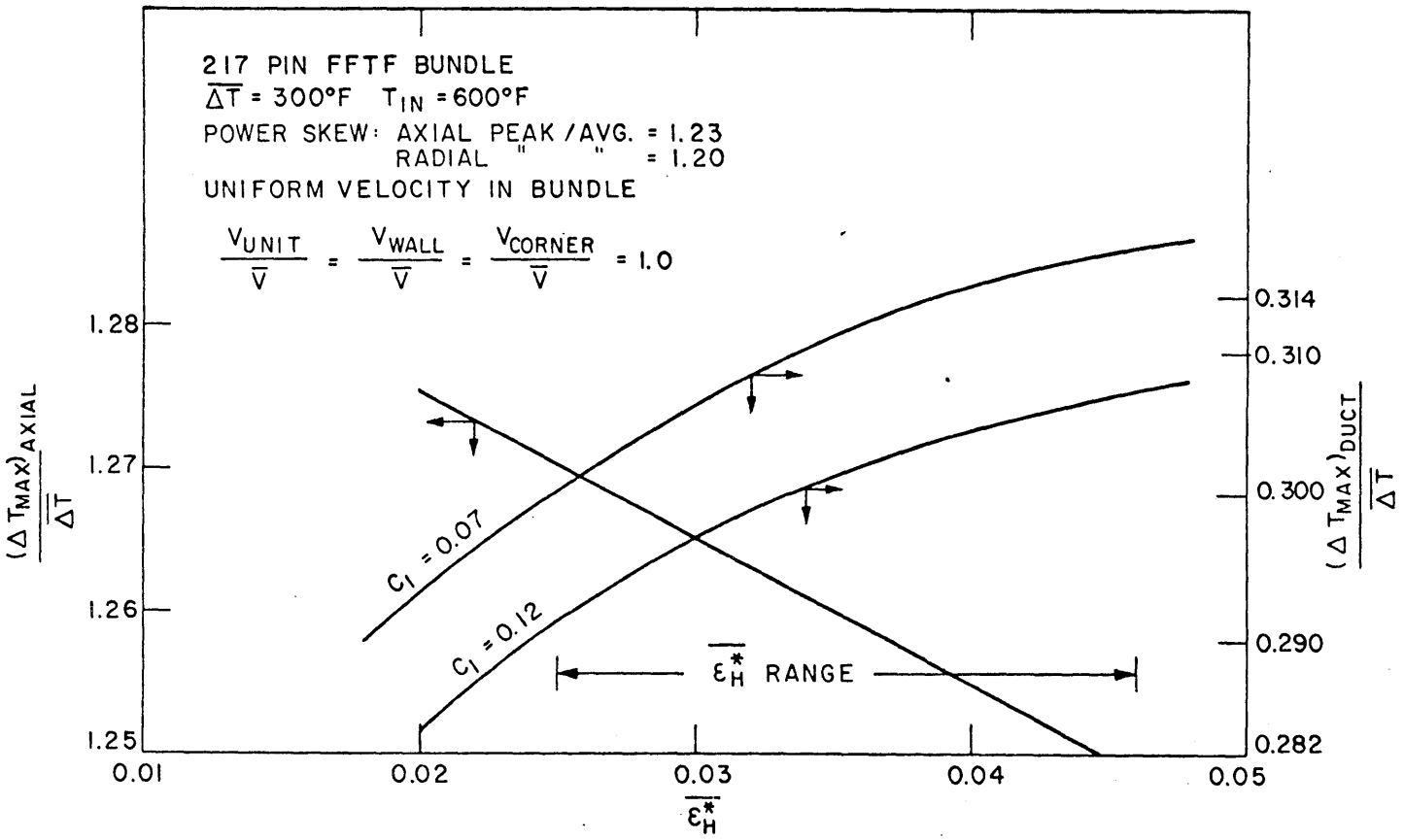
217 PIN FFTF BUNDLE
$\overline{\Delta T}$ = 300°F T_{IN} = 600°F
POWER SKEW: AXIAL PEAK / AVG. = 1.23
RADIAL " " = 1.20
UNIFORM VELOCITY IN BUNDLE
$\frac{V_{UNIT}}{\overline{V}} = \frac{V_{WALL}}{\overline{V}} = \frac{V_{CORNER}}{\overline{V}} = 1.0$
$\frac{(\Delta T_{MAX})_{AXIAL}}{\overline{\Delta T}}$
1.28
1.27
1.26
1.25
$C_1 = 0.07$
$C_1 = 0.12$
$\overline{\varepsilon_H^*}$ RANGE
0.01
0.02
0.03
0.04
0.05
$\overline{\varepsilon_H^*}$
0.314
0.310
0.300
0.290
0.282
$\frac{(\Delta T_{MAX})_{DUCT}}{\overline{\Delta T}}$

FIG. 4.3

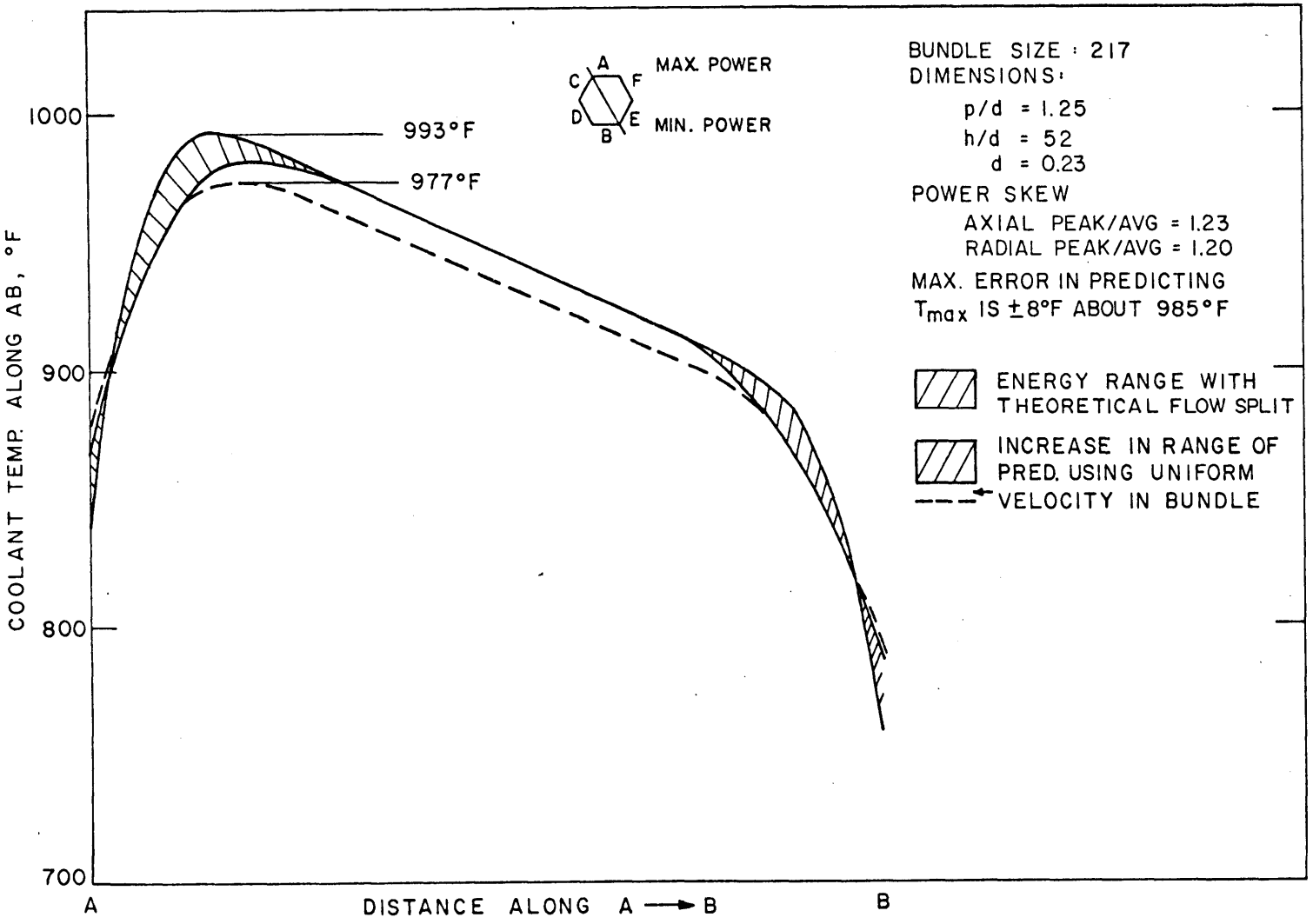
1000
900
800
700
COOLANT TEMP. ALONG AB, °F
993°F
977°F
A
C
F
D
E
B
MAX. POWER
MIN. POWER
BUNDLE SIZE : 217
DIMENSIONS:
p/d = 1.25
h/d = 52
d = 0.23
POWER SKEW
AXIAL PEAK/AVG = 1.23
RADIAL PEAK/AVG = 1.20
MAX. ERROR IN PREDICTING
T_{max} IS ±8°F ABOUT 985°F
ENERGY RANGE WITH THEORETICAL FLOW SPLIT
INCREASE IN RANGE OF PRED. USING UNIFORM VELOCITY IN BUNDLE
A
DISTANCE ALONG A → B
B

FIG. 4.4

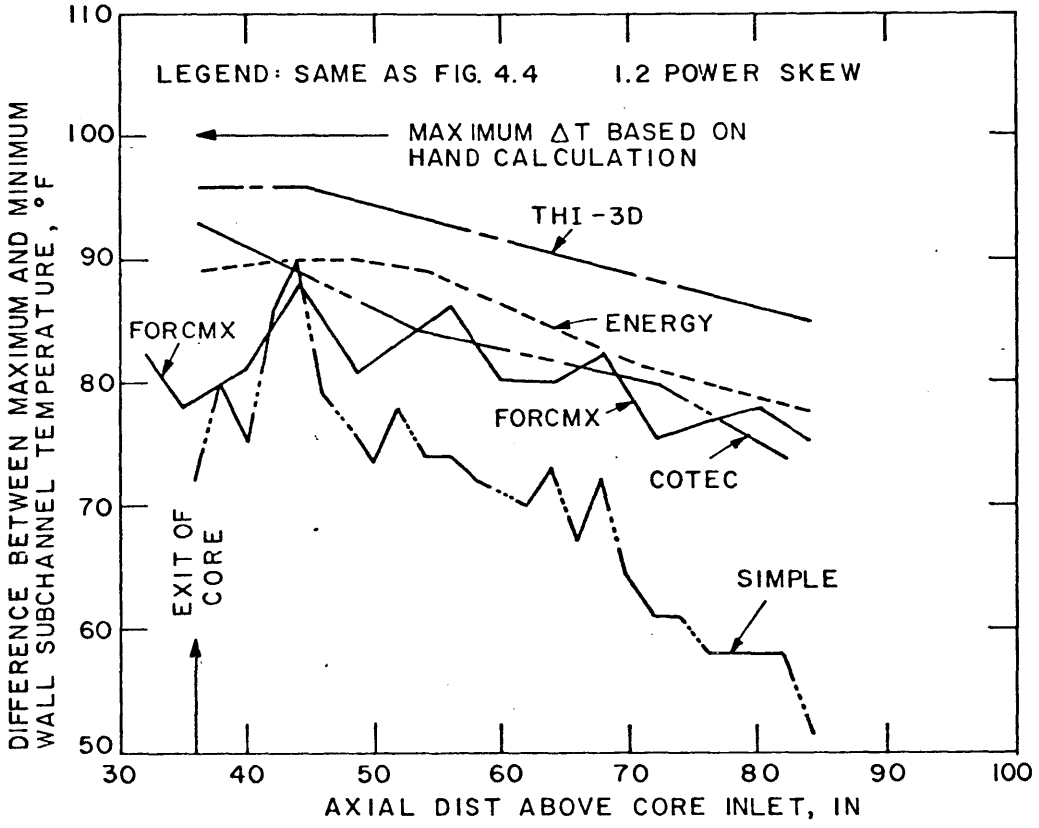
LEGEND: SAME AS FIG. 4.4 1.2 POWER SKEW
MAXIMUM ΔT BASED ON HAND CALCULATION
THI-3D
ENERGY
FORCMX
FORCMX
COTEC
SIMPLE
EXIT OF CORE
DIFFERENCE BETWEEN MAXIMUM AND MINIMUM WALL SUBCHANNEL TEMPERATURE, °F
AXIAL DIST ABOVE CORE INLET, IN
110
100
90
80
70
60
50
30
40
50
60
70
80
90
100

FIG. 4.5

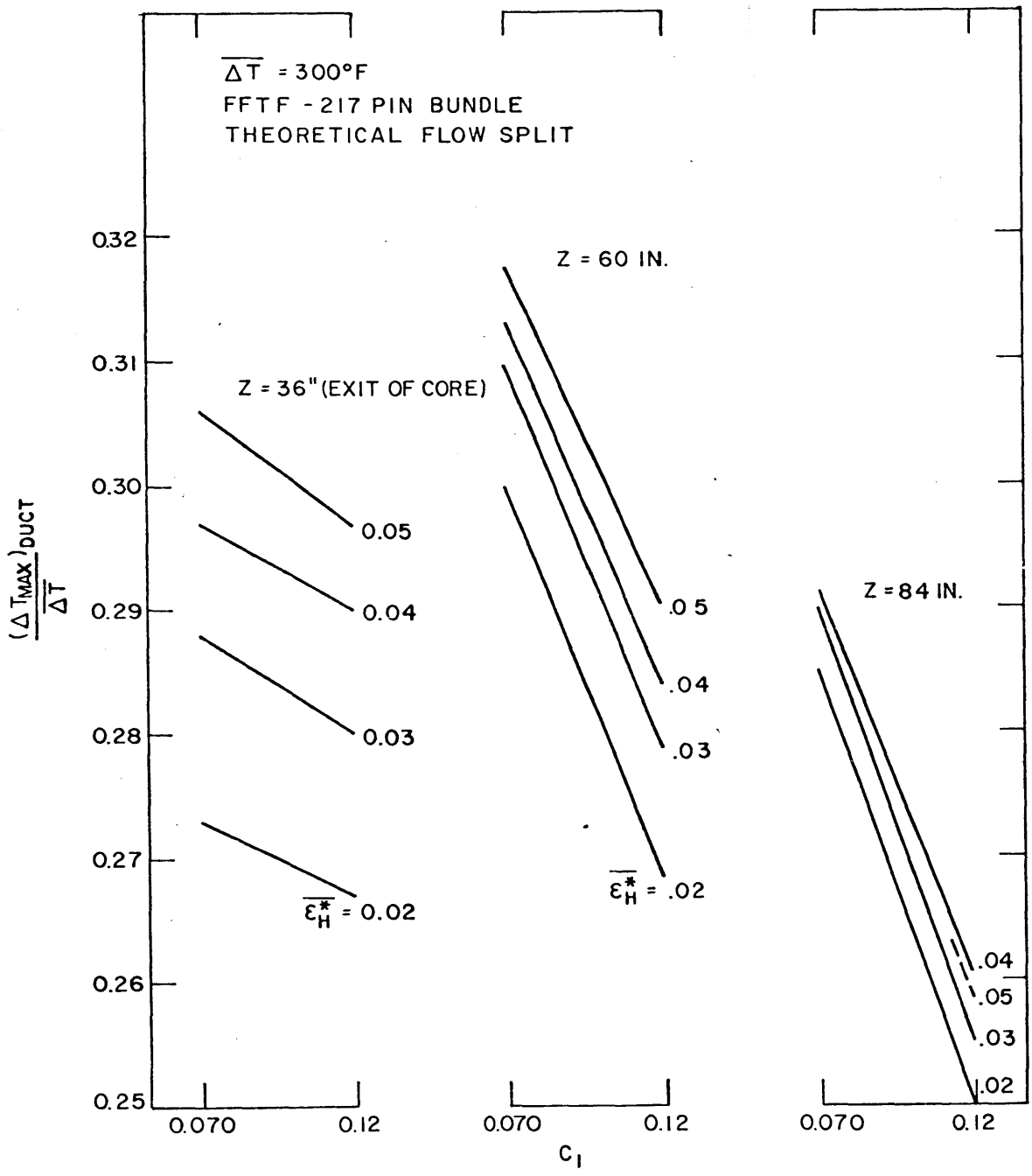
$\overline{\Delta T}$ = 300°F
FFTF - 217 PIN BUNDLE
THEORETICAL FLOW SPLIT
$\frac{(\Delta T_{MAX})_{DUCT}}{\overline{\Delta T}}$
0.32
0.31
0.30
0.29
0.28
0.27
0.26
0.25
Z = 36" (EXIT OF CORE)
0.05
0.04
0.03
$\overline{\varepsilon_H^*}$ = 0.02
Z = 60 IN.
.05
.04
.03
$\overline{\varepsilon_H^*}$ = .02
Z = 84 IN.
.04
.05
.03
.02
0.070
0.12
0.070
0.12
0.070
0.12
C_1

FIG. 4.6

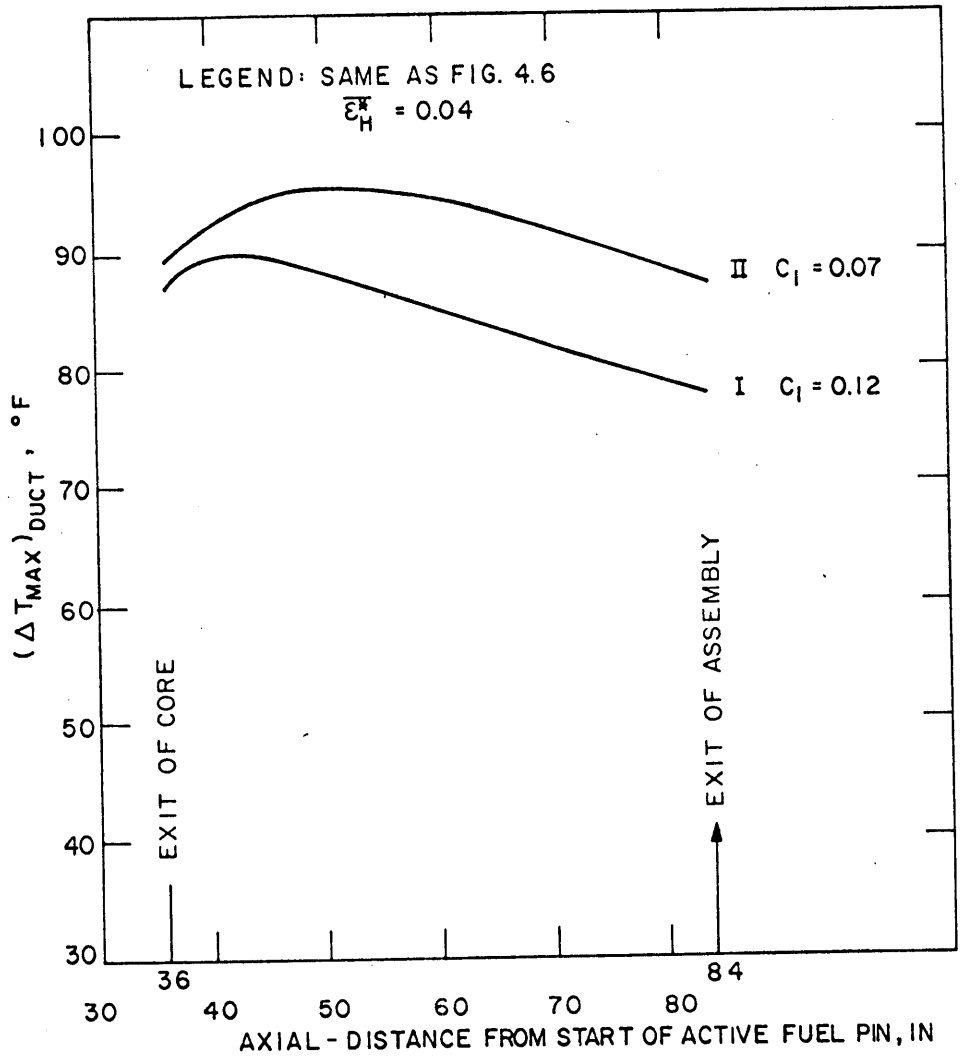
LEGEND: SAME AS FIG. 4.6
$\overline{\varepsilon_H^*}$ = 0.04
II C_1 = 0.07
I C_1 = 0.12
$(\Delta T_{MAX})_{DUCT}$, °F
100
90
80
70
60
50
40
30
EXIT OF CORE
EXIT OF ASSEMBLY
36
84
30
40
50
60
70
80
AXIAL - DISTANCE FROM START OF ACTIVE FUEL PIN, IN

FIG. 4.7

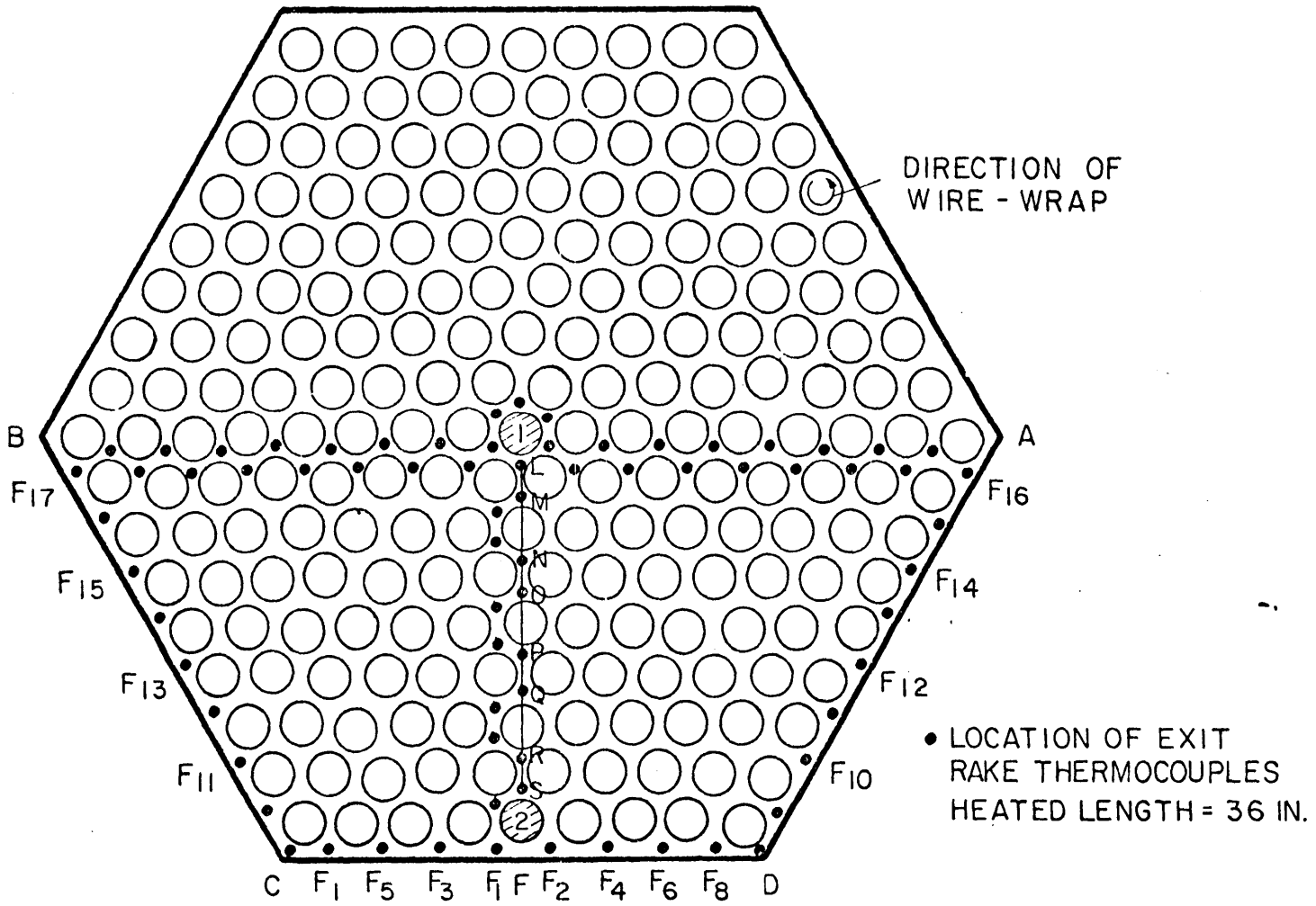
DIRECTION OF
WIRE - WRAP
B
A
F17
F16
F15
F14
F13
F12
F11
F10
C
F1
F5
F3
F7
F
F2
F4
F6
F8
D
1
2
L
M
N
O
P
Q
R
S
• LOCATION OF EXIT
RAKE THERMOCOUPLES
HEATED LENGTH = 36 IN.

FIG. 5.1

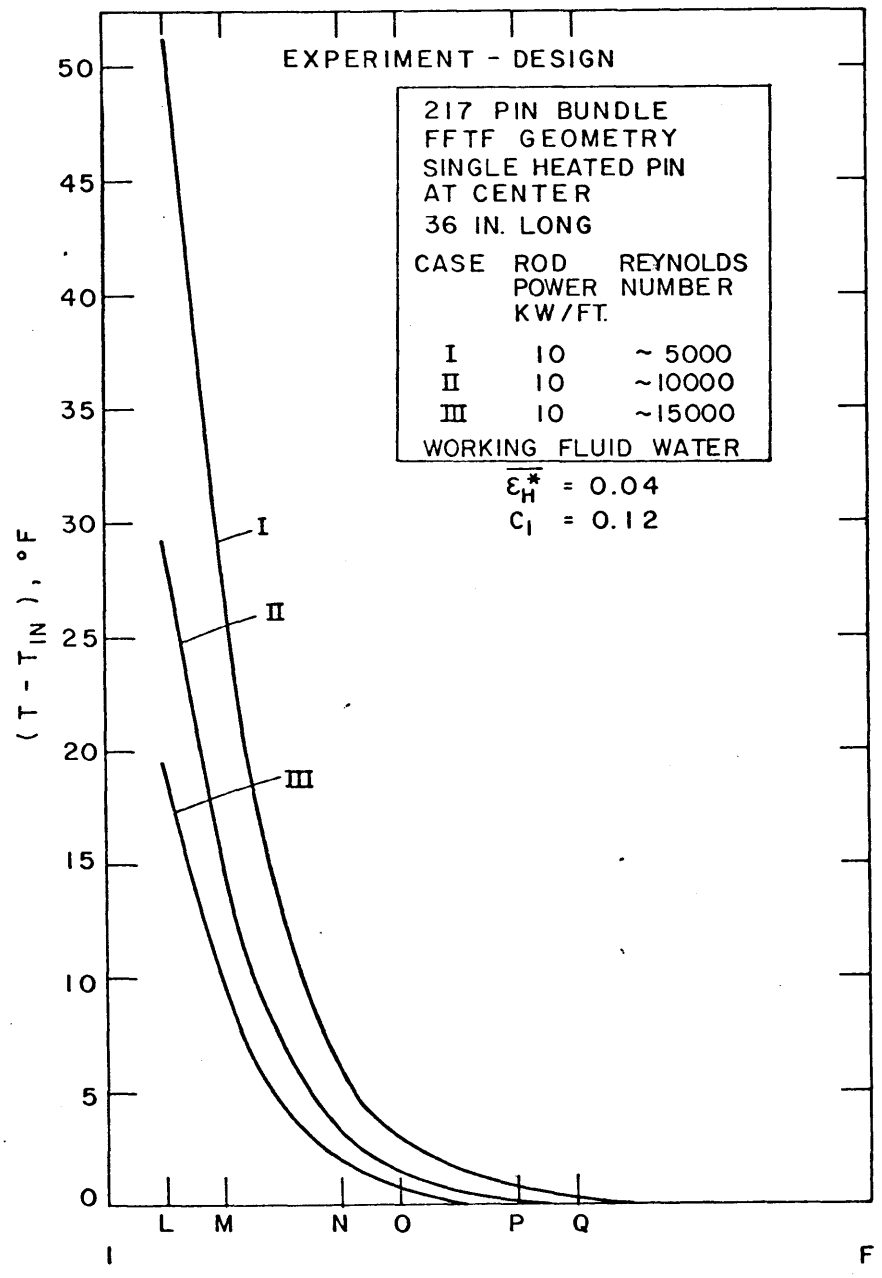
EXPERIMENT - DESIGN
217 PIN BUNDLE
FFTF GEOMETRY
SINGLE HEATED PIN
AT CENTER
36 IN. LONG
CASE ROD POWER KW/FT. REYNOLDS NUMBER
I 10 ~ 5000
II 10 ~10000
III 10 ~15000
WORKING FLUID WATER
$\overline{\varepsilon_H^*}$ = 0.04
C_1 = 0.12
$(T - T_{IN})$, °F
50
45
40
35
30
25
20
15
10
5
0
I
II
III
L M N O P Q
I
F

FIG. 5.2

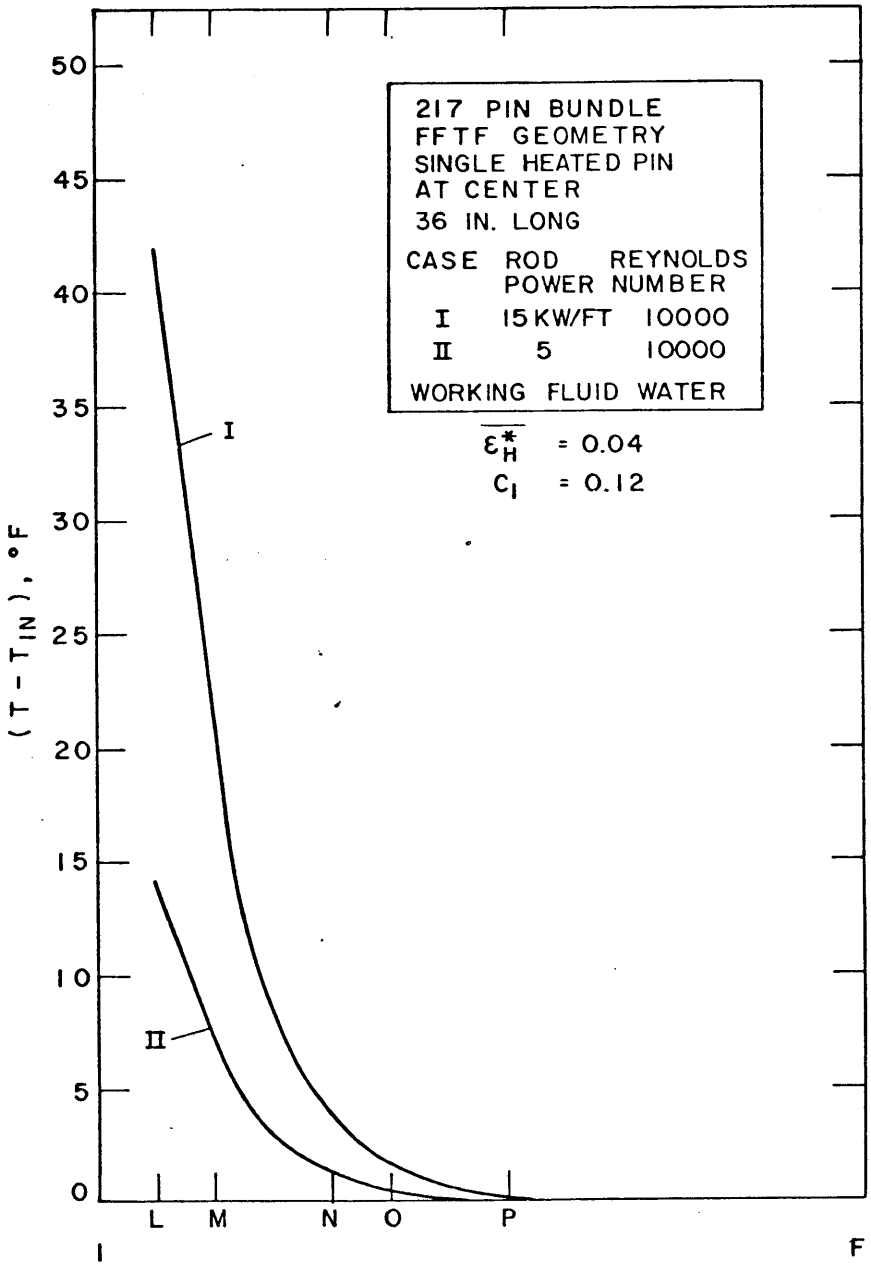
217 PIN BUNDLE
FFTF GEOMETRY
SINGLE HEATED PIN
AT CENTER
36 IN. LONG
CASE ROD POWER REYNOLDS NUMBER
I 15 KW/FT 10000
II 5 10000
WORKING FLUID WATER
$\overline{\varepsilon_H^*}$ = 0.04
C_1 = 0.12
$(T - T_{IN})$, °F
50
45
40
35
30
25
20
15
10
5
0
I
II
L
M
N
O
P
I
F

FIG. 5.3

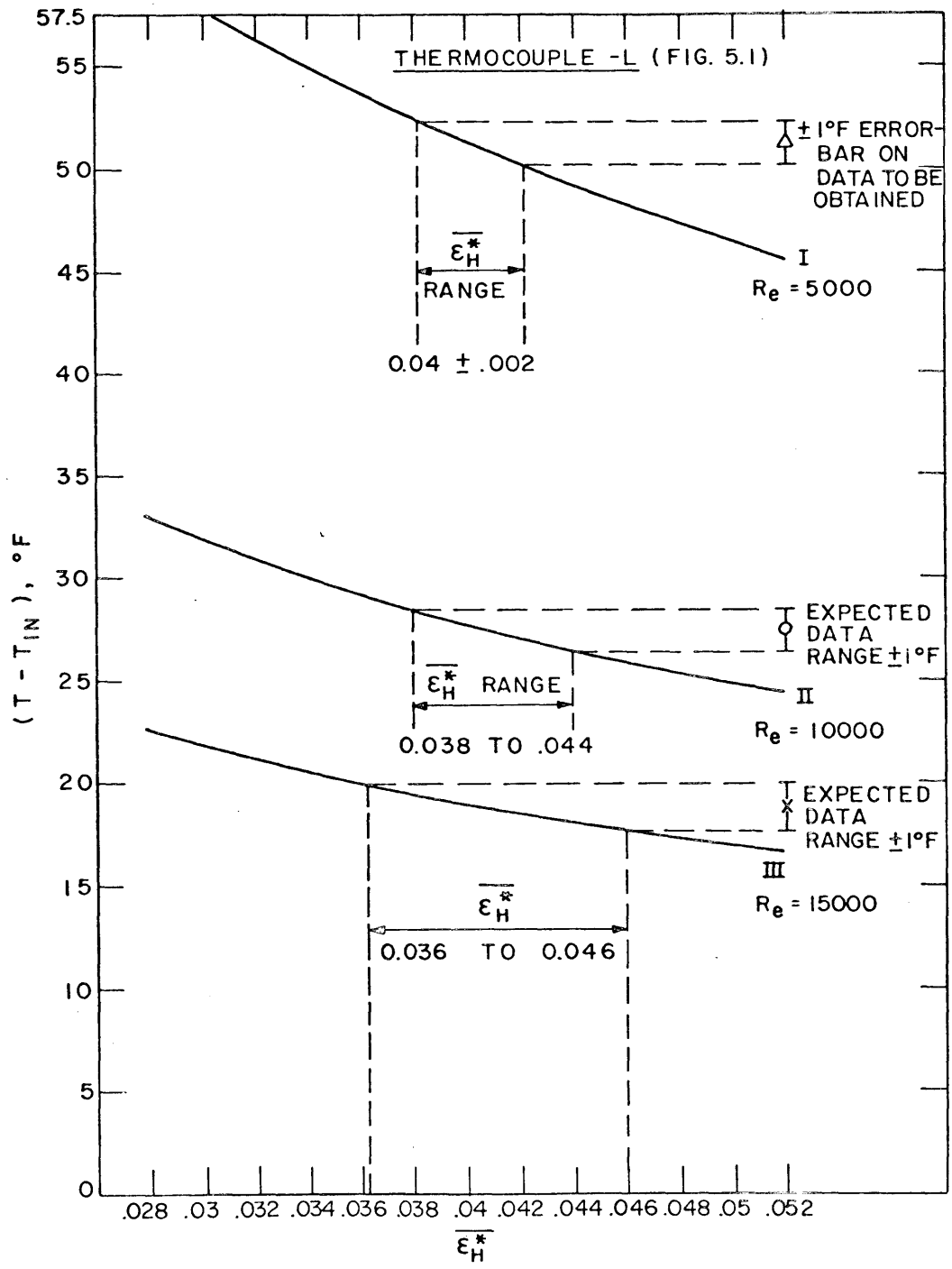
THERMOCOUPLE -L (FIG. 5.1)
±1°F ERROR-BAR ON DATA TO BE OBTAINED
$\overline{\varepsilon_H^*}$ RANGE
0.04 ± .002
I
R_e = 5000
EXPECTED DATA RANGE ±1°F
$\overline{\varepsilon_H^*}$ RANGE
0.038 TO .044
II
R_e = 10000
EXPECTED DATA RANGE ±1°F
$\overline{\varepsilon_H^*}$
0.036 TO 0.046
III
R_e = 15000
$(T - T_{IN})$, °F
$\overline{\varepsilon_H^*}$
57.5
55
50
45
40
35
30
25
20
15
10
5
0
.028 .03 .032 .034 .036 .038 .04 .042 .044 .046 .048 .05 .052

FIG. 5.4

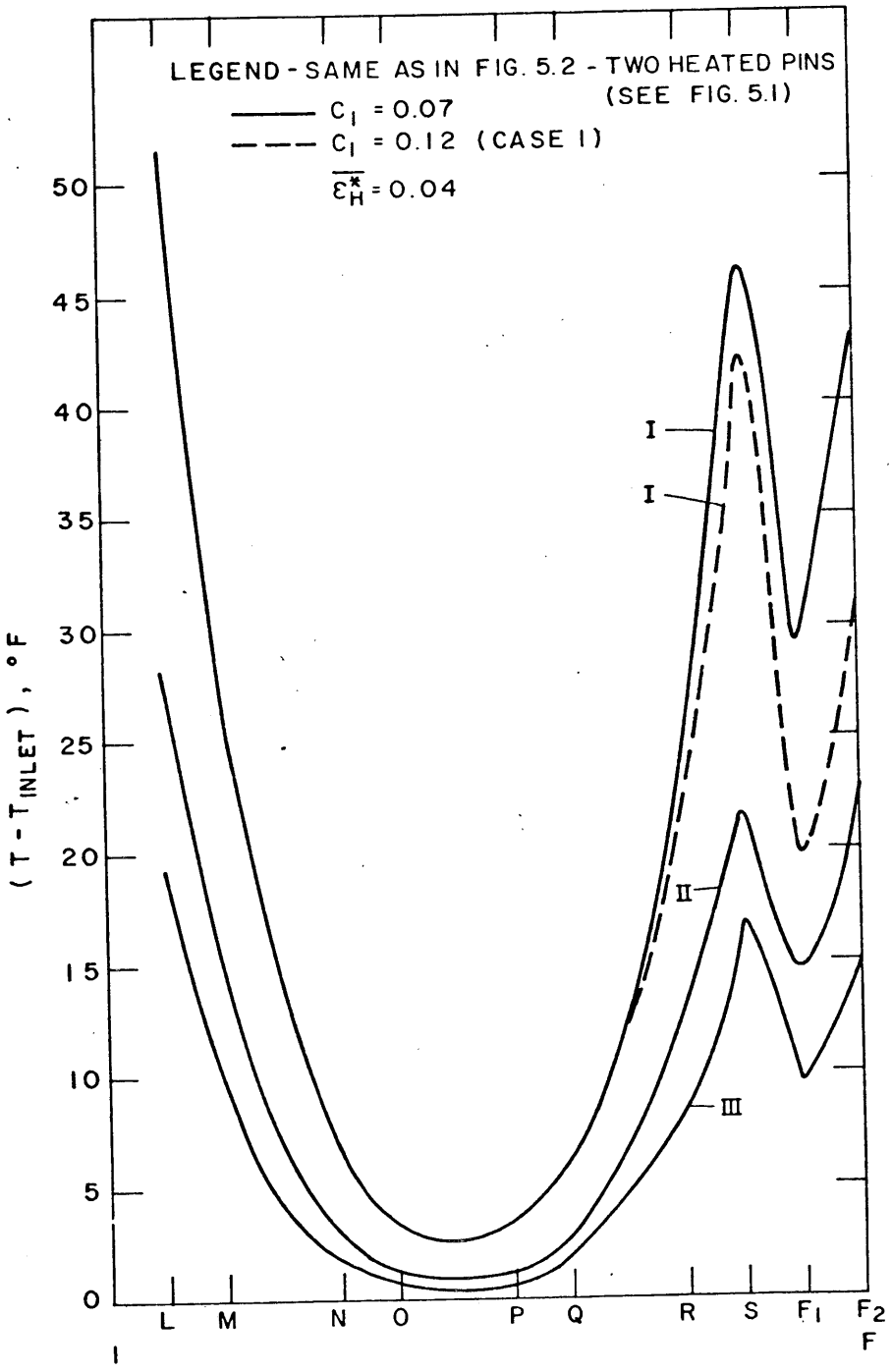
LEGEND - SAME AS IN FIG. 5.2 - TWO HEATED PINS
(SEE FIG. 5.1)
C_1 = 0.07
C_1 = 0.12 (CASE 1)
$\overline{\varepsilon_H^*}$ = 0.04
(T - T_{INLET}), °F
50
45
40
35
30
25
20
15
10
5
0
I
I
II
III
L
M
N
O
P
Q
R
S
F_1
F_2
I
F

FIG. 5.5

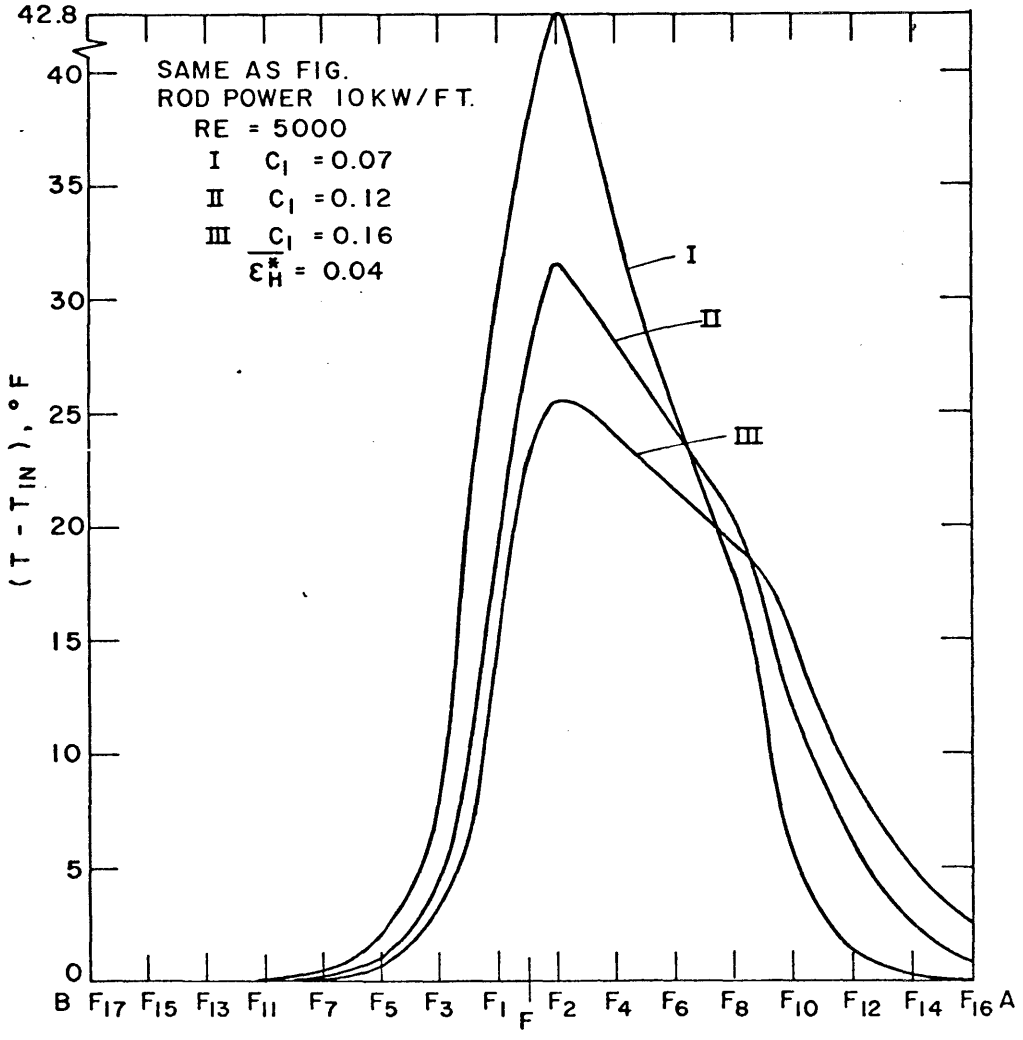
42.8
40
35
30
25
20
15
10
5
0
SAME AS FIG.
ROD POWER 10KW/FT.
RE = 5000
I C_1 = 0.07
II C_1 = 0.12
III C_1 = 0.16
$\frac{C_1}{\varepsilon_H^*}$ = 0.04
I
II
III
$(T - T_{IN})$, °F
B F_{17} F_{15} F_{13} F_{11} F_7 F_5 F_3 F_1 F F_2 F_4 F_6 F_8 F_{10} F_{12} F_{14} F_{16} A

FIG. 5.6

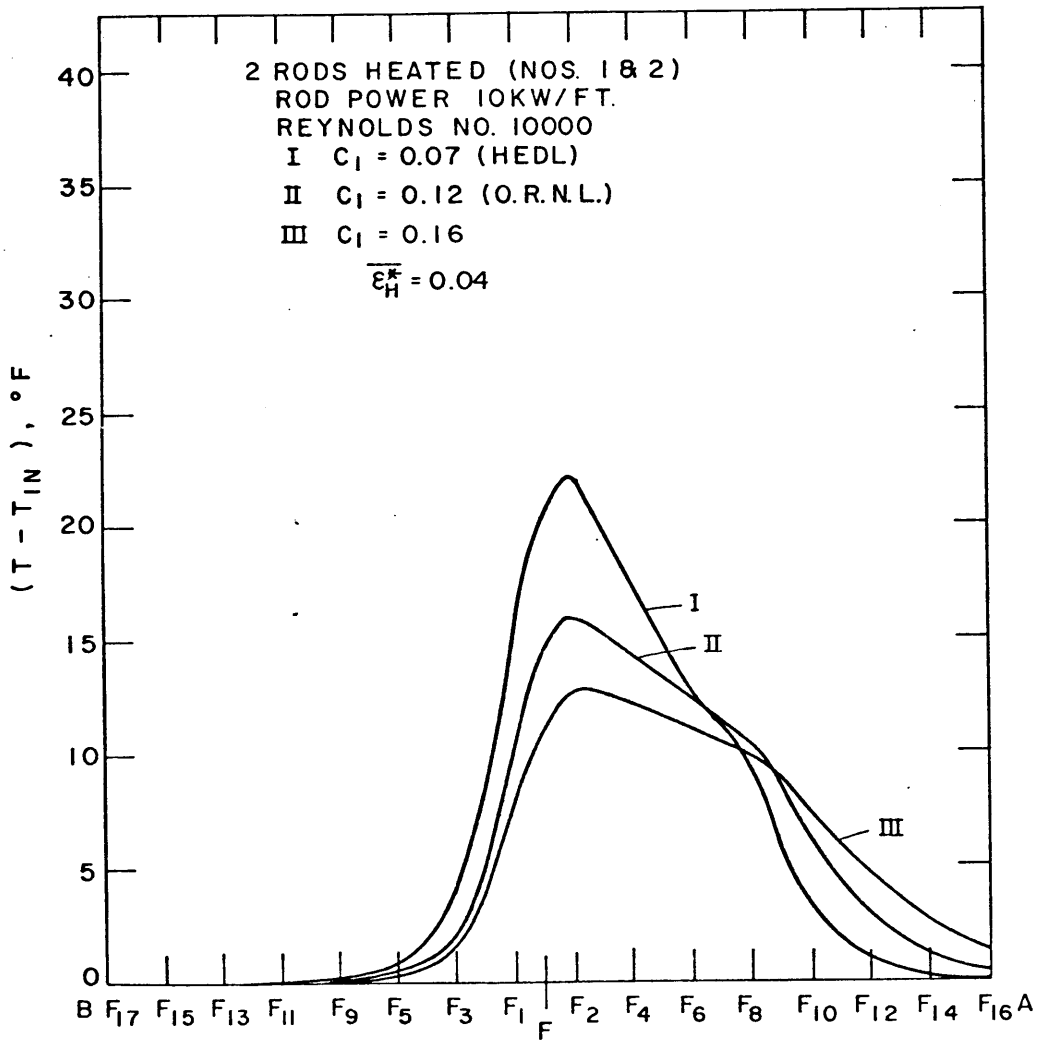
2 RODS HEATED (NOS. 1 & 2)
ROD POWER 10KW/FT.
REYNOLDS NO. 10000
I C_1 = 0.07 (HEDL)
II C_1 = 0.12 (O.R.N.L.)
III C_1 = 0.16
$\overline{\varepsilon_H^*}$ = 0.04
$(T - T_{IN})$, °F
0
5
10
15
20
25
30
35
40
I
II
III
B F_{17} F_{15} F_{13} F_{11} F_9 F_5 F_3 F_1 F F_2 F_4 F_6 F_8 F_{10} F_{12} F_{14} F_{16} A

FIG. 5.7

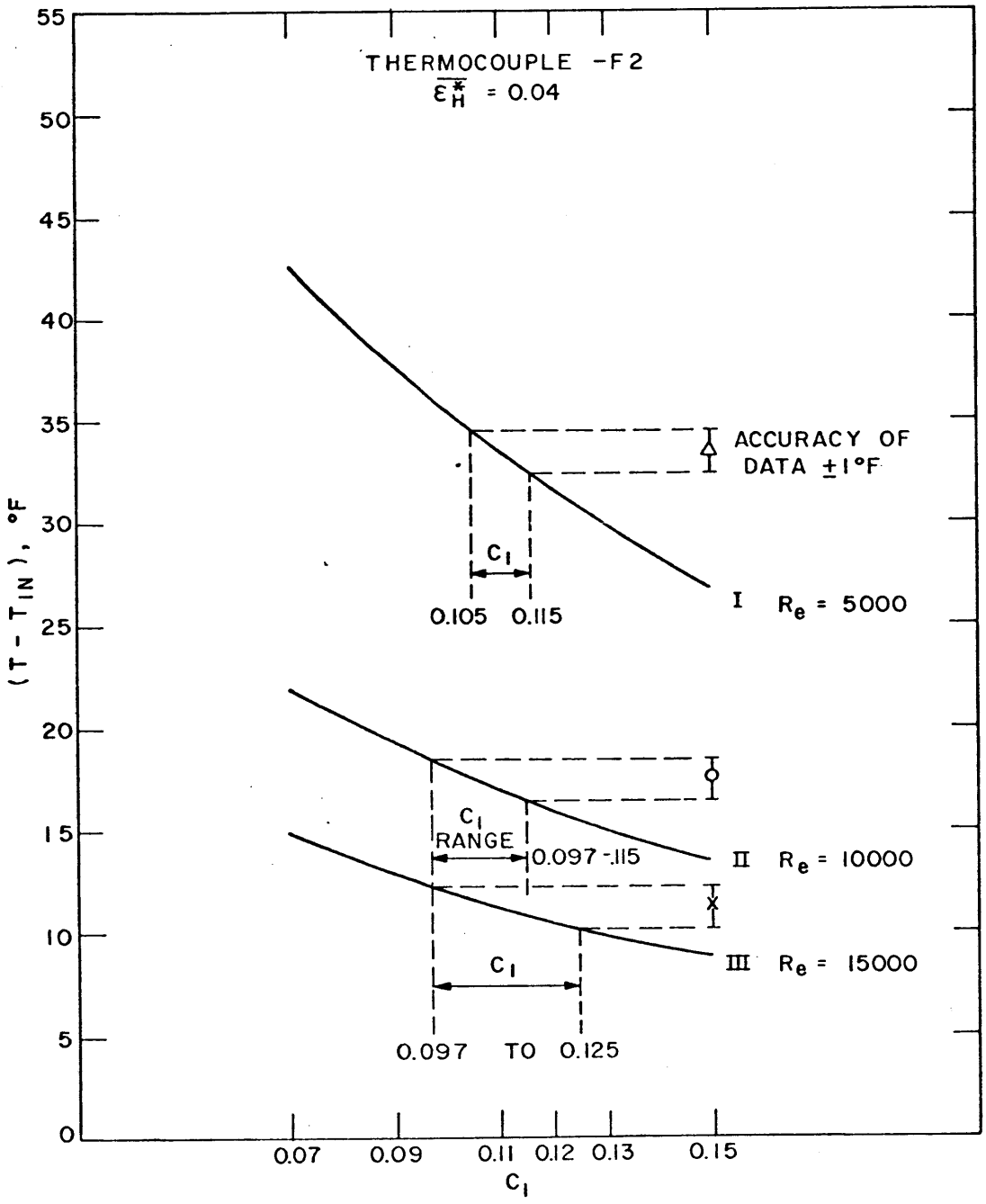
THERMOCOUPLE -F2
$\overline{\varepsilon_H^*}$ = 0.04
ACCURACY OF DATA ±1°F
C_1
0.105 0.115
I R_e = 5000
C_1 RANGE
0.097 -.115
II R_e = 10000
C_1
0.097 TO 0.125
III R_e = 15000
$(T - T_{IN})$, °F
C_1
55
50
45
40
35
30
25
20
15
10
5
0
0.07
0.09
0.11
0.12
0.13
0.15

FIG. 5.8

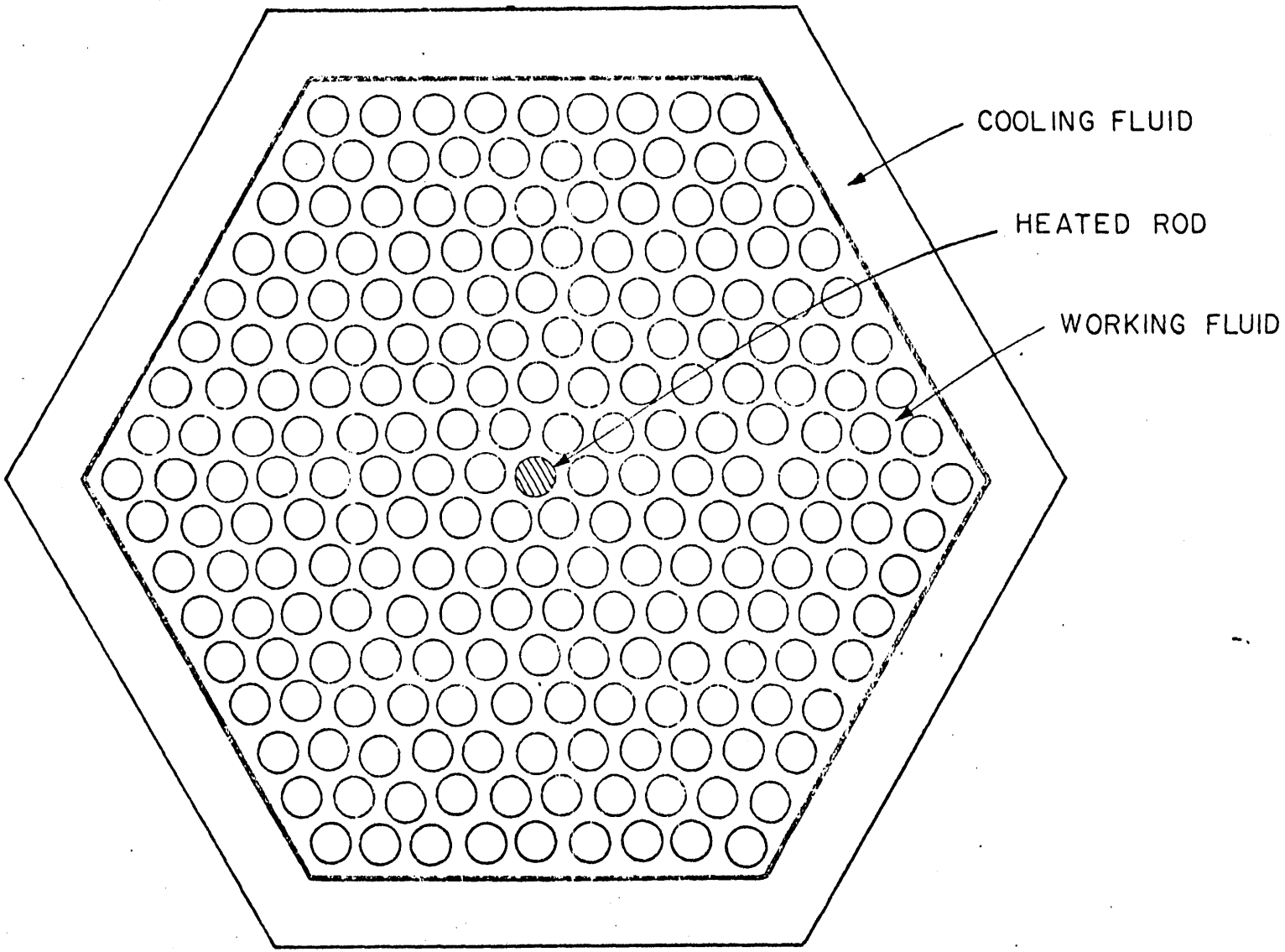

FIG. 5.9

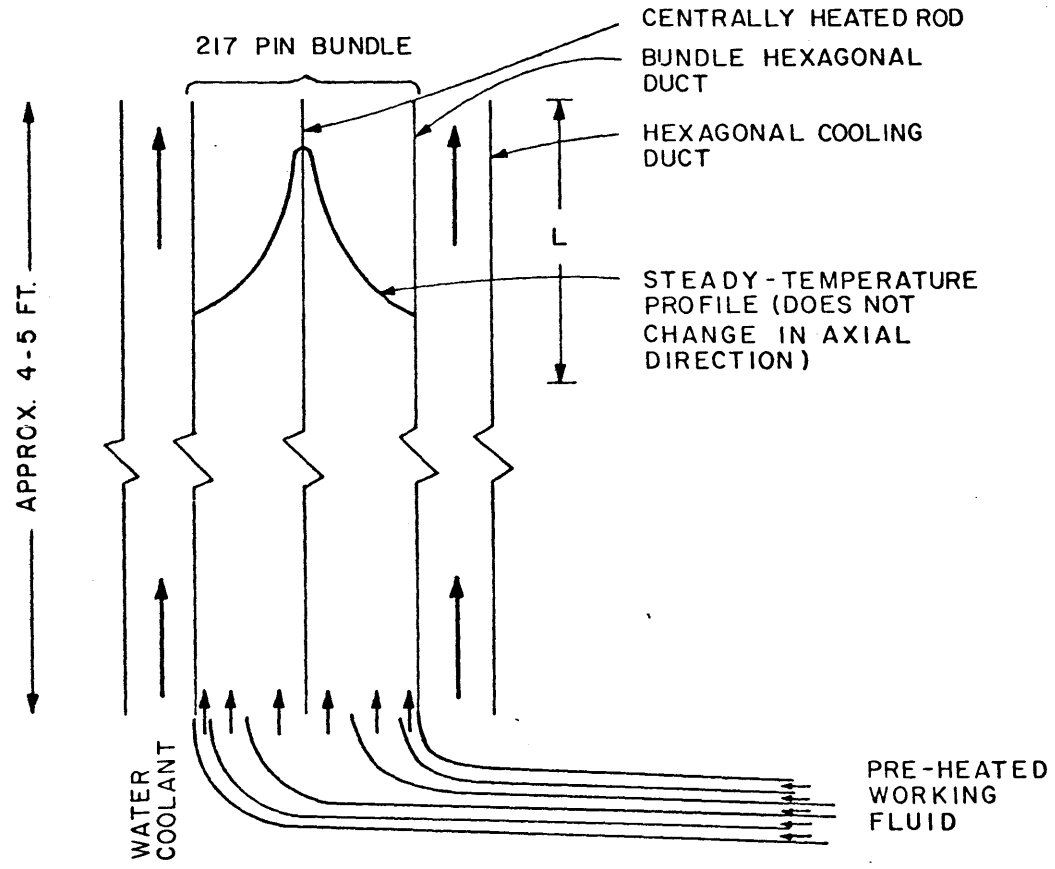
217 PIN BUNDLE
CENTRALLY HEATED ROD
BUNDLE HEXAGONAL DUCT
HEXAGONAL COOLING DUCT
L
STEADY-TEMPERATURE PROFILE (DOES NOT CHANGE IN AXIAL DIRECTION)
APPROX. 4-5 FT.
WATER COOLANT
PRE-HEATED WORKING FLUID

FIG. 5.10

Nomenclature

C	concentration
C_o	initial concentration at injection
C^*	dimensionless concentration C/C_o
C_1	coefficient representing swirl flow ($= \bar{V}_g/\bar{V}$)
C_p	specific heat of coolant
d	pin diameter
d_e	hydraulic diameter of inner channels
F	fraction of diametric tolerance accommodated within the bundle
h	wire-wrap axial pitch
Δp	increase in pitch due to tolerance
p	rod pitch
P_r	Prandtl number
Q	total heat transfer
R_e	Reynolds number
S_c	Schmidt number
T_{cold}	temperature of working fluid
T_{hot}	injection temperature of fluid
T^*	dimensionless temperature, $T^* = \frac{T-T_{cold}}{T_{hot}-T_{cold}}$
T_{max}	maximum coolant temperature within an assembly
$(\Delta T_{max})_{ax.}$	maximum rise in axial coolant temperature
$(\Delta T_{max})_{duct}$	maximum temperature difference between any two points in the duct at any axial level
$\overline{\Delta T}$	average axial temperature rise
$\bar{V}$	average bundle velocity
$\bar{V}_g$	average circumferential velocity in the gap between fuel rod and duct wall

ε_H	enhanced effective eddy diffusivity
ε_H^*	dimensionless enhanced effective eddy diffusivity ($\varepsilon_H^* = \varepsilon_H / (\bar{V}_{de} d_e)$)
ρ_1	density
γ	kinematic viscosity ($\gamma = \mu / \rho$)
μ	dynamic viscosity

APPENDIX

7A. Data Analysis and Calibration of ENERGY

Our primary concern at present is the analysis of data relevant to fuel assemblies. Although the current typical LMFBR fuel assembly has a $p/d \sim 1.25$ and $h/d \sim 50$, the data analyzed covers a large variation about these geometrical parameters. This should be useful in thermal-hydraulic optimization studies.

Table I shows the various types of experiments used to obtain data. This table is ordered in terms of increasing bundle size since the bundle size "effect" is of major concern. Table II lists the same data in terms of the two most important parameters characterizing a wire wrapped fuel rod assembly. The data analysis will be presented by increasing size of the bundle.

1*. ANL-CT-7 pin Bundle (Ref. 6)

Lorenz and Ginsberg performed a 7-pin wire-wrap experiment with salt (NaCl) injection into upward flowing water. The subchannel flows are sampled isokinetically at a fixed measuring point located near the exit of the test section. Salt can be injected at various axial distances from the fixed measuring plane. The salt concentration of the extracted flow is measured using in-line conductivity cells. The authors claim to have obtained reliable bulk concentration data within the first spacer pitch. In addition, axial subchannel flow rate measurements were made for both wall and central channels. As pointed out by Lorenz and Ginsberg the isokinetic sampling

*Numbers according to Table I

technique permits measurement of bulk (subchannel-average) properties, thereby yielding more meaningful results for use in subchannel analysis codes than if discrete point wise measurements were made.

Fig. 1 shows the subchannel flow rates at three different Reynolds numbers. There was no obvious Reynolds number dependence on flow rates. The subchannel flow rates are expected to be periodic (with different periodicity for central and wall channels). As indicated by Lorenz the reason for central subchannel (#2) data falling on a straight line is that measurements of subchannel flow rates were taken every 1/6th spacer pitch at positions where the wire-wraps were in the gaps. At these locations, one would expect little variation in central subchannel flow rates. As also seen in Fig. 1 Lorenz could predict the axial average subchannel flow rates by theoretical flow split predictions assuming bare rods. Fig. 2 shows the variation of concentration with axial distance. Only one set of data for injection into a wall channel has been reported.

ENERGY - Analysis and Calibration

Since data for only one wall channel was reported the two coefficients $\overline{\varepsilon_H^*}$ and C_1 could not be determined from the single set of data. However Novendstern's method for determining flow split in wire-wrapped bundles was used to see if the data reported in Fig. 1 can be predicted. The model of Ref. 7 has been programmed into the computer code DROP. Ref. 7 predicts

that the ratio of velocities in the central, wall and corner channels to the bundle average velocity for the Lorenz 7 pin bundle (without tolerance) is 0.9336, 1.08 and 0.8627 respectively. The ratio of the flow rates for these respective channels to the total flow rate is 0.042, 0.0977 and 0.0267. Noting that the 7-pin bundle of Lorenz combines the wall and corner channels into their peripheral channel, one finds that the ratio of flow rates in the central and peripheral channels to the total flow rate is 0.042 and 0.1244 respectively. This is almost exactly the flow division obtained experimentally. If the coefficients A and B in the expression $f = \frac{A}{Re^B}$ are different than those used by Novendstern[7], a different flow split will be predicted. This is perhaps why Lorenz found the natural flow split assuming bare rods to predict the data well. As will be seen later only the 7 pin bundle flow split can be predicted by the theoretical model. As the bundle size increases the theoretical and experimental flow splits appear to diverge (Fig. 3.1).

The attenuation of the concentration ratio, C/C_o, for the injection channel of the 7-pin bundle is shown in Fig. 2. A comparison of the attenuation rate of C/C_o for the peripheral channel of a 91 pin bundle, of same p/d and h/d ratios is discussed later in this section under subsection 8. Values of $\overline{\varepsilon_H^*}$ and C_1 could not be obtained from the single set of data reported.

2. Battelle - 7 pin Laser Study (Ref. 5)

The Battelle - 7 pin Laser study was performed on a bundle with h/d and p/d of nearly the same order of magnitude as most of the other bundles in our investigation. However the diameter of the pins was 0.866 in. Three different Reynolds numbers were used in the turbulent flow regime. No information on flow split can be derived from this set of data since the spatial velocity distribution across a subchannel was not measured. However one of the measurements made of direct use to us is the ratio of the circumferential velocity in the gap between the rod and the duct wall to the average bundle velocity. This ratio when averaged over the circumference of the bundle is the coefficient C_1 in ENERGY. The value of C_1 reported in Ref. 5 is approximately 0.18.

3. Cadarache 7-pin Hot Water Injection Study (Ref. 8)

The 7-pin hot water injection study was designed to investigate the effect of Reynolds number, helicoidal pitch of the spacer wires,h,and p/d, the ratio of the distance between pin centers to the pin diameter. Table III gives the characteristic dimensions of the bundles studied. Cold water at 68°F was circulated upward in an hexagonal can 80 cm. long containing the wire wrapped rod bundle. Hot

water at about 140°F was injected into one of the sub-channels at a variable level. In Fig. 3 the orientation of the spacer wire at the injection point was always the same. At the outlet of the pin bundle the temperatures were measured by thermocouples at the center of these channels.

The details of the thermocouple design are not given and hence it is difficult to estimate the range of error about the mean measured temperature. The data was not taken at a distance more than one wire wrap pitch down-stream of the injection plane. It is assumed that the rods were hollow, thereby permitting very little or no heat transfer through them. Figs. 3 and 4 show the plot of the dimensionless temperature attenuation $(\frac{T - T_{cold}}{T_{hot} - T_{cold}})$ for the injection channel vs axial distance. It can be seen that this temperature attenuation rate depends upon the location of the wire wrap with respect to the injec-tion point. For example, at the entrance the wire is located at approximately the five o'clock position with respect to channel 1 and about to enter it. However the wire is located at the 6:30 position with respect to channel 4 and is not entering it at the injection plane. The experimenter found by hot water injection into each channel of bundle 2 that the minimum attenuation of temperature (minimum mixing rate) took place for injection into channel 1 and the average attenuation of temperature was for injection into channel 4. Similar temperature maps are available for both the donor and injection channels for

injection into average and minimum subchannels for each bundle.

ENERGY - Analysis and Calibration

The ENERGY analysis of the data was basically limited to the analysis of the injector channel data. The reason for this is given below. ENERGY smears (axially-averaged) the effect of wire-wrap into an enhanced effective eddy diffusivity $\overline{\varepsilon_H^*}$. For the injector channel every wire traverse (3 traverses per lead length) of the subchannel causes mixing between the uniform cold temperature of the adjacent channels and the hot injection temperature and, hence, degradation of the injection channel temperature. Thus the injector channels could be simulated better within the limitations of the ENERGY model than the channels adjacent to the injector channel.

The ENERGY analysis of the data proceeds as follows. For interior injection it was found that the mixing coefficient $\overline{\varepsilon_H^*}$ was nearly independent of C_1. Figs. 3 and 4 show the $\overline{\varepsilon_H^*}$ values and the predicted temperature attenuation rate. As discussed before for bundle 2 the data in Fig. 3 yields the average $(\overline{\varepsilon_H^*})_{min}$ whereas the data in Fig. 4 yields the $(\overline{\varepsilon_H^*})_{avg}$. In this manner the $(\overline{\varepsilon_H^*})_{avg}$ for bundles 1 through 5 were determined for the interior channels. It is seen that $\overline{\varepsilon_H^*}$ is very sensitive to the temperature attenuation rate and small errors in experimental

measurements can lead to large errors in $\overline{\varepsilon_H^*}$. Assuming a $\pm$ 1°F accuracy on coolant exit temperature measurement it was found that for bundle 2 for interior injection $(\overline{\varepsilon_H^*})_{min} = 0.033 \pm 0.01$ and $(\overline{\varepsilon_H^*})_{avg} = 0.083 \pm 0.02$.

The wall channel analysis is complicated by the fact that there are two unknowns $\overline{\varepsilon_H^*}$ and C_1. It was assumed that $\overline{\varepsilon_H^*}$ was uniform in the bundle. Then C_1 was varied until the temperature attenuation data and the predictions matched for wall channel injection. Due to the many assumptions made in the analysis of the wall channels the values of C_1 obtained would not be representative of the true swirl flow in the bundle and large error bars would be associated with the results (approx. $\pm$ 50%). For this reason the values of C_1 so determined must be further verified by more experimental data. Table III shows the $\overline{\varepsilon_H^*}$ and C_1 values for the various bundles analyzed. It was further confirmed by these experiments that $\overline{\varepsilon_H^*}$ is not a function of Reynolds number for highly turbulent flows. An interesting result from the data on bundles 1, 3 and 5 shows that there is a maximum in mixing rates for p/d in the range $1.14 < p/d < 1.355$. However the exact p/d for which this maximum occurs cannot be determined from SKOK's data. No information on internal-swirl flow could be obtained from analysis of this data.

4. ORNL - 19 pin FFM-IIA Bundle (Ref. 9)

The Oak Ridge National Lab. FFM-IIA data was taken in a 19 pin bundle with the geometry similar to the FFTF bundle. Fig. 5 shows a cross-section of the wire-wrapped bundle. Liquid sodium was used to cool the electrically heated pins. The heated length of the rods is 21 in. The coolant enters the bundle approx. 6 in. below the plane where the rods are heated in order to provide a fully developed flow field at the entrance to the heated section. Thermocouples are located in the rod walls and also in the wire wraps. An exit rake is located 3 in. above the exit of heated bundle and is instrumented with thermocouples which directly measure coolant temperatures at the center of various subchannels. The axial power profile is uniform. The hexagonal duct wall is surrounded by guard heaters to minimize heat losses.

Many data sets are reported for various power skews (Fig. 5) and Reynolds numbers from about 1000 to 70000.

ENERGY Analysis and Calibration:

The analysis of the ORNL data was performed first for the case of all heated pins at various power skews. The ENERGY equations were solved with the following additional assumptions:

a) k, ρ, C_p, u were evaluated at the average temperature over the flow cross-section and taken as uniform at each axial position; they varied and were re-evaluated at successive axial positions.

b) A uniform value of $\overline{\varepsilon_H^*}$ was assumed throughout the bundle.

For each of the test runs the best $\overline{\varepsilon_H^*}$ and C_1 was determined by choosing the magnitudes which gave calculated exit fluid temperature distribution that agreed with the measured value. Fig. 6, 7, 8 show the data and the calculated temperature profile. It was found that C_1 only affects the edge row temperatures. Therefore $\overline{\varepsilon_H^*}$ was evaluated directly by using the data within the bundle. Then C_1 is varied until the best agreement with data is obtained in the outer region. The magnitude of $\overline{\varepsilon_H^*}$ is shown in Fig. 9. It was found that both $\overline{\varepsilon_H^*}$ and C_1 are independent of Reynolds number for Re $\geq$ 15000. The optimum values of $\overline{\varepsilon_H^*}$ and C_1 were found to be 0.04 $\pm$ .01 and 0.12 $\pm$ .02 respectively from various sets of data where all pins are heated.

It is interesting to note that the same $\overline{\varepsilon_H^*}$ matches data for various power skews. This result was anticipated and confirms our physical interpretation of $\overline{\varepsilon_H^*}$ as a parameter dictated by bundle geometry.

The major problem encountered was in analyzing the single heated pin data. As discussed in Ref. 1 (see Fig. 10) computer programs like THI-3D and COTEC have also not been able to predict this data satisfactorily. The single pin tests, however, raise several interesting questions, which cannot be fully resolved without additional experimental data. The large asymmetry in radial temperature profile

for a centrally heated pin can be attributed to either an internal swirl flow (i.e. due to only 2 rows of pins the wall circumferential flow is able to penetrate almost to the center of the bundle) or due to bowing of the heated pin. The single pin tests were conducted at 8-10 kw/ft. Distortion of the FFM bundle under power and flow has been observed via X-ray photography and image enhancement technique. The distortion appeared to be power dependent[9]. These radiograph tests were made above 8 kw/ft, at which power level the spacing between the wall and the rod appeared to vary in the axial direction. On one side of the bundle the rod to wall gap increased and on the opposite side it decreased. This change of wall to rod gap in the circumferential direction should not affect C_1 since the latter is a space average quantity. However, if inidvidual heater pins distorted in the axial direction at these power levels,then asymmetry in radial temperature distribution for a centrally heated pin should be expected.

Only for large internal swirl flow can such severe asymmetries in temperature exist. If large internal swirl exists then the inherent assumptions in ENERGY should prevent it from matching the radial temperature profiles for the 20% and 300% power skew cases. For this reason it is believed that if internal swirl exists at all it is small in magnitude and it does not affect temperature distribution at the exit of the bundle. It is our interpretation that the severe radial temperature asymmetry for the

centrally heated pin run is primarily due to rod bowing. Other single heated pin runs were also analyzed. The runs with single heated pins at the wall were also used to determine C_1. The predictions for these runs matched with data much better than for the centrally heated pin case.

The accuracy of the coolant thermocouple was assumed to be $\pm$ 1.5°F. The thermocouples located in the rod walls and in the wire wrap gave a local temperature which was difficult to use to compare with ENERGY predictions of subchannel averaged temperatures.

One subchannel temperature (marked XX in Fig. 5) was overpredicted by all U.S. codes including THI-3D for the uniform power case. No reasons for this are obvious and it needs to be resolved.

5. M.I.T. 61 pin Laser Study (Ref. 4)

The M.I.T. 61 pin bundle is being instrumented for salt-injection tests. In the meantime a Laser Doppler Velocimeter (LDV) is being used to measure the axial and swirl flow in the wall channels. Two different wire-wrap leads of 6 in. and 12 in. have been tested. LDV is probably the most accurate means of determining point velocity measurements within subchannels at present.

Fig. 11a shows the portion of the 61 pin bundle tested along with the points at which the axial and transverse velocities were measured over two wire wrap pitches.

In addition, detailed point velocity measurements were made within the subchannel which has the points C and B on its boundaries. The tests were performed both in the laminar and turbulent flow regimes.

Fig. 11b shows the fully developed axial velocity profile over the wire wrap pitch 6-8 in. from the inlet. The abscissa shows the location of the wire wrap (see numbered rod in Fig. 11a) with respect to the channel. The ratio of the average velocity in the wall channel to bundle average velocity was found to be 1.04 and 1.19 in the turbulent and laminar flow regimes respectively for h/d = 48. The corresponding values for the 6 in. lead run (h/d = 24) were 1.02 and 1.24 respectively. The theoretical flow split yields a value of 1.10 for $\bar{V}_{wall}/\bar{V}_{bundle}$ for turbulent flow and 1.22 for laminar flow when no tolerances are taken into account. Whereas the theoretical flow split without tolerances appears to agree in the laminar flow case it yields a value approximately 6% higher than the experimentally measured value. When tolerances are taken into account a range is obtained for the flow split (see Section 3.1).

Another interesting result is that C_1 lies between 0.12 and 0.14 for h/d = 48 and $C_1 \simeq 0.21$ for h/d = 24. The value of C_1 for h/d = 48 is close to $C_1 = 0.12$ (h/d = 52) determined from the ORNL data. It is necessary to point out that the swirl velocity was measured only at the midpoint between the rod and gap and $C_1 = 0.13$ includes a correction for the assumed velocity profile which is applied to the

measured point velocity in order to determine an average velocity in the gap. An error analysis[4] shows that the approximate total error in measuring swirl velocity is between 11 and 15%. The swirl velocity at the points C, B and A (in rod to wall gaps) were found to be very nearly equal for all wire-wrap locations. If the average subchannel swirl flow increased in going from C to A one would expect for all wire wrap orientations a higher swirl velocity at A than at C. This was not the case. This clearly shows that, contrary to the data in Ref. 12, the swirl flow is not a function of the subchannel position on the flat of the hexagonal duct wall. Although the magnitude of the swirl flow changes with different wire wrap positions no significant gradients in swirl flow along the duct wall were found at fixed axial positions.

The entrance length required to attain fully developed flow was found to lie between 6 and 8 in. This result agrees with a similar result obtained in Ref. 19.

6. Japanese 91 pin Salt Injection Tests (Ref. 13)

The Japanese 91 pin alkaline (Fig. 12) salt injection tests were performed using a 0.248 in. diameter fuel pin and a p/d ratio of 1.20. Pitot tubes at the exit of the bundle measure the local velocity distribution in the subchannels. In addition dynamic and static deformation of the fuel rods produced by flow was measured by a strain gauge fixed on the surface of the fuel rod for the purpose of

knowing vibration and deformation of the rods. Pressure drop was obtained by measuring distribution of static pressure by a pressure gauge and obtaining pressure distribution at each water temperature and flow rate. For the mixing tests, sodium chloride solution was injected into water flowing through the fuel assemblies and concentration distribution of sodium chloride was measured at the exit end of the fuel assemblies. The detector probes are fixed to a probe fixing plate (Fig. 12) and placed at the center of several subchannels as shown in Fig. 13. The subchannel velocity was measured with a standard deviation of 8.1% and the standard deviation of flow measurement is 24.3%. The latter is higher because of axial bowing of rods which were determined from the vibration and deformation tests.

The mixing tests for the fuel assembly were performed with salt injection in central and noncentered interior subchannels. However only one single data point is available for central injection in the turbulent flow regime and no data points are available for turbulent flow for the eccentric salt injection.

Only the peak velocity profiles in each subchannel across the bundle have been reported. The peak velocity profile shows a W shaped distribution. The peak velocities near the wall are higher than their immediate neighbors and an increase in the peak velocity in the central regions is observed.

Relations obtained between the coefficient of friction f and Reynolds number Re from the pressure drop data show that they are in good agreement with the Blasius's equation for cylindrical tubes provided the representative lengths and flow velocity were calculated including the wire spacers.

ENERGY - Analysis and Calibration:

One cannot infer the average velocity distribution from the reported peak subchannel velocity distributions. Consequently it is extremely difficult to determine a flow split from the reported peak velocity distribution. However a W shaped velocity distribution across a 91 pin bundle has also been reported earlier by Bump et al.[14]. If the average velocity distribution is in fact W shaped then non-uniform mixing coefficients might also be expected across the bundle. The degree of non-uniformity in transverse velocity distribution and its effect on mixing coefficient distribution is not yet resolved. Obviously if the non-uniformity in velocity distribution across the bundle is large, measurements of velocities in typical wall, corner and central channels is of no major gain. Unless the various codes take into account the "correct" velocity distribution the mixing coefficients obtained by calibrating the code with temperature data based on assumed velocity distribution would be erroneous. An outline of an experiment which would yield a variation of mixing coefficient across the bundle, if one exists, is given in Section 5.

The ENERGY code was used to obtain $\overline{\varepsilon_H^*}$ for the single set of data available for the fuel assembly in the turbulent flow regime. Fig. 14 shows the experimental data along with the best ENERGY fit. The $\overline{\varepsilon_H^*}$ so obtained was equal to 0.025 $\pm$ 0.01 at a Reynolds number of about 7600. It is interesting to note that Fig. 14 shows a slight asymmetry in salt concentrations about the injection point. For example, probes 3 and 3' are located at the same radial distance from the injection point, yet probe 3' records a lower concentration than the probe 3. This asymmetry could be due to inlet perturbation effects or internal swirl or due to vibration and/or axial non-uniform deformation of fuel pins observed in the tests. ENERGY predicts a radially symmetrical distribution about the injection point since there is no provision for taking into account internal swirl flow. In any case, the internal swirl flow appears to be very small. This has also been discussed earlier regarding the analysis of the ORNL data.

7. Karlsruhe Heated Pin Experiments (Ref. 15, 16, 17)

The Karlsruhe 61 pin experiments employ one or several electrically heated rods and sodium as coolant to determine mixing rates for several ratios of wire pitch to rod diameter. The rod diameter used in their study is 0.2362 in. which is very close to the FFTF geometry. However the p/d ratio is 1.315 and h/d ratios tested are 16.67, 33.34 and 50.

The test section consisting of the 61 rod bundle is inserted in a box which is conically supported in the sodium vessel of the test loop. The sodium enters a mixing chamber and flows downwards through the bundle, first through a 500 mm. long hydraulic entrance region and then through the 1000 mm. long section with the heated rod. At the outlet of the bundle, 50 NiCr-Ni thermocouples of 0.5 mm. diameter (Fig. 15) are installed in the different subchannels to register the radial temperature profiles in the bundle cross-section.

The experiments were made within the range $10^4 \leq Re \leq 10^5$. The sodium temperature at the test section inlet was in the range 300 - 500°C. The tolerance on pin-to-pin spacing was less than 0.1 mm. Great care was taken to ensure any azimuthal variation of the heat flux due to fabrication tolerances in the heaters. In addition great care was taken in installing and in knowing the precise location of thermocouples within each subchannel. The thermocouple accuracy was not reported. We have assumed it to be $\pm$ 1°F.

Data was taken, with the central rod heated, at two different Reynolds numbers for the three different h/d ratios. In addition Ref. 17 reports an experiment with two heated rods, one at the center and one at the wall for h/d ratio of 16.67.

ENERGY - Analysis and Calibration:

Figs. 16 and 17 show two series of measured sodium temperature profiles. Plotted are the differences between local subchannel and sodium inlet temperatures as a function of the radial subchannel position for bundles with wire wrapped rods of different leads. In both runs the heating power of the center rod was nearly constant but the mass flow rate varied. It is seen that the sodium temperature profiles decrease very rapidly away from the central rod in the radial direction.

As the h/d ratio decreases mixing increases and the radial temperature gradient proportionality decreases. The measured temperature profiles were used to determine $\overline{\varepsilon_H^*}$ using the ENERGY code. The $\overline{\varepsilon_H^*}$ values were first determined from Fig. 16. The same values of $\overline{\varepsilon_H^*}$ could predict the data well in Fig. 17 even though the Reynolds number was doubled to approx. 33000. The values of $\overline{\varepsilon_H^*}$ determined from this experiment are:

h/d = 16.67	$\overline{\varepsilon_H^*} = 0.028$
h/d = 33.34	$\overline{\varepsilon_H^*} = 0.044$
h/d = 50	$\overline{\varepsilon_H^*} = 0.088$

The Karlsruhe experimenters do not report any asymmetry in radial temperature profiles. One may then assume that the effects of wire start position at entrance or internal swirls do not affect the exit temperature distribution. The swirl flow near the duct wall cannot be determined from the single heated pin experiment.

Ref. 16 and 17 report experiments with two heated rods. The temperature distribution from Ref. 16 is shown in Fig. 18. Although an ENERGY analysis was not made because it is not specifically known which reported data points correspond to which subchannel, yet several interesting points are brought out by the experiments. The influence of swirl flow near the wall penetrates almost to the central regions of the bundle. This is seen from the difference in temperatures measured, at the same radial distance from center, along M - C and M - F in Fig. 18. It is possible that part of the difference could be due to an internal swirl and one should not wholly attribute it to the penetrating effect of the wall swirl. However one cannot know which of these is predominant from a 61 pin experiment, where there are only 4 rows of rods from the wall to the center. Since the MISTPAL-II code[16] is reportedly able to predict the temperature distribution along MF and MC well although it does not have an internal swirl model in it, one is led to believe that the penetrating effect of wall swirl is dominating over any internal swirl that may exist.

Another interesting point is that MISTRAL-II uses uniform mixing coefficients in the bundle to match the data. This shows that the degree of interaction (in terms of mixing) between the inner and wall regions is not significantly smaller than the interaction between the subchannels within the inner core of the bundle. Although very near the wall (along MX) the temperature gradients are very small

(as found in Ref. 12), the steepness of temperature gradients existing in the radial direction near the wall is of the magnitude of the temperature gradients existing near the center of the bundle. This shows that the mixing coefficients are of the same order of magnitude in the radial direction except very close to the wall.

8. ANL-RAS- Hot Water Injection Tests (Ref. 12)

The ANL-RAS mixing tests were conducted with water in a 91-element bundle. The major emphasis is placed on investigation of flow characteristics in the peripheral channels. Hot water tracer was injected into selected wall channels and the axial and radial movement of tracer was detected with thermocouples mounted on the rod walls. Great care has been taken in developing and designing fast response thermocouples and the injection system. The injector design, its position and the injection flow rate have been optimized in order to get a consistent set of reliable results. It was found that the subchannel centered injector provides the best representation of the condition analyzed with codes using the rectangular edge subchannel geometry. Moreover with the centered injector there is greater probability of uniform mixing across the injection subchannel. Injection velocities slightly greater than nominal velocity through the bundle were found to give best mixing within the injection subchannel. Only one wire-wrap staring orientation was used in this experiment for obtaining data.

Fig. 19 shows the circumferential and axial progression of the dye and thermal tracer. It was found that the maximum concentration of the tracer lags behind the tracer front with the wire wrap angle almost midway between the two. Comparison of the thermal tracer results with the previous dye-tracer (Ref. 18) results show excellent agreement. Both the locus of the maximum concentration and dye front show an in-phase periodic behavior. As the wire wrap moves from the adjacent interior subchannel into the edge subchannel the swirl flow is seen to increase.

The thermal-tracer studies of Ref. 12 also indicate that the swirl flow varies not only with wire wrap position as was found in Ref. 8, but also with the position of the subchannel across the face of the bundle. The subchannels near the downstream corner of a face (in the direction of swirl flow) have the higher swirl flow. The authors of Ref. 12 believe that the corners are particularly important in the swirl flow mechanism. As the size of the bundle increases, they feel, "corner interaction" is less causing swirl flow to decrease. These experiments also show that the interaction between the edge subchannels and interior subchannels is low.

The ENERGY ANALYSIS and Calibration studies are given for subsections VIII and IX simultaneously at the end of subsection IX.

9. ANL-CT- Salt Injection Tests (19)

The ANL-CT-91 pin tests were performed on a 2:1 bundle size. The rod dia. p/d and h/d ratios are 0.5 in., 1.24 and 48. The working fluid is water. The Reynolds number was varied from 9000 to 24000.

The main feature of this experiment is the isokinetic sampling technique. An electrolyte tracer is injected into the flowing water stream and isokinetically withdrawn at the exit of the bundle (see Refs. 6, 19 for details on isokinetic sampling technique) which permits one to measure both mixed mean subchannel concentrations and flow rates. Thus any errors in trying to determine subchannel average quantities from point measurements are avoided. Confidence in the accuracy of this technique in obtaining reliable concentration gradients in the first wire-wrap pitch of an assembly was first obtained on a 7-pin bundle.[6]

Considerable effort has been devoted to optimize the injector design and flow rates so as to get accurate measurements of concentrations downstream of the injection point. In addition care is taken to ensure that the initial wire orientation remain fixed with respect to the injection position.

The flow split ($V_{channel}/\overline{V}$) obtained from these experiments by isokinetically sampling the flow show different results than the predictions based on hydraulic diameter concept. The subchannel to the bundle average velocity ratio for the central, edge and corner subchannels was found to be 1.01, 0.99 and 0.94

respectively. Time-of-flight measurements on the RAS-91-pin bundle[12] using a thermal pulse and the AI 217 pin bundle[20] using a salt tracer pulse yielded edge channel velocity split to be 1.03 and 1.00 approximately.

There was no Reynolds number effect on the concentration data or on the flow split data. In order to assess how long it takes for the flow to fully develop two extreme entrance conditions were employed; on a 70% circular plan blockage of the central region of the bundle and the other a 50% annular planar blockage of the peripheral regions. The isokinetic velocity measurements show identical results at 2 1/2 spacer pitches from the entrance. Obviously any initial flow maldistributions have died away. Similar results were obtained for blockages near the exit.

Fig. 20 shows the trace of the maximum concentration and the dye front for wire wrap orientation A. Fig. 21 shows the same for wire wrap orientation B at the injection point. It is seen that the average slopes of both sets of data and similar data from thermal-tracer experiments (Fig. 19) are very close to each other. In addition for the same wire-wrap orientation the trace of the maximum concentration and the dye front are also in phase for the two different experiments (Ref. 12 and 19). These similarities in data exist in spite of the diameter and wire wrap pitch in Ref. 19 being twice that of Ref. 12 showing h/d is a correlating parameter.

ENERGY - Analysis and Calibration

A pulse-flow model was incorporated in ENERGY to take into account an enhanced translation in movement of the wave-front. As shown in Fig. 22 due to smearing effect in lumped parameter codes, the calculated wave front is always located ahead of the actual wavefront; the difference between the two depends upon the mesh size. Although the trace of the maximum concentration is not affected by smearing to any appreciable extent the predicted tracer front is affected. Fig. 23 shows that the pulse flow model results match the tracer maximum concentration as well as the dye front for C_1=0.14. The tracer front was represented by lines of constant concentration between 0.005 and 0.05. It is necessary to note that the predicted wavefront follows the experimental wavefront closely from inlet to exit.

Fig. 24 shows comparison between the data and the ENERGY model without the pulse flow model in the wall region. It was again found that C_1=0.14 is able to predict the trace of maximum concentration well. However, as discussed earlier, the tracer front initially travels ahead of the experimental tracer front due to the "smearing-effect." It is necessary to point out that we believe that the bulk of the tracer injected must travel in the direction of the velocity vector. Thus the trace of the maximum concentration represents the velocity vector and the tracer front is ahead of all the

maximum concentration line due to turbulent diffusion effects.

10. GE-127 pin Hot Water Injection Tests (Ref. 22)

The 127 pin bundle was 72 in. long and contained a hexagonal flow duct. The diameter of the pins is 0.25 in., p/d and h/d are 1.28 and 24 respectively. The Reynolds number of the test was about 55000. Hot water is injected and mixing rates were inferred from temperature measurements downstream. Fig. 25 shows the main test loop. The loop temperature was maintained at 100^{o}F. Approximately 2% of the main flow was diverted from the loop, just upstream from the main pump, heated in a 900,000 Btu/h boiler to 161.4^{o}F, increased in pressure up to 125 psi with a small 2 hp jet pump and re-injected into the center of the bundle. Fig. 26 shows the cross-section of dummy fuel bundle and Fig. 27 shows the mechanical details of hot water injection. Lateral dispersion of hot water was inhibited for a length of one inch above the injection tube by a "dam" in the form of a filler rod welded to each of six rods surrounding the central injection tube. The flow rate in the injection flow channel is approximately made equal to the flow rates in the 6 central channels. Care was exercised in the adjustment of injection and main flow rates during experimentation so as to minimize any localized lateral dispersion due to mismatch in flow velocities.

Lattice temperature measurements downstream from the hot water injection point were measured at every 1 in. axial

distance from 6 in. to 65 in. Fig. 28 shows the lattice temperature probe assembly. This probe assembly was designed to fit within the tube which simulated fuel rods and could measure the temperature of the moving fluid in any one of the six channels surrounding the instrumented rod without perturbing the flow. The probe assembly could be moved along the 72 in. length of the dummy fuel rod and could be rotated within any particular tube so as to orient the thermocouples preferentially in any direction. In order to confirm the directional temperature sensitivity of the probe assembly two dimensional heat transfer calculations were done on the probe assembly, dummy fuel rod and water environment for several assumbed circumferential temperature distributions. One severe distribution is shown in Fig. 29. In this case the thermocouple response was calculated to be 95^{o}F showing considerable directional sensitivity.

It is obvious from Fig. 26 that estimation of swirl flow in the wall regions cannot be made from this setup. Therefore the effort was concentrated on determining $\overline{\varepsilon_H^*}$ for the particular geometry and flow conditions.

In order to determine $\overline{\varepsilon_H^*}$ for salt and hot water injection experiments, the following procedure was adopted. The temperature rise for various channels is determined from the ENERGY code by varying the input parameter $\overline{\varepsilon_H^*}$. Fig. 30 shows a plot of temperature rise vs. $\overline{\varepsilon_H^*}$ for several channels, at the 12 in. axial level and at the 36 in. level. On the same figure the

recorded data is plotted showing a $\pm$ 1°F spread due to assumed thermocouple accuracy. It is interesting to note that the slope of the curve in Fig. 30 for the injection channel at 12 in. is large but for other channels the slope is not large at 12 in. At 36 in. the slope of all the curves are small. The only meaningful estimate of the range of $\overline{\varepsilon_H^*}$ can be obtained from the injection channel data at 12 in. For other channels, when a $\pm$ 1°F spread on data is superimposed on the plotted computer curves, it is seen that almost any value of $\overline{\varepsilon_H^*}$ should predict a temperature rise within the data range. Thus usefulness of the data 6 to 14 in. beyond injection is limited. The value of $\overline{\varepsilon_H^*}$ so determined as found to lie between 0.050 and 0.060. The procedure described above is only the first step in data analysis. The next step, a refinement on Step I, is described below.

Since at the injection point there is a perturbation of the main flow stream due to injection of salt or hot water, it is quite conceivable that these perturbation effects may last several inches downstream of injection point. The data is then analyzed by taking the inlet plane in the computer program to be several inches downstream of the injection point in the experiment. For this data inlet was assumed to be 12 in. downstream of injection point and data at this 12 in. location was assumed as the initial channel condition. Fig. 31 shows the data for the injection channel and also the predictions of ENERGY for 5 different cases. Set I shows the predictions

for the case where the inlet to ENERGY is at the same plane as the injection point. For other curves the 12 in. level in the experiment is the starting point for the calculations. It is seen that curves I and II do not match although $\overline{\varepsilon_H^*}$ = 0.062 for both . This was found to be due to a lack of energy balance in the data between inlet and 12 in. level. The total energy at the 12 in. level, as calculated by taking the sum of the product of flow and enthalpy over all channels, was found to be greater than the total energy in the injection plane. The data at 12 in. is probably more reliable (as discussed below) and free of any inlet perturbation effects. The inlet energy balance was corrected to match that at the 12 in. level. On superimposing a $\pm$ 1°F error band on the data $\overline{\varepsilon_H^*}$ was found to be in the range 0.040 to 0.070 or an approximate average of 0.055 $\pm$ 0.015.

The data after the 12 in. axial level is probably more reliable because of the following reason. It was found that the radial temperature distribution across the bundle had a peak which rotated circumferentially as the fluid travelled up the bundle. Perhaps an internal swirl had generated due to slightly asymmetric injection into the six inner channels. This internal swirl appears to die off at about 12 - 18 in. when the radially peak temperature stops rotating. Thus as one proceeds axially downstream the reliability of the data increases but its sensitivity to $\overline{\varepsilon_H^*}$ decreased (Fig. 30). Therefore the 12 in. level data was chosen as a reliable

set of data to start calculations and yet maintain reasonable sensitivity to $\overline{\epsilon_H^*}$ variations.

11. HEDL-217 PIN SALT INJECTION TESTS

The HEDL 217 pin tests are the only set of experiments on a full size FFTF fuel assembly geometry. Considerable effort, therefore, has been devoted to developing an understanding of the experimental set up instrumentation, test procedure and results.

Three types of pins were used for the assembly (1) Dummy pins, (2) Instrumented pins, and (3) injection pins. The HEDL description of their sensors is as follows: "Fifty-eight instrumented pins were fabricated from laminated phenolic tubing, NEMA grade XXX. Three basic electrode arrangements were necessary to provide the required measurement patterns. The fabrication of the pins was similar for each of the arrangements. First, the 1/4 inch OD x 3/15 in. ID phenolic tubing wall was drilled with the required electrode pattern, then a length of 17 guage B & S Forms air insulated copper wire (0.045 in. dia.) was pulled through the tube and out each hole. Each pin had eight electrodes. The tube bore was filled with epoxy resin to provide an insulating seal. Each pin was then centerless ground to an outside diameter of 0.23 in. and the exposed copper electrodes nickel plated. The pins were trimmed to length and a lower end cap which engages the lower grid, was attached with epoxy glue. The

end cap slot was oriented as required to assure the proper electrode location and wire wrap phase."

A salt solution can be injected into the subchannels from three injection pins marked 1, 2, 3 in Fig. 32. An equal amount of fluid is withdrawn in order to minimize any disturbance of the main fluid stream. In order to insure that the injected salt solution completely mixed within the subchannel with the mainstream fluid three fins were provided which isolate the subchannel up to 2 3/4 in. from the salt injection point. The addition of surface area due to the fins was compensated by a reduction in wire-wrap surface area so that there is no axial reduction in flow in the injected subchannel. Fig. 32 shows the three injection rods, wall injection location and instrumented rod locations. A few subchannels were surrounded by two instrumented pins.

As indicated by Ref. 23, not much effort was devoted to an orderly instrumentation development including injector design and its effect on results. However, Ref. 12 states based on their experience that the injection effect on results is expected to be small.

The mass balance obtained show a 13% error for interior injections and up to 37% error for wall injections.

The sensitivity of the electrodes to electrolyte concentration was localized to the volume of the fluid immediately adjacent to the exposed electrode surface. Thus point measurements were obtained in these tests as opposed to subchannel

average measurements obtained by isokinetic sampling techniques. Thus if high concentration gradients exist within a channel the reading would have been weighted toward the concentration closest to the probe. This effect is termed striping. The authors of the HEDL report feel that near the injection point and a few inches downstream high intrachannel concentration gradients existed and probe readings were not the bulk concentration of the subchannels. However, downstream where concentrations in adjacent channels were similar, the striping effect would be negligible.

Typical results for central injection are shown in Fig. 33 (a,b,c,d). The injection concentration was 2165 ppm (the mass balance shows 1991 ppm at 6 in. axial level, Fig. 33a). At 12 in. the concentration in the injection channel has dropped down to 194 ppm, the mass balance shows 2206 ppm. At the 36 in. level the concentration in the injection channel is down to 63 ppm but the mass balance is further up to 2370 ppm. In addition to the mass balance being slightly off there was an apparent drift (which could be due to a net mass transport in the direction of the wire twist or due to inlet perturbation effect) in the direction of the wire rotation.

Typical results for wall injection are shown in Fig. 34 a,b,c,d. It is seen that there is considerable interaction between the wall and the first row of interior subchannels. In addition one finds that in going from zero to an axial level of 36 in. the maxima in concentration moves only (4-5) subchannels

along the circumference of the duct while the tracer front advances only 2 subchannels ahead of the first corner channel in its path. The mass balances for wall injection were poor as the probes were damaged either from vibration or from swelling of the epoxy due to exposure to water. (Ref. 12)

In none of the tests performed did the authors (of Ref. 23) find any dependence of their results on Reynolds number in the range $10000 \leq Re \leq 30000$.

ENERGY - Analysis and Calibration:

The two major issues, apart from ENERGY calibration, that have to be resolved by an ENERGY analysis were as follows. First, whether the swirl flow, measured by C_1 in ENERGY is lower than found for the ORNL and ANL bundles of similar geometry. If it is lower then is it due to improper response of instrumentation or is it a bundle size effect. Second, is the drift observed for internal injection caused by internal swirl or is it caused by an inlet perturbation effect?

Table IV gives the HEDL runs analyzed. Runs 4, 11, 14 and 19 were analyzed for interior injection and Run 2 for wall injections. The method of analysis of this data was similar to that described earlier in subsection X for the GE-127 pin data analysis. Initially the injection plane of the tracer was used as the starting level for code calculations. It was found that the exit concentrations at the 36 in. level could not be matched for any value of $\overline{\varepsilon_H^*}$ and C_1. Next the 12 in. level HEDL data was used as the starting plane for code calculations.

Every set of data analyzed could be predicted well at the 36 in. level if calculations were started at the 12 in. level of the HEDL data. A typical ENERGY comparison with data is shown in Fig. 35. The $\overline{\epsilon_H^*}$ found (Table 4) lies in the range 0.015 to 0.030. The range for $\overline{\epsilon_H^*}$ so found is not large considering the uncertainties in mass balance. However, one important conclusion can be readily drawn. Since ENERGY using the 12 in. plane as initial condition can predict the data one can conclude that there is no internal swirl in the bundle. If internal swirl exists its effect on exit salt concentration is negligibly small. The so-called "drift" of two channels to the left of injection channel is an injection perturbation effect. When the starting level for the calculations was taken at the 6 in. level of the data the exit (36 in) concentrations could not be predicted as well. This shows that the inlet perturbation effects probably persisted up to 9 in. from the injection plane. The $\overline{\epsilon_H^*}$ found from HEDL tests is considerably lower (30-40%) than that found from the ORNL heated pin test. In order to explain this difference the data was examined closely. As seen in Fig. 33 some of the channels had two probes in them. The probes pointing in a direction opposite to wire map rotation (wire wrap rotation and swirl flow are clockwise for HEDL tests) always measured higher concentrations than the other probe in the channel. Often the difference in the concentration measured by the two probes was large. If other channels had

been equipped with more than one probe it would have been easier to estimate the average concentration in the channel. Obviously point measurements are difficult to use in calibrating lumped parameter codes. Another reason for obtaining low $\overline{\varepsilon_H^*}$ in these tests is the possibility of change in accuracy of data with salt concentration.[24] If the salt concentration is increased to a high value, the electrical resistance that is measured by conductivity cells is low and accuracy is small.[24] If the salt concentration is very low the accuracy with which concentrations can be measured is high and the concentration gradients might be low within a subchannel. However, very small errors in trying to relate point measurements to bulk subchannel values could give a wide spread in the $\overline{\varepsilon_H^*}$ values. An intermediate concentration range is desirable. However the wall probes in the HEDL data are subject to (laminar) boundary layer effects which can increase electrical resistance many times leading to a loss in accuracy.[24]

Figs. 36a and b show the rate at which the maximum in subchannel concentration travels along the duct wall. The slope of the trace of the maxima is considerably smaller than found from the ANL data (Figs. 19, 20). Since the maxima in concentration represents the swirl velocity more closely than does the tracer front it is obvious that the swirl velocity is smaller for this 217 pin bundle than for the 91 pin bundle. Fig. 37 shows that for the HEDL bundle $C_1 \approx 0.07$, which could also be determined from Figs. 36a and 36b.

Contrary to the observations in the ANL (Ref. 12) considerable interaction with the interior channel took place.

The reasons for obtaining a lower C_1 for these tests have been discussed in the main text. Either the point probes located in the rod walls do not accurately measure salt concentration in the wall channels or there is an actual bundle size effect.

7.2 Definition of Mixing Mechanisms

Energy redistribution in a wire-wrapped fuel assembly takes place by the following mechanisms:

(a) Thermal Conduction - characterized by the thermal diffusivity, α.

(b) Turbulent Exchange on a Molecular Level (including flow scattering) without a net transfer of fluid. The dimensionless group characterizing turbulent exchange is, $W_{Tij}/\bar{W}$, where W_{Tij} is the turbulent exchange rate and $\bar{W}$ is the average bundle flow rate.

(c) Cross-Flow - any convection of fluid due to a radial pressure gradient can be classified as cross-flow. Cross-flow can be subdivided into two categories: (1) Diversion Cross-Flow: That fraction of the total cross-flow between any two sub-channels that occurs due to a pressure gradient set up by virtue of the dissimilarities in local hydraulic characteristics (either geometrically, hydrodynamically or thermally induced). For example, (figure 1) as the wire lead to a diameter increases to very large values ($\frac{h}{d} \rightarrow \infty$) the hydraulic diameter of channels i and j would be locally different at various axial levels causing flow to redistribute itself by diversion cross-flow. Thus the varying axial and transverse flow resistance in the

presence or absence of wire wrap can cause diversion cross-flow.

Diversion cross-flow may be characterized by the term, $W_{Dij}/\overline{W}$

(2) Flow-Sweep: For wire-wrapped rod bundles of p/d > 1.18 the axial flow has no direct vertical path through the bundle (1) but at regular intervals crosses the wire and is swept from one channel to another due to the favorable pressure gradient set up by the wire. This sweeping effect of the wire would extend a small distance below and above the location where the wire crosses the gap. Thus the axial momentum of flow in a subchannel is periodically changed by the presence of the wire. The fraction of axial momentum carried by the sweep flow in the transverse direction can be considerably greater than that carried by diversion cross-flow, depending upon the wire lead to diameter ratio. For rod bundles with p/d < 1.18 a part of the fluid can flow vertically upwards in a bundle and part of it will be periodically swept into other channels. The flow field for such a bundle would be even more complex than for a bundle with p/d > 1.18.

Flow sweep may be characterized by the term, $W_{Sij}/\overline{W}$ (or W_{Sij}/W_i).

Swirl Flow: The sweep flow in the wall channels has characteristics which are different from that in the central channels. Whereas the sweep flow between two subchannels in the central parts of the bundle changes direction periodically, the sweep flow between two wall channels is always in the same

direction. This sweep flow along the housing wall is known as the swirl flow. The swirl flow, perhaps, fluctuates about a mean value. It is characterized by the term, $V_\theta/\overline{V}$, where V_θ is the velocity in the gap between the rod and the wall and $\overline{V}$ average axial bundle velocity.

Most experimental effort has been to quantitatively determine these four mechanisms individually if possible and their dependence upon geometrical and flow parameters. The major emphasis has been in determining flow sweeping, perhaps because it is the least understood and the most important means of momentum and energy transfer. Once these mechanisms are known, they are direct input into the subchannel analysis computer programs as they are now formulated.

Appendix

Titles for Illustrations

Figure No.	
1	Experimentally Determined Subchannel Flow Rates (Ref. 6)
2	Experimentally Determined Concentration Profiles (Ref. 6)
3	Min. Temp. Attenuation For Interior Injection
4	Avg. Temp. Attenuation For Interior Injection
5	Oak Ridge Test Bundle and Test Parameters
6	Parametric Study to Det. $\overline{\varepsilon^*_H}$ and C_1
7	Exit Temperature Distribution
8	Comparison of Exit Temperatures For 300% Skew (B)
9	Variation of $\overline{\varepsilon^*_H}$ vs. Reynolds No.
10	Comparison of Exit Temperatures For Single Rod Heated Case
11a	Locations of Measuring Points
11b	Variation of C_1 Along Duct Wall
11c	Variation of Axial Velocity For One Wire Wrap Pitch Axial Length
12	Measuring Equipment of the Mixing Effect (Ref. 13)
13	Arrangement of the Injection and the Detection Sub-channels (Core Fuel, Center Injection) (Ref. 13)
14	Predicted and Experimental Distribution of Concentration For Fuel Assembly
15	Testsection With 61 -Rod-Bundle (Ref. 16)
16	Temperature Rise for Radial Subchannels
17	Temperature Rise for Radial Subchannels
18	Temperature Distribution at Outlet of 61 Pin Assembly (Ref. 15)
19	Comparison of the Circumferential and Axial Progression of Present Thermal-tracer Studies With Previous Dye-tracer Studies. (Ref. 12)

Figure No.

TABLE I

REF. \ NO. OF PINS	7	19	37	61	91	127	217
ANL - RAS ANL - CT ANL - CT	①(b)				⑧(a) ⑨(b)		
ORNL		④(c)					
MIT				⑤(d)			
BATALLE	②(d)						
JAPANESE				⑥(b)			
HEDL							⑪(b)
G E						⑩(a)	
KARLSRUHE				⑦(c)			
CADARACHE	③(a)						

LEGEND ① 1,2,---11 NUMBER ASSIGNED TO EACH EXPERIMENT FOR USE IN TABLE 3.2
② TYPE OF EXPERIMENT (a) HOT WATER INJECTION (b) SALT INJECTION
(c) HEATED PIN (d) LASER

TABLE 2

p/d \ h/d	14	17	19	21	24	26.5	28	34	43	48	50	52	55
1.065			3*										
1.1													
1.14	3			3			3						
1.20									6	1 8			
1.24										9		4 11	
1.25					5					5			
1.28					10								2
1.315		7						7			7		
1.355						3							

* NUMBERS REFER TO TABLE - I

Table III: SKOK-Bundles & Energy Coefficients

Bundle No.	p/d	h/d	Dia. of Pin. In.	$(\overline{\varepsilon_H^*})_{AVG}$	C_1
1	1.355	26.5	0.667	0.0255	0.13
2	1.142	14.3	0.827	0.083	0.22
3	1.142	21.4	0.827	0.055	0.16
4	1.142	28.6	0.827	0.041	0.14
5	1.065	19.5	0.906	0.027	X
			Error-Bars	$\pm$ 25% of $\overline{\varepsilon_H^*}$	$\pm$ 50% of C_1

Table 4

	HEDL Run	Bulk Conc. (ppm)	Flow (gpm)	Re	$\overline{\varepsilon_H^*}$	C_I
Interior Injection	4	4145	430	~ 20000	0.017	
	11	8290	215	~ 10000	0.015	
	14	4347	615	~ 28000	0.02	*
	19	2165	430	~ 20000	0.03	
Wall Injection	2	1802	430	~ 20000	X	0.07

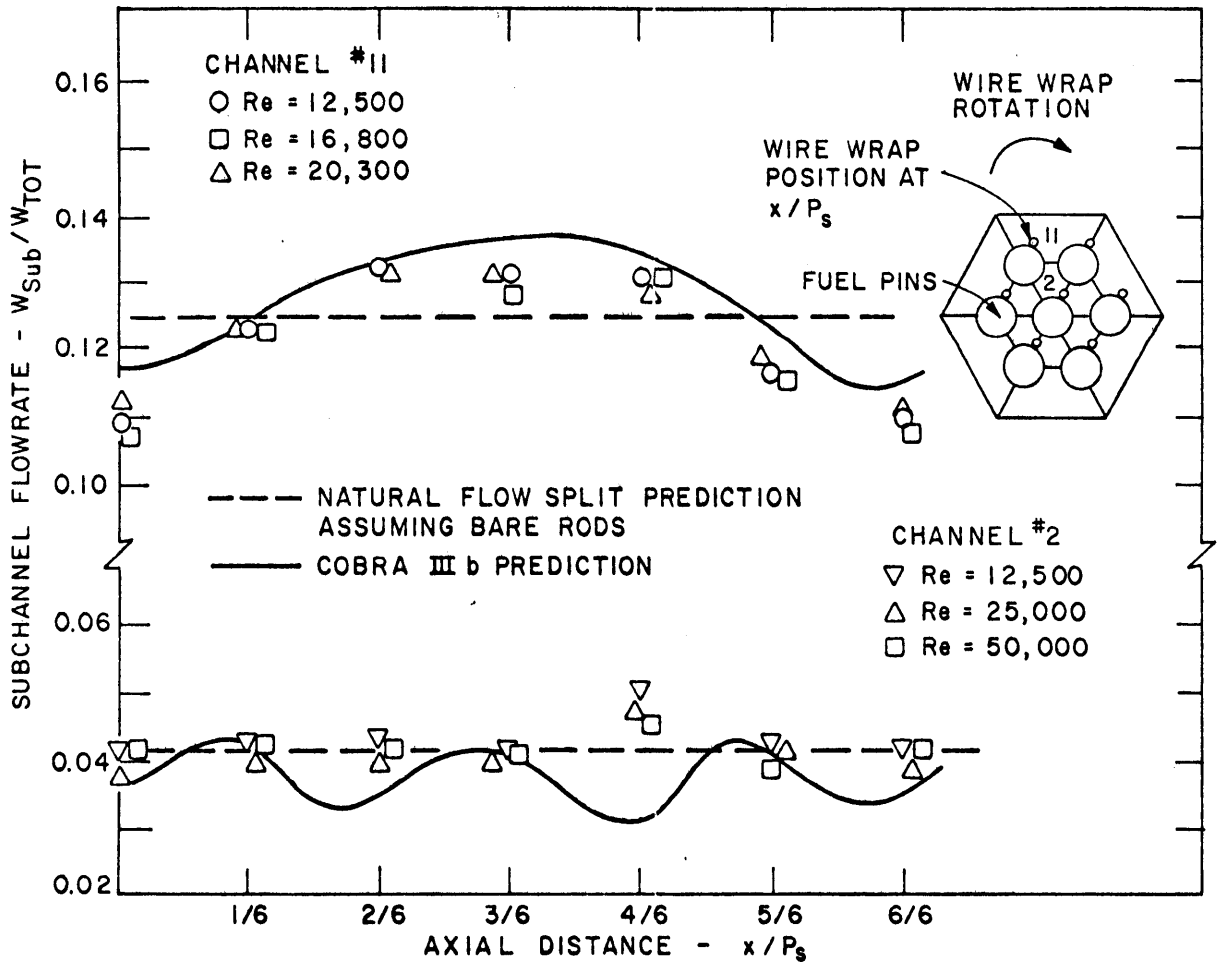
CHANNEL #11
Re = 12,500
Re = 16,800
Re = 20,300
WIRE WRAP ROTATION
WIRE WRAP POSITION AT x / Ps
FUEL PINS
11
2
NATURAL FLOW SPLIT PREDICTION ASSUMING BARE RODS
COBRA III b PREDICTION
CHANNEL #2
Re = 12,500
Re = 25,000
Re = 50,000
SUBCHANNEL FLOWRATE - WSub / WTOT
0.16
0.14
0.12
0.10
0.06
0.04
0.02
1/6
2/6
3/6
4/6
5/6
6/6
AXIAL DISTANCE - x / Ps

FIG. 1

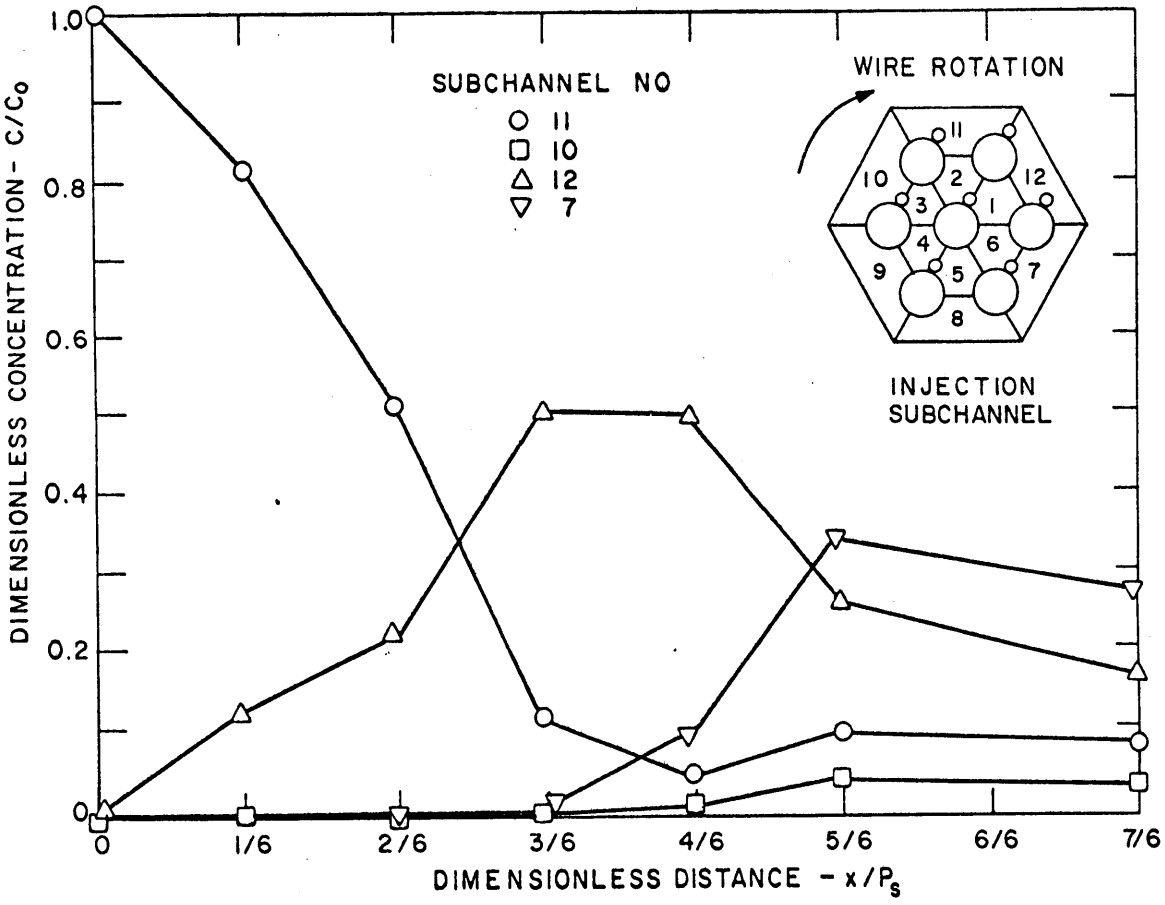
1.0
0.8
0.6
0.4
0.2
0
DIMENSIONLESS CONCENTRATION - C/C0
SUBCHANNEL NO
11
10
12
7
WIRE ROTATION
11
10
2
12
3
1
4
6
9
5
7
8
INJECTION SUBCHANNEL
0
1/6
2/6
3/6
4/6
5/6
6/6
7/6
DIMENSIONLESS DISTANCE - x/Ps

FIG. 2

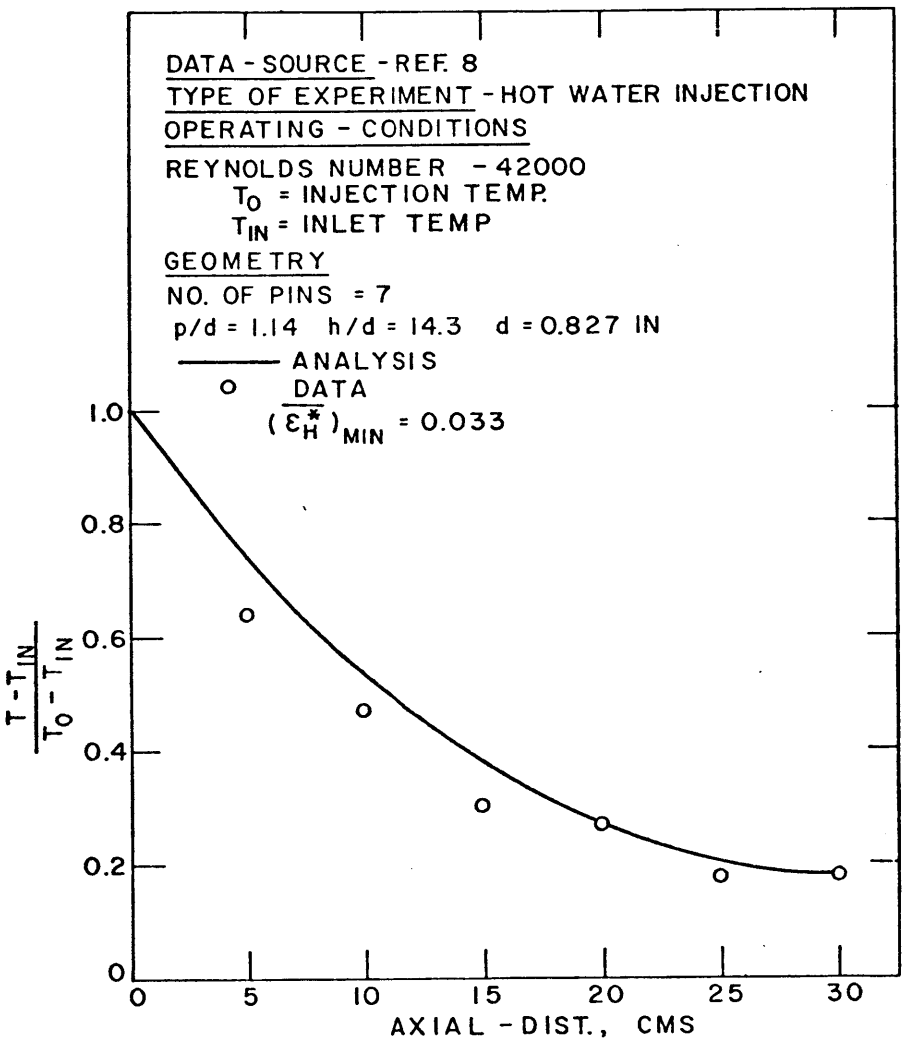
DATA - SOURCE - REF. 8
TYPE OF EXPERIMENT - HOT WATER INJECTION
OPERATING - CONDITIONS
REYNOLDS NUMBER - 42000
T_O = INJECTION TEMP.
T_{IN} = INLET TEMP
GEOMETRY
NO. OF PINS = 7
p/d = 1.14 h/d = 14.3 d = 0.827 IN
ANALYSIS
DATA
$(\overline{\varepsilon_H^*})_{MIN}$ = 0.033
$\frac{T-T_{IN}}{T_O-T_{IN}}$
1.0
0.8
0.6
0.4
0.2
0
0
5
10
15
20
25
30
AXIAL - DIST., CMS

FIG. 3

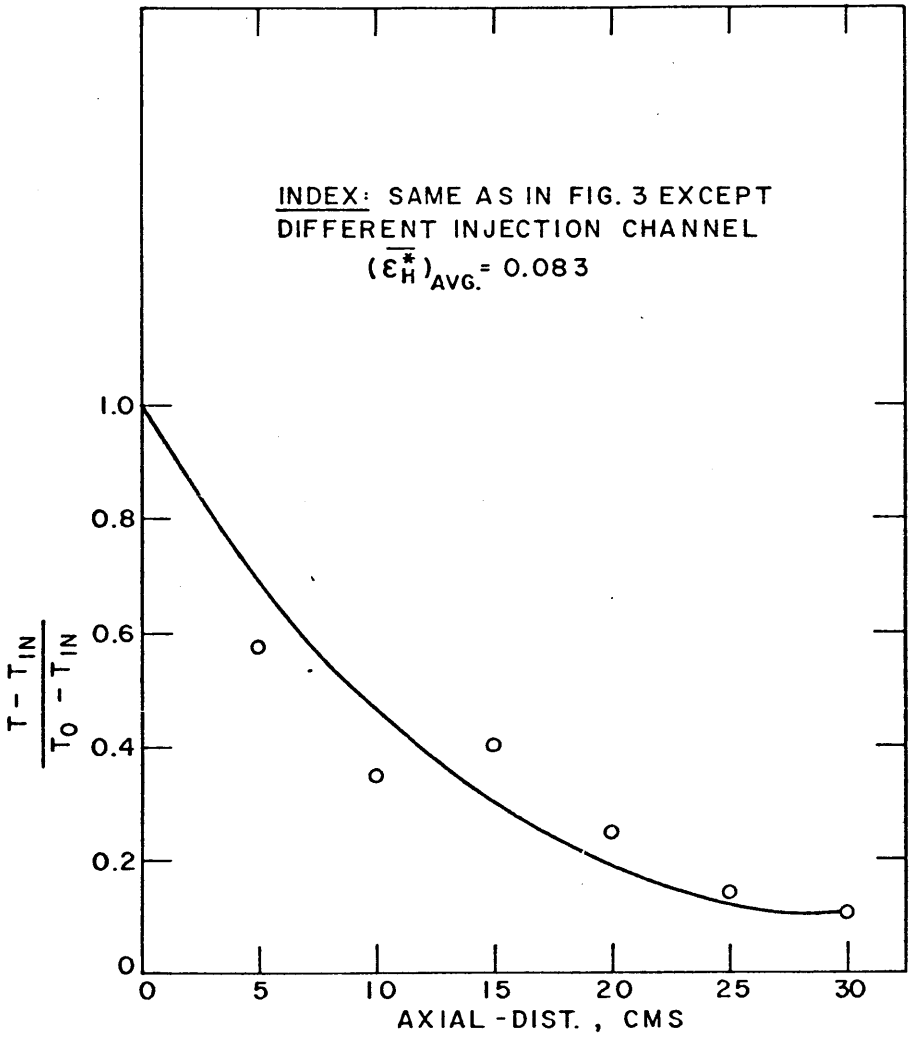
INDEX: SAME AS IN FIG. 3 EXCEPT
DIFFERENT INJECTION CHANNEL
$(\overline{\varepsilon_H^*})_{AVG.} = 0.083$
$\frac{T - T_{IN}}{T_O - T_{IN}}$
1.0
0.8
0.6
0.4
0.2
0
0
5
10
15
20
25
30
AXIAL - DIST. , CMS

FIG. 4

x ≡ LOCATION OF EXIT THERMOCOUPLE

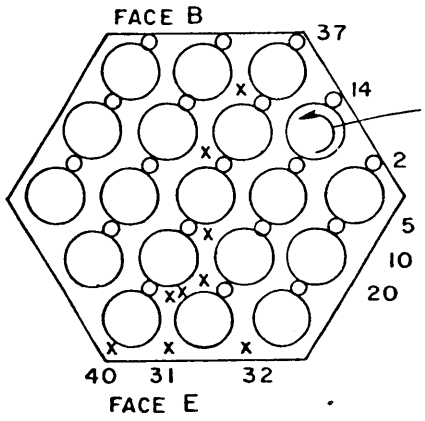

CHANNEL NO.

WIRE - WRAP DIRECTION

TEST PARAMETERS: REF. 9

1. FLUID - LIQUID Na
2. FLOW RATE - UP TO 56 GPM (Re - 1,000 TO 70,000)
3. POWER SKEW
   a. ALL RODS UNIFORMLY HEATED
   b. EACH ROD HEATED INDIVIDUALLY
   c. B 20 % HIGHER THAN E
   d. E 20 % HIGHER THAN B
   e. B 300 % HIGHER THAN E
   f. E 300 % HIGHER THAN B
4. d = 0.23 IN.
   h/d = 52
   p/d = 1.24

FIG. 5

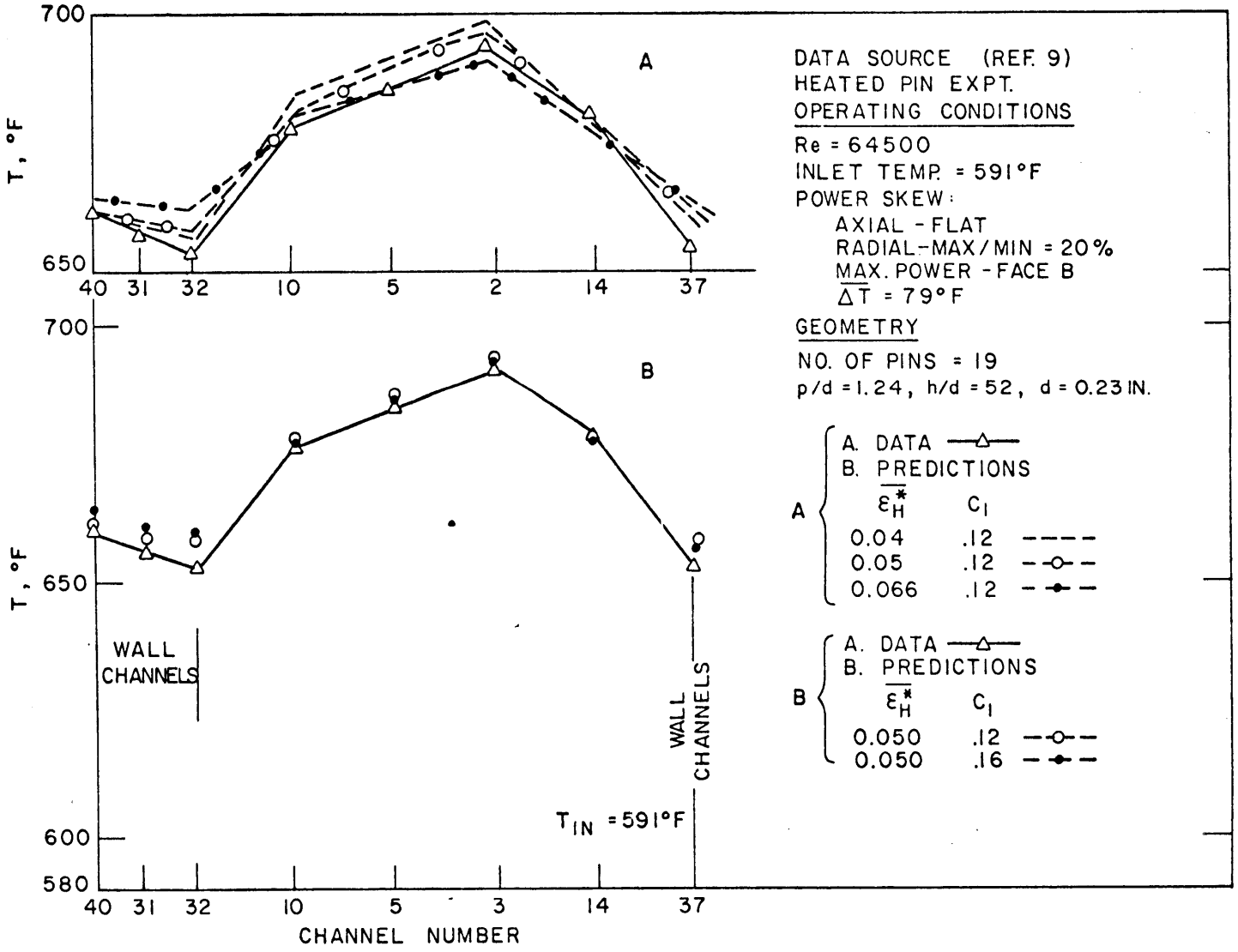
700
650
T, °F
A
40 31 32 10 5 2 14 37
700
650
600
580
T, °F
B
WALL CHANNELS
WALL CHANNELS
T_{IN} = 591°F
40 31 32 10 5 3 14 37
CHANNEL NUMBER
DATA SOURCE (REF. 9)
HEATED PIN EXPT.
OPERATING CONDITIONS
Re = 64500
INLET TEMP. = 591°F
POWER SKEW:
AXIAL - FLAT
RADIAL-MAX/MIN = 20%
MAX. POWER - FACE B
$\overline{\Delta T}$ = 79°F
GEOMETRY
NO. OF PINS = 19
p/d = 1.24, h/d = 52, d = 0.23 IN.
A
A. DATA
B. PREDICTIONS
$\overline{\varepsilon_H^*}$ C_1
0.04 .12
0.05 .12
0.066 .12
B
A. DATA
B. PREDICTIONS
$\overline{\varepsilon_H^*}$ C_1
0.050 .12
0.050 .16

FIG. 6

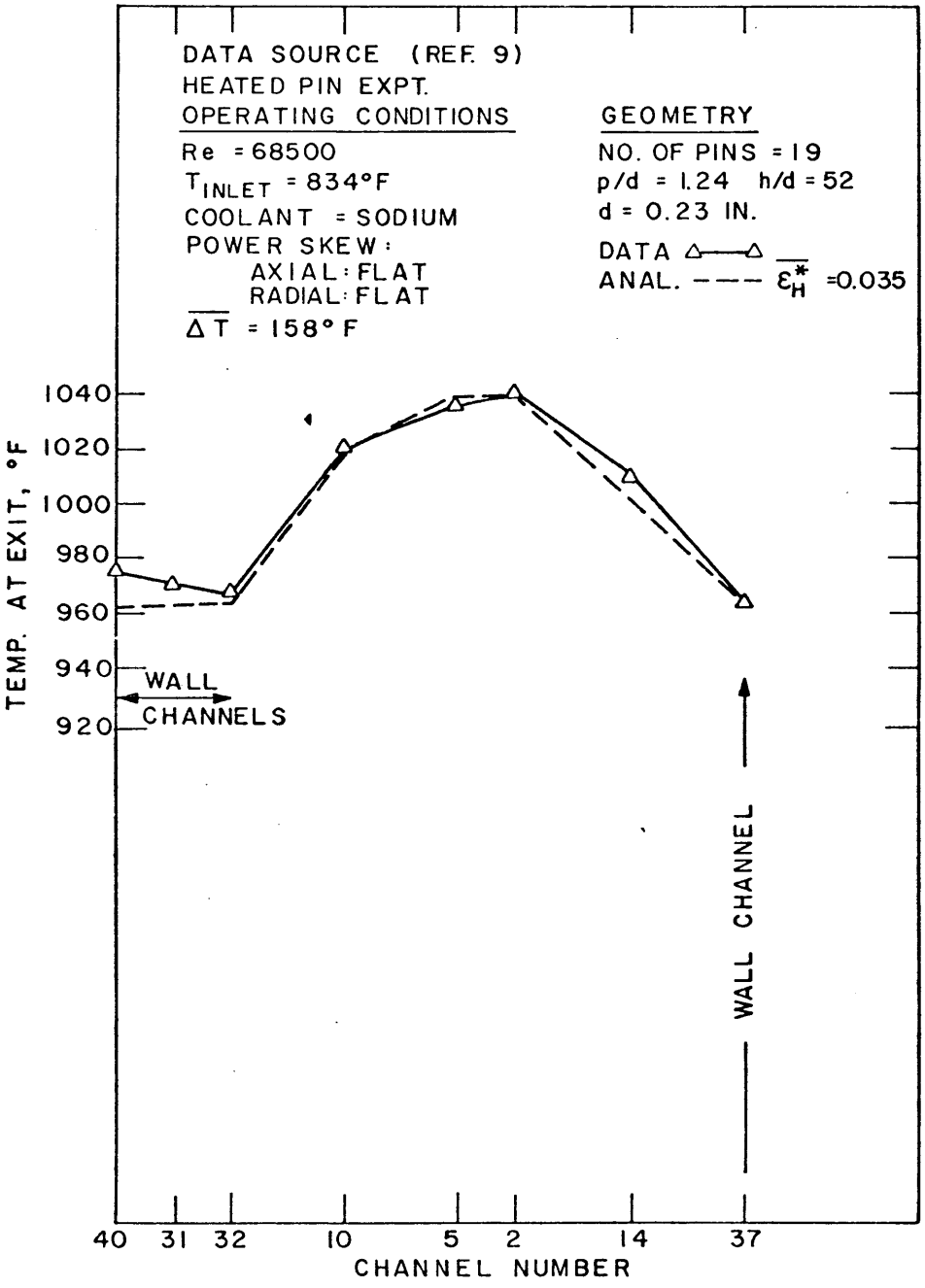
DATA SOURCE (REF. 9)
HEATED PIN EXPT.
OPERATING CONDITIONS
Re = 68500
T INLET = 834°F
COOLANT = SODIUM
POWER SKEW:
AXIAL: FLAT
RADIAL: FLAT
ΔT = 158° F
GEOMETRY
NO. OF PINS = 19
p/d = 1.24 h/d = 52
d = 0.23 IN.
DATA
ANAL. ε*H =0.035
TEMP. AT EXIT, °F
1040
1020
1000
980
960
940
920
WALL
CHANNELS
WALL CHANNEL
40 31 32 10 5 2 14 37
CHANNEL NUMBER

FIG. 7

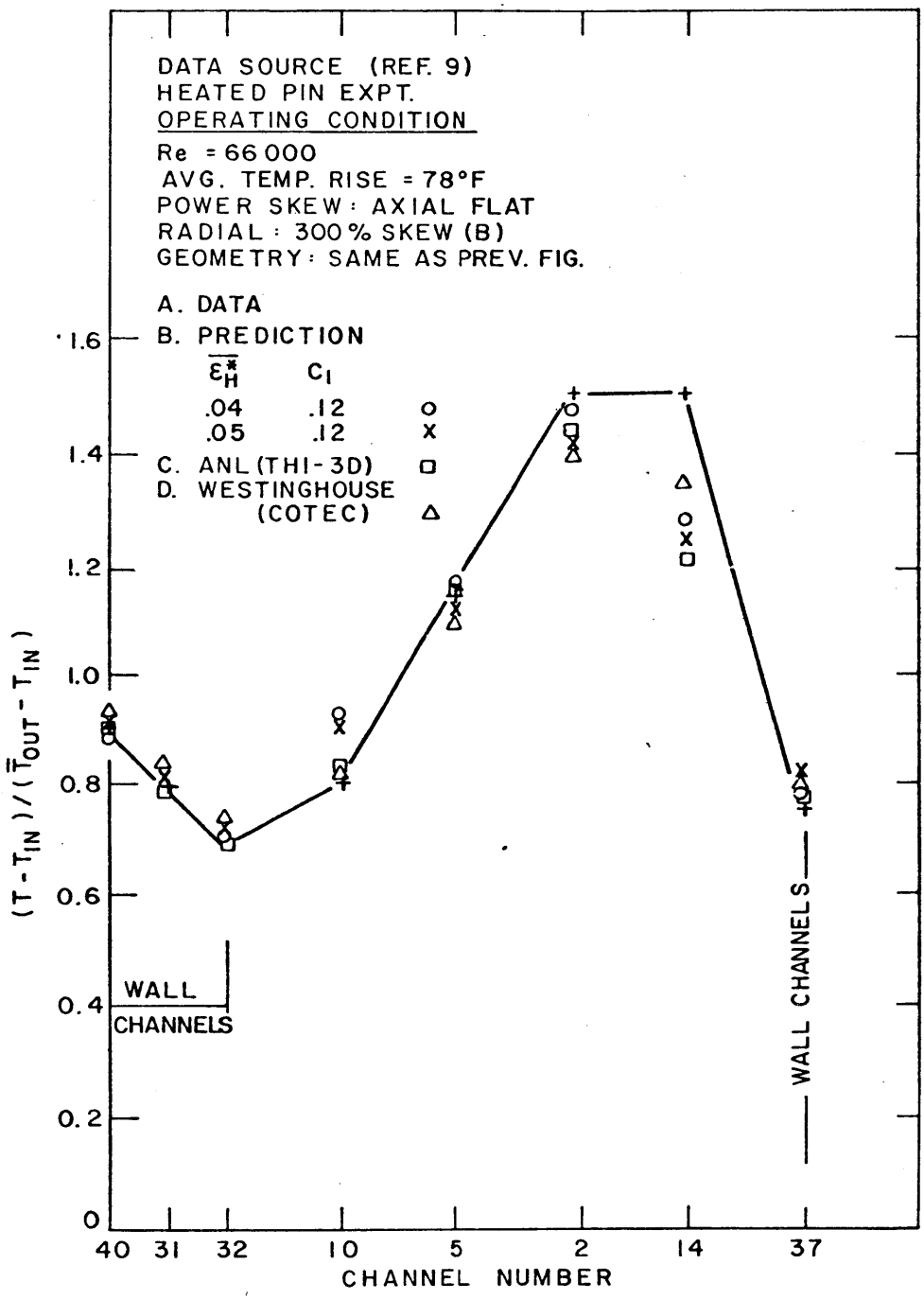
DATA SOURCE (REF. 9)
HEATED PIN EXPT.
OPERATING CONDITION
Re = 66 000
AVG. TEMP. RISE = 78°F
POWER SKEW: AXIAL FLAT
RADIAL: 300% SKEW (B)
GEOMETRY: SAME AS PREV. FIG.
A. DATA
B. PREDICTION
$\bar{\varepsilon}^*_H$ C_1
.04 .12
.05 .12
C. ANL (THI-3D)
D. WESTINGHOUSE (COTEC)
$(T-T_{IN})/(\bar{T}_{OUT}-T_{IN})$
1.6
1.4
1.2
1.0
0.8
0.6
0.4
0.2
0
WALL CHANNELS
WALL CHANNELS
40 31 32 10 5 2 14 37
CHANNEL NUMBER

FIG. 8

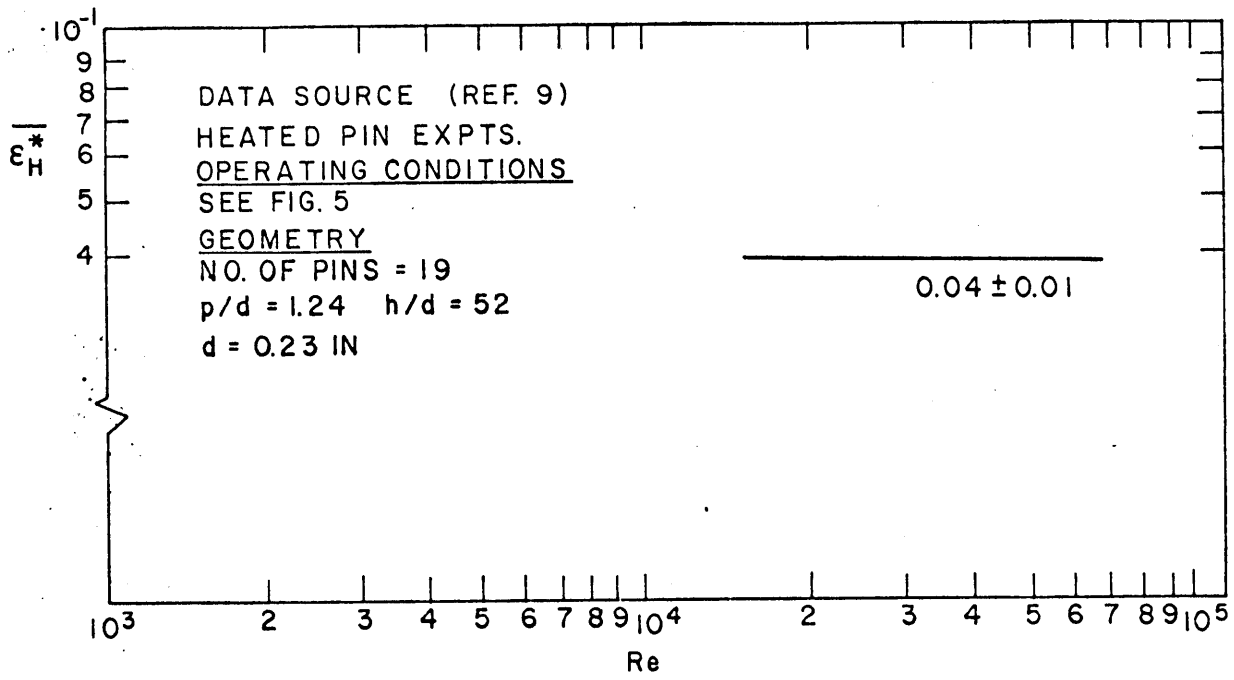
10^{-1}
9
8
7
6
5
4
$\overline{\varepsilon_H^*}$
DATA SOURCE (REF. 9)
HEATED PIN EXPTS.
OPERATING CONDITIONS
SEE FIG. 5
GEOMETRY
NO. OF PINS = 19
p/d = 1.24 h/d = 52
d = 0.23 IN
0.04 ± 0.01
10^3 2 3 4 5 6 7 8 9 10^4 2 3 4 5 6 7 8 9 10^5
Re

FIG. 9

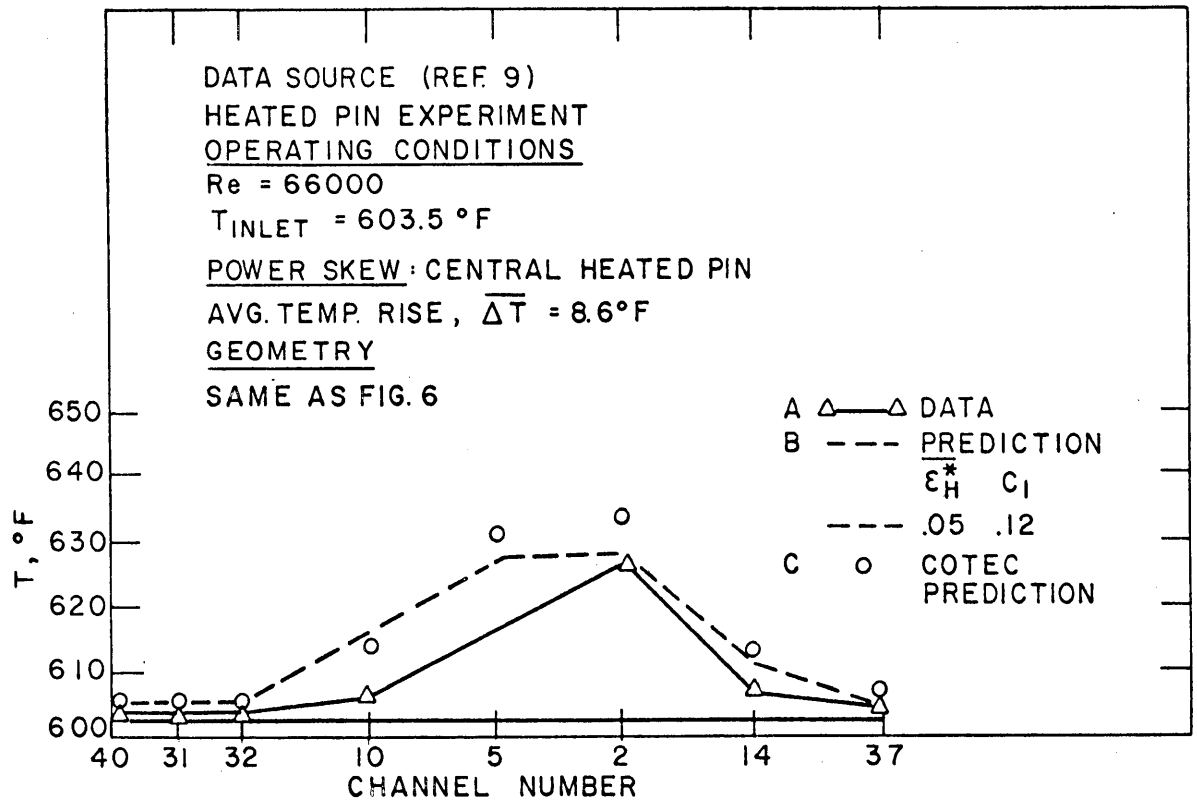
DATA SOURCE (REF. 9)
HEATED PIN EXPERIMENT
OPERATING CONDITIONS
Re = 66000
T_{INLET} = 603.5 °F
POWER SKEW: CENTRAL HEATED PIN
AVG. TEMP. RISE, $\overline{\Delta T}$ = 8.6°F
GEOMETRY
SAME AS FIG. 6
A DATA
B PREDICTION
$\overline{\varepsilon_H^*}$ C_1
.05 .12
C COTEC PREDICTION
650
640
630
620
610
600
T, °F
40 31 32 10 5 2 14 37
CHANNEL NUMBER

FIG. 10

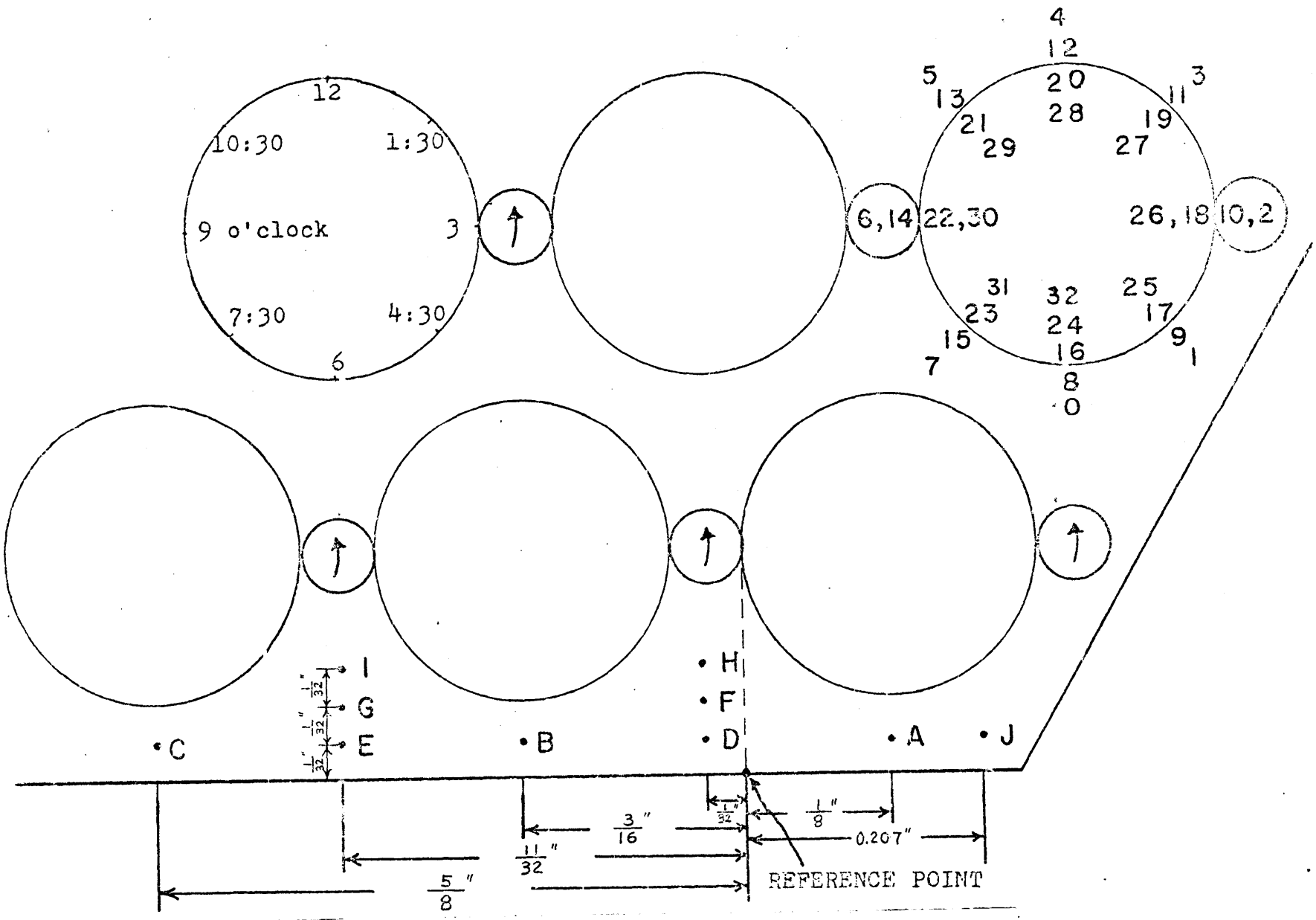
12
10:30
1:30
9 o'clock
3
7:30
4:30
6
4
12
5
20
3
13
11
28
21
19
29
27
6,14
22,30
26,18
10,2
31
32
25
23
24
17
15
16
9
7
1
8
0
I
G
E
C
B
H
F
D
A
J
1/32"
1/32"
1/32"
5/8"
11/32"
3/16"
1/32"
1/8"
0.207"
REFERENCE POINT

FIG. 11a

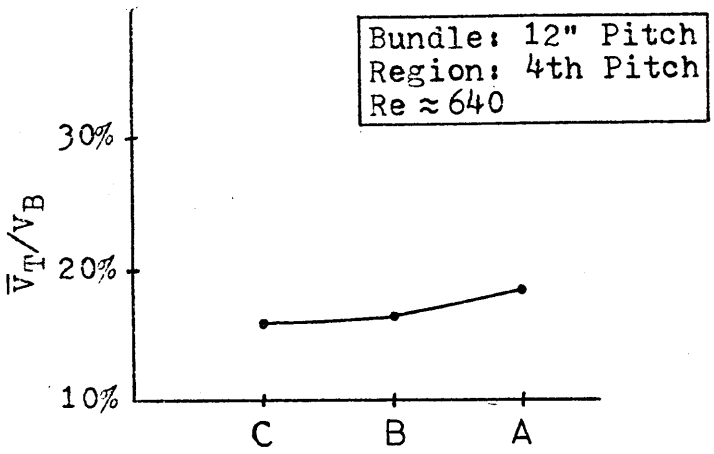

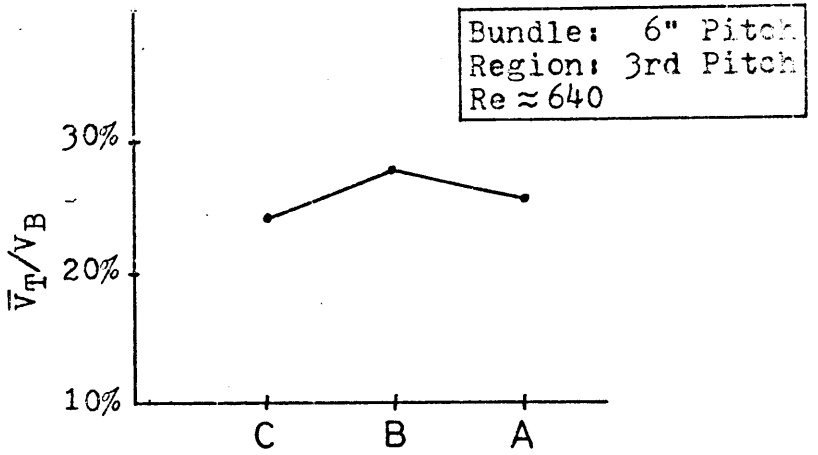

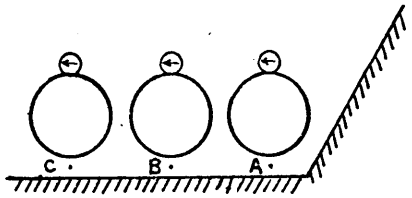

Measurement Positions

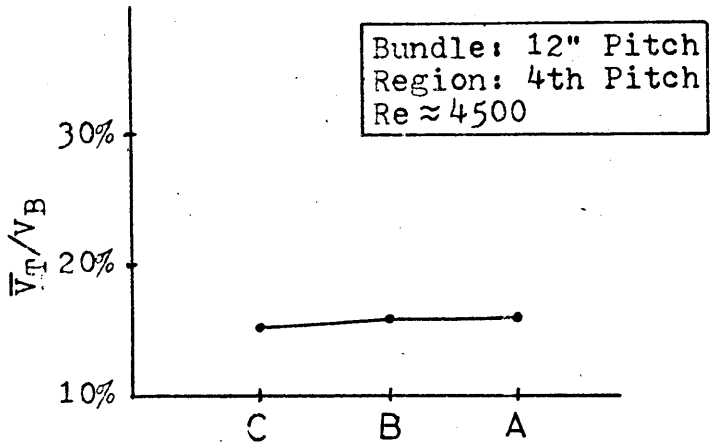

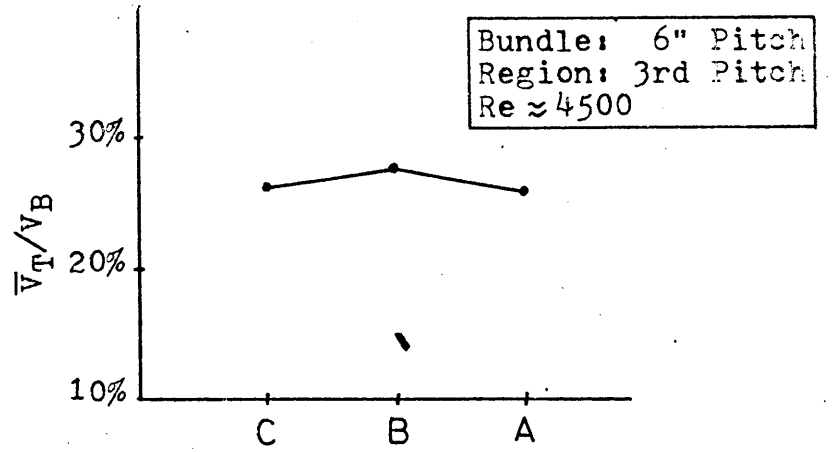

FIG. 11b

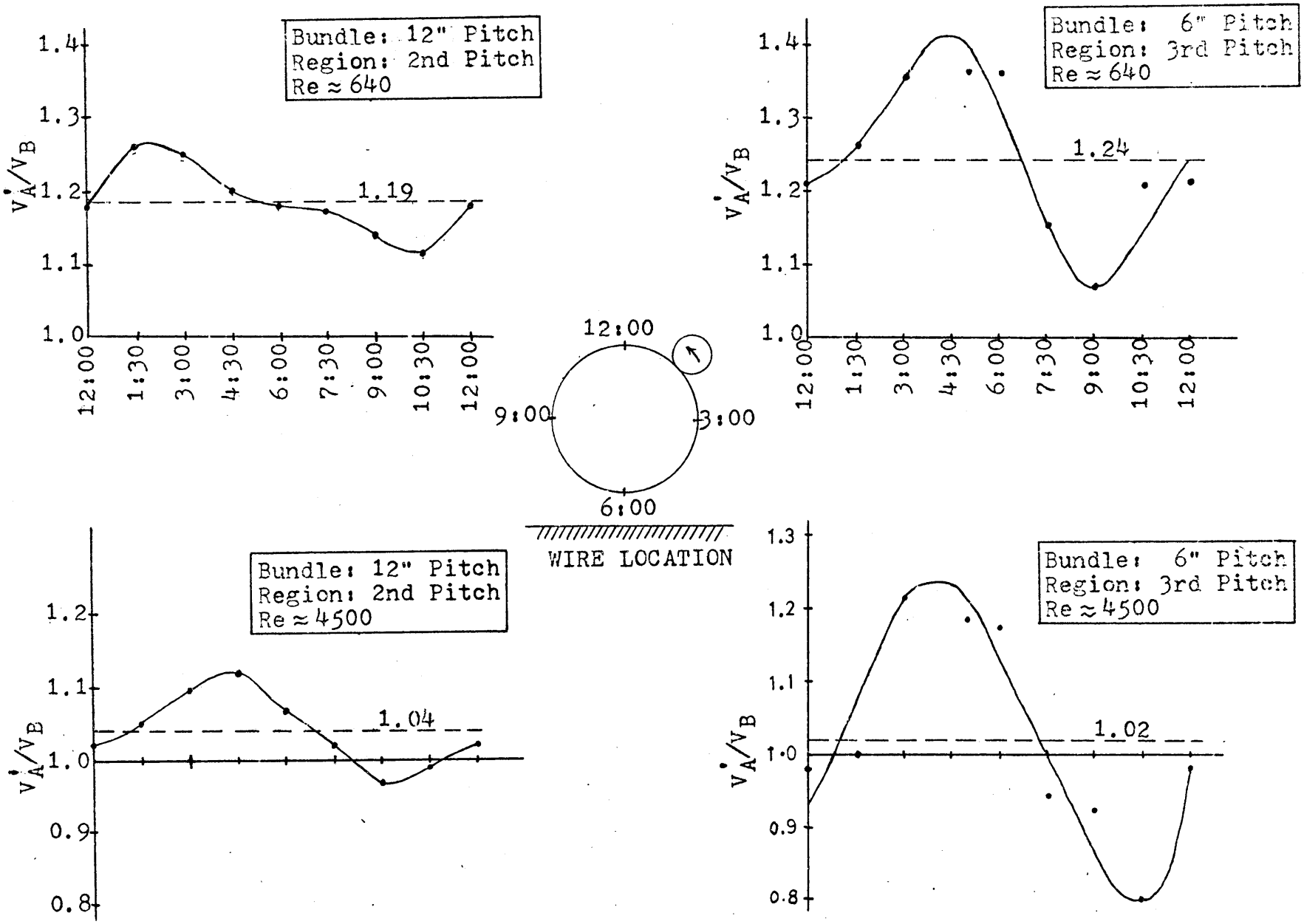
Bundle: 12" Pitch
Region: 2nd Pitch
Re ≈ 640
1.19
Bundle: 6" Pitch
Region: 3rd Pitch
Re ≈ 640
1.24
12:00
9:00
3:00
6:00
WIRE LOCATION
Bundle: 12" Pitch
Region: 2nd Pitch
Re ≈ 4500
1.04
Bundle: 6" Pitch
Region: 3rd Pitch
Re ≈ 4500
1.02
V_A'/V_B

FIG. 11c

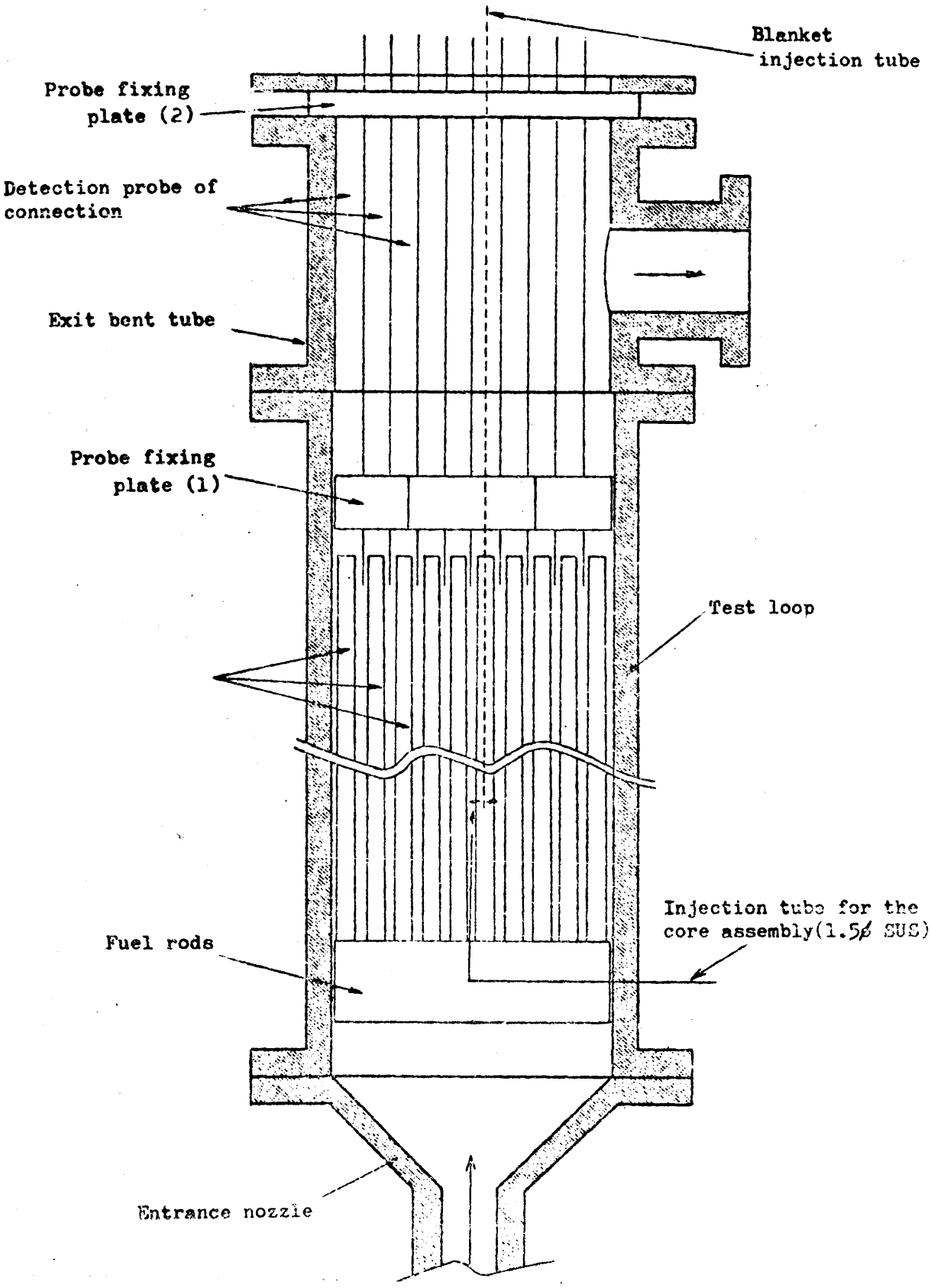
Blanket injection tube
Probe fixing plate (2)
Detection probe of connection
Exit bent tube
Probe fixing plate (1)
Test loop
Injection tube for the core assembly(1.5ϕ SUS)
Fuel rods
Entrance nozzle

FIG. 12

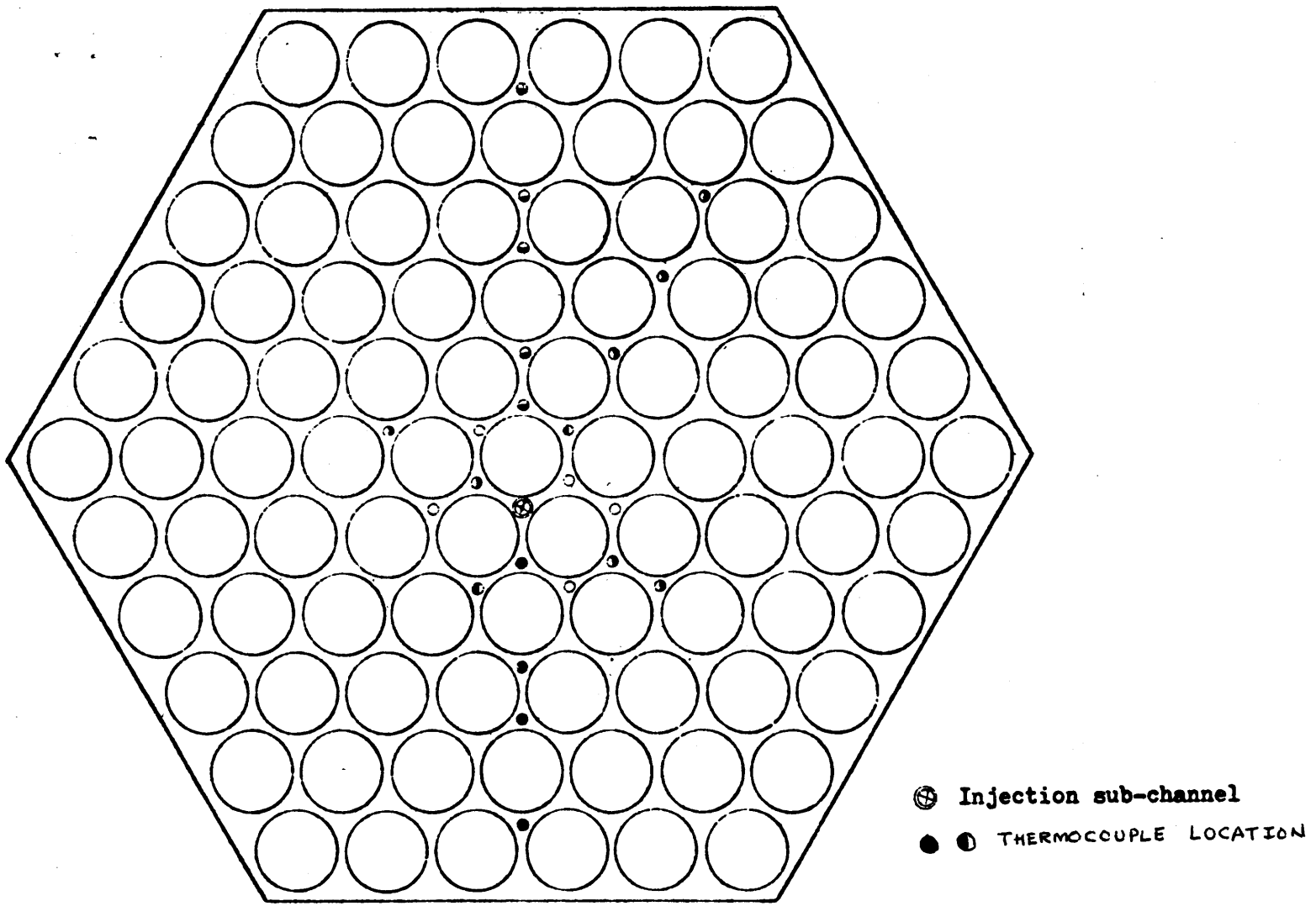

FIG. 13

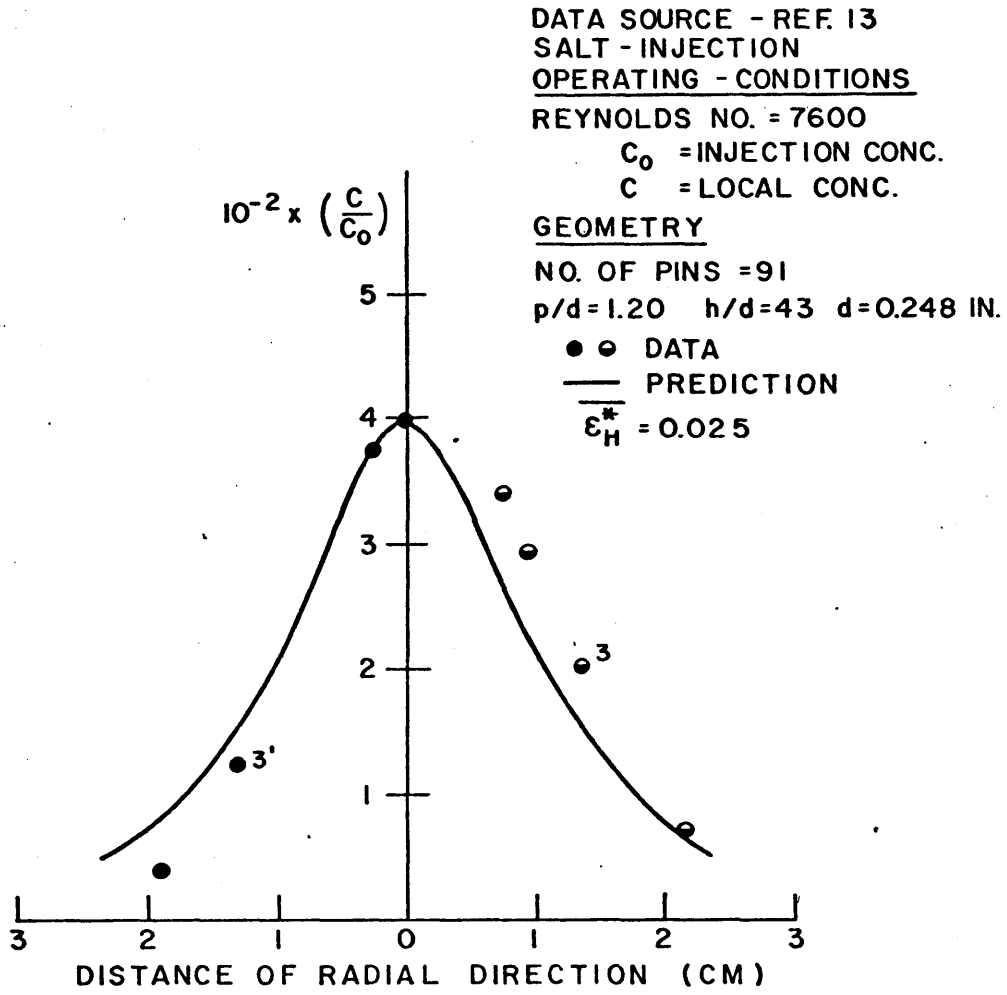
DATA SOURCE - REF. 13
SALT - INJECTION
OPERATING - CONDITIONS
REYNOLDS NO. = 7600
C_o = INJECTION CONC.
C = LOCAL CONC.
GEOMETRY
NO. OF PINS = 91
p/d = 1.20 h/d = 43 d = 0.248 IN.
DATA
PREDICTION
$\overline{\varepsilon_H^*}$ = 0.025
$10^{-2} \times \left(\frac{C}{C_o}\right)$
5
4
3
2
1
3'
3
3 2 1 0 1 2 3
DISTANCE OF RADIAL DIRECTION (CM)

FIG. 14

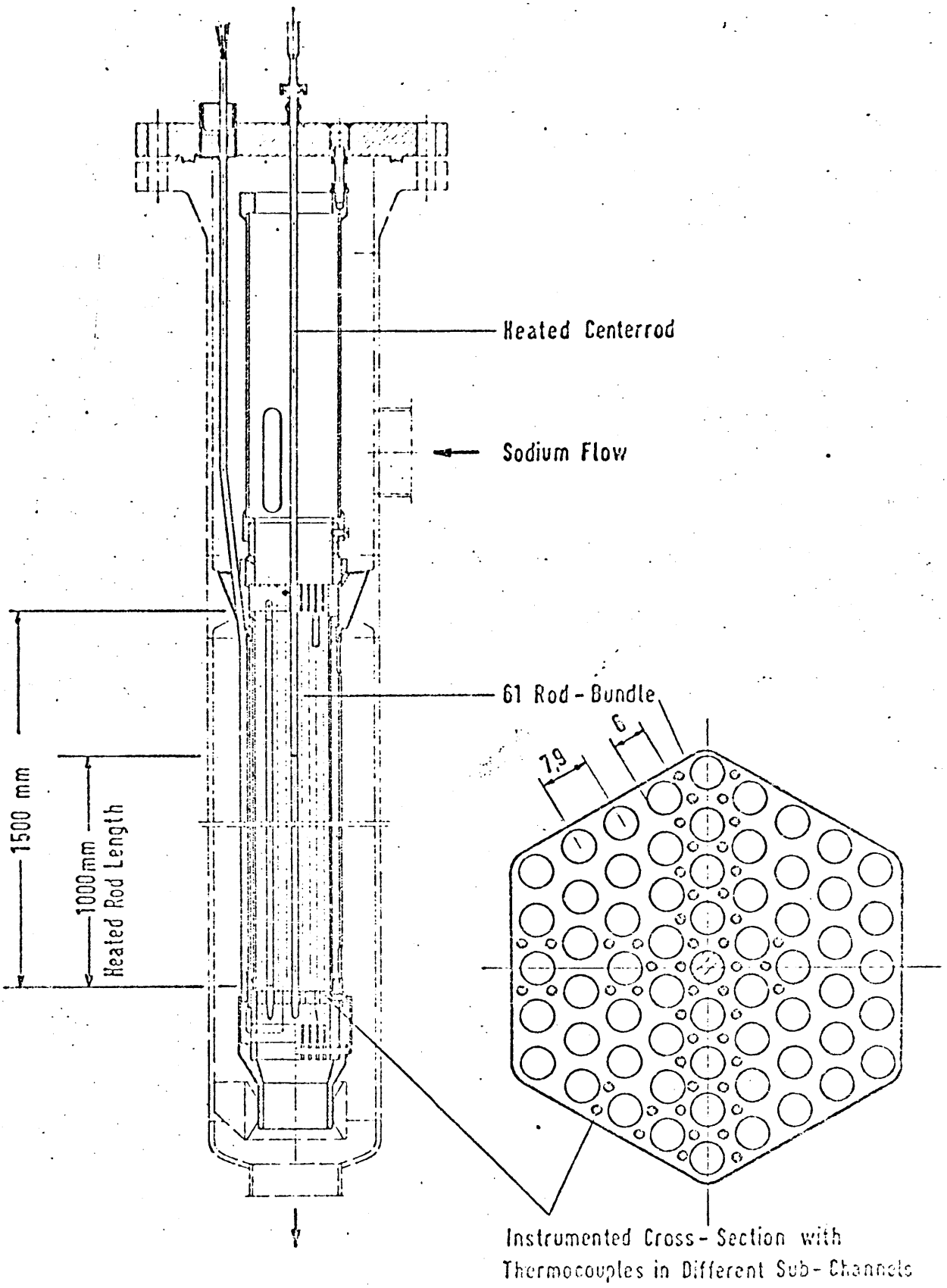
Heated Centerrod
Sodium Flow
61 Rod-Bundle
1500 mm
1000mm
Heated Rod Length
7.9
6
Instrumented Cross-Section with
Thermocouples in Different Sub-Channels

FIG. 15

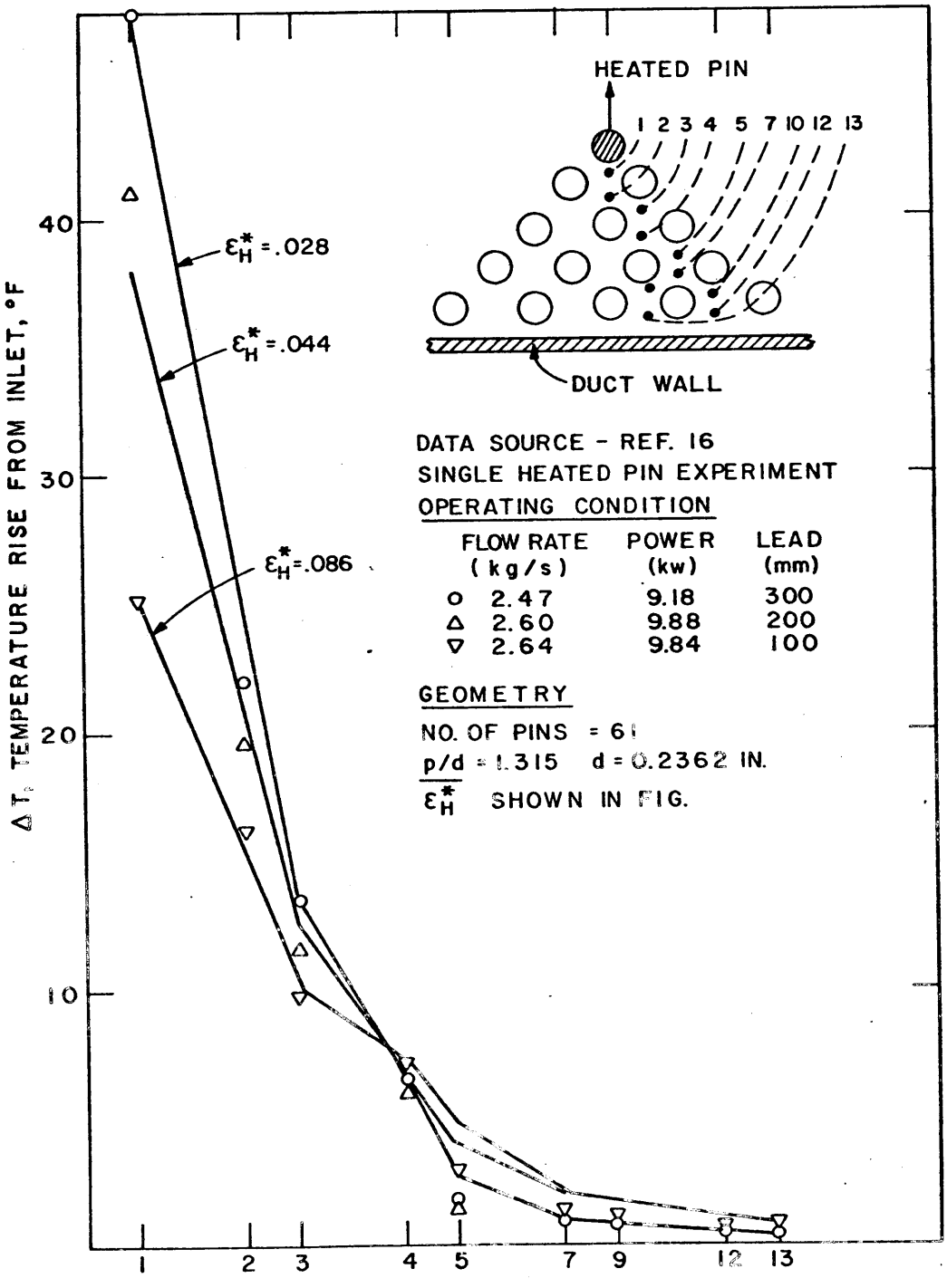
HEATED PIN
1 2 3 4 5 7 10 12 13
DUCT WALL
ε_H^* = .028
ε_H^* = .044
ε_H^* = .086
ΔT, TEMPERATURE RISE FROM INLET, °F
40
30
20
10
1
2
3
4
5
7
9
12
13
DATA SOURCE - REF. 16
SINGLE HEATED PIN EXPERIMENT
OPERATING CONDITION
FLOW RATE (kg/s)
POWER (kw)
LEAD (mm)
o 2.47 9.18 300
Δ 2.60 9.88 200
∇ 2.64 9.84 100
GEOMETRY
NO. OF PINS = 61
p/d = 1.315 d = 0.2362 IN.
ε_H^* SHOWN IN FIG.

FIG. 16

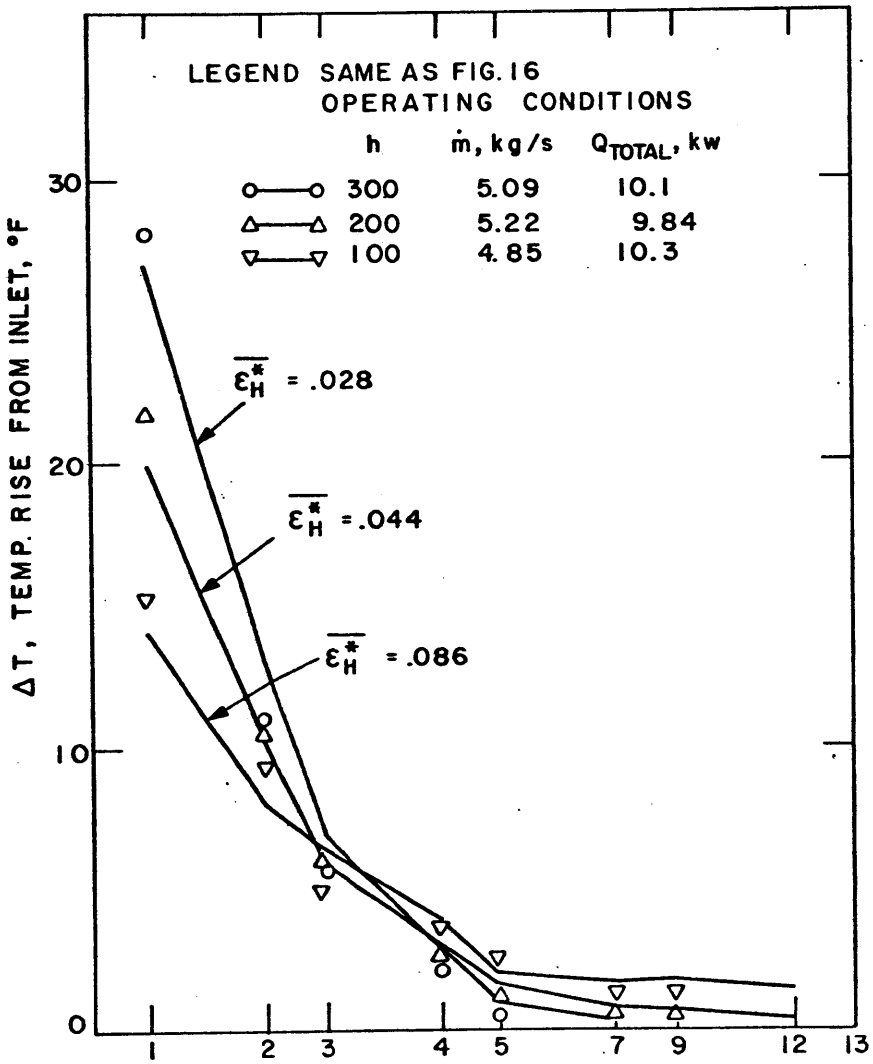
LEGEND SAME AS FIG. 16
OPERATING CONDITIONS
h
ṁ, kg/s
Q_{TOTAL}, kw
300 5.09 10.1
200 5.22 9.84
100 4.85 10.3
$\overline{\varepsilon_H^*}$ = .028
$\overline{\varepsilon_H^*}$ = .044
$\overline{\varepsilon_H^*}$ = .086
ΔT, TEMP. RISE FROM INLET, °F
0
10
20
30
1
2
3
4
5
7
9
12
13

FIG. 17

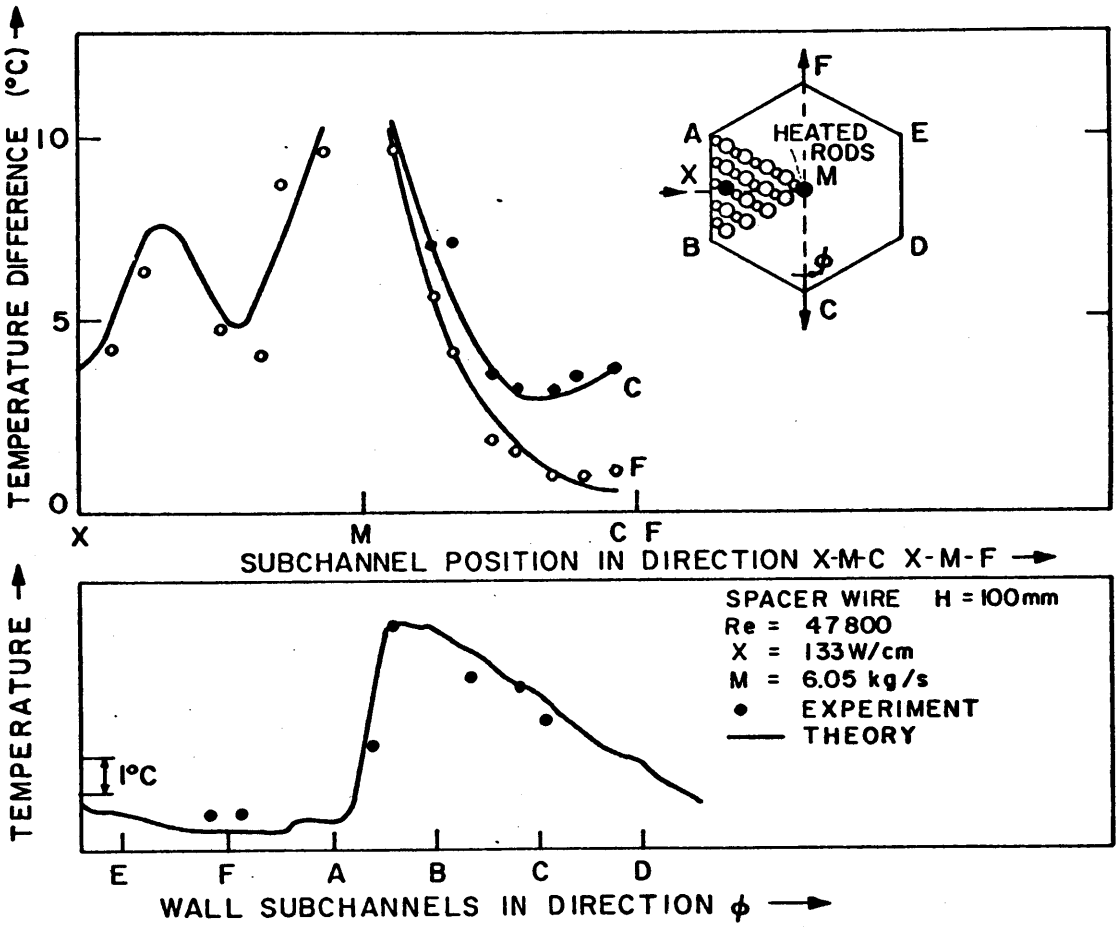
TEMPERATURE DIFFERENCE (°C)
10
5
0
X
M
C F
C
F
HEATED RODS
A
B
C
D
E
F
X
M
ϕ
SUBCHANNEL POSITION IN DIRECTION X-M-C X-M-F
TEMPERATURE
1°C
SPACER WIRE H = 100mm
Re = 47800
X = 133W/cm
M = 6.05 kg/s
EXPERIMENT
THEORY
E
F
A
B
C
D
WALL SUBCHANNELS IN DIRECTION ϕ

FIG. 18

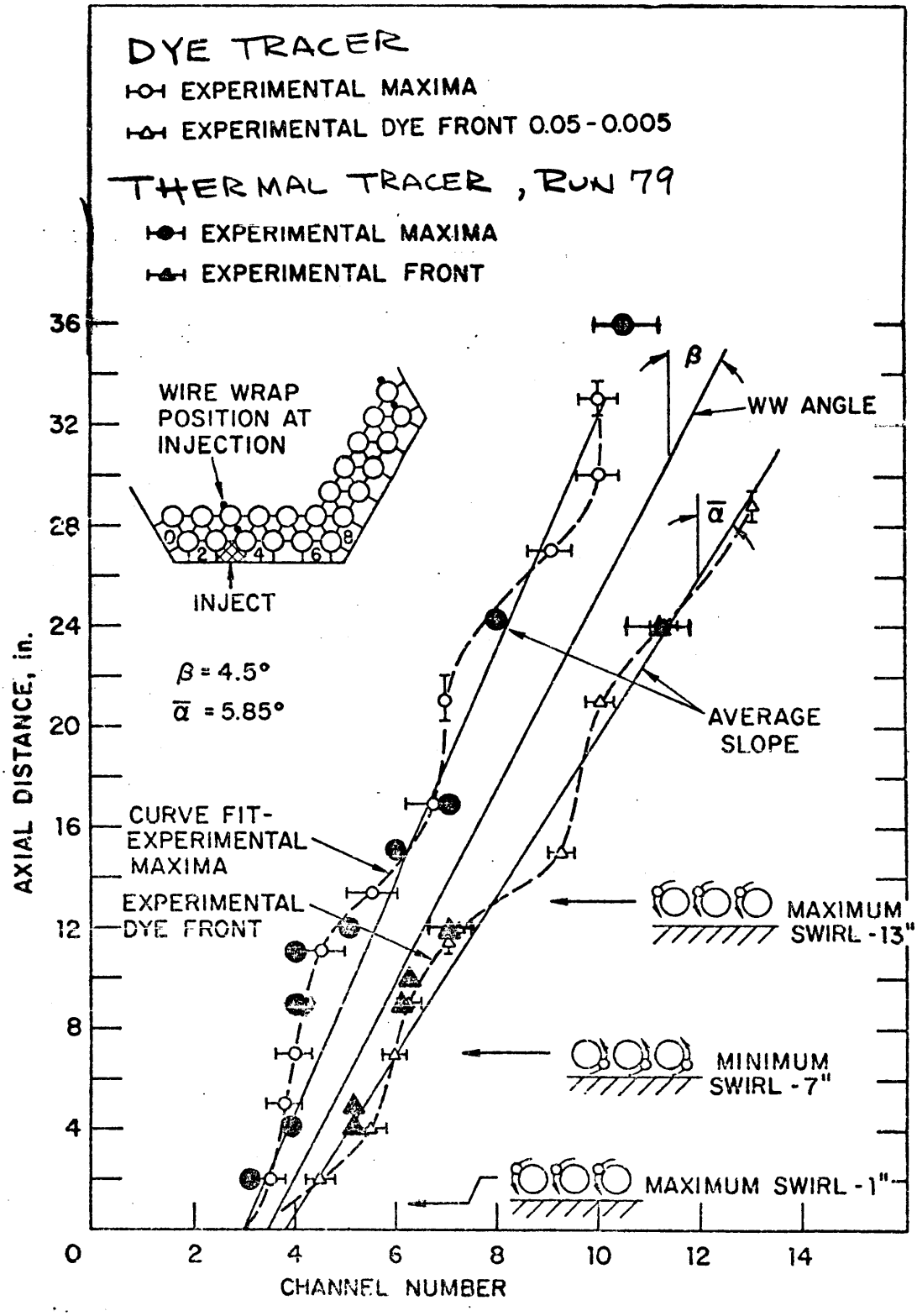
DYE TRACER
EXPERIMENTAL MAXIMA
EXPERIMENTAL DYE FRONT 0.05 - 0.005
THERMAL TRACER, RUN 79
EXPERIMENTAL MAXIMA
EXPERIMENTAL FRONT
WIRE WRAP POSITION AT INJECTION
INJECT
β = 4.5°
ᾱ = 5.85°
β
WW ANGLE
ᾱ
AVERAGE SLOPE
CURVE FIT - EXPERIMENTAL MAXIMA
EXPERIMENTAL DYE FRONT
MAXIMUM SWIRL - 13"
MINIMUM SWIRL - 7"
MAXIMUM SWIRL - 1"
AXIAL DISTANCE, in.
CHANNEL NUMBER
0
2
4
6
8
10
12
14
16
20
24
28
32
36

FIG. 19

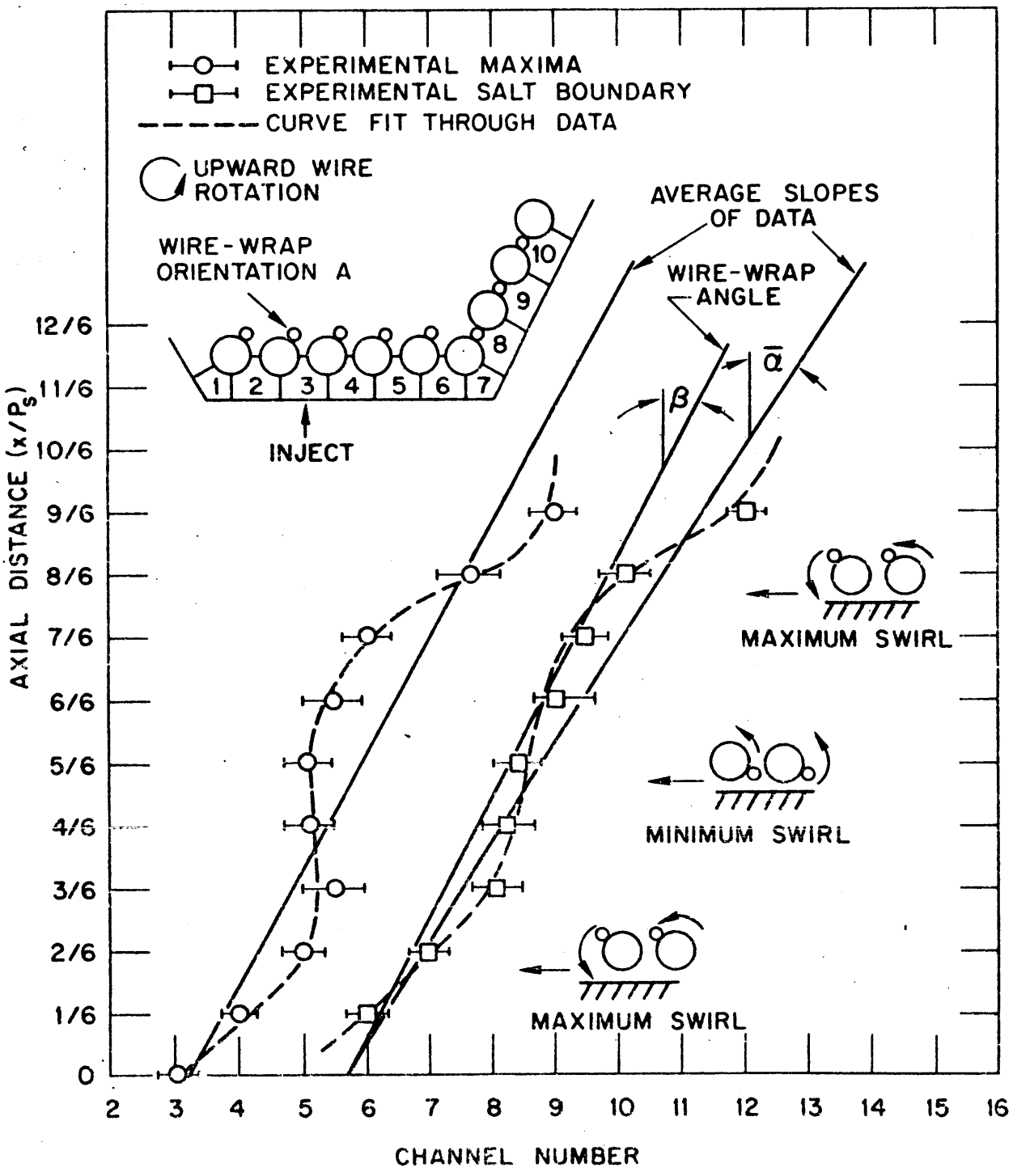
EXPERIMENTAL MAXIMA
EXPERIMENTAL SALT BOUNDARY
CURVE FIT THROUGH DATA
UPWARD WIRE ROTATION
WIRE-WRAP ORIENTATION A
INJECT
AVERAGE SLOPES OF DATA
WIRE-WRAP ANGLE
MAXIMUM SWIRL
MINIMUM SWIRL
MAXIMUM SWIRL
AXIAL DISTANCE (x/Ps)
CHANNEL NUMBER
12/6
11/6
10/6
9/6
8/6
7/6
6/6
5/6
4/6
3/6
2/6
1/6
0
2
3
4
5
6
7
8
9
10
11
12
13
14
15
16

FIG. 20

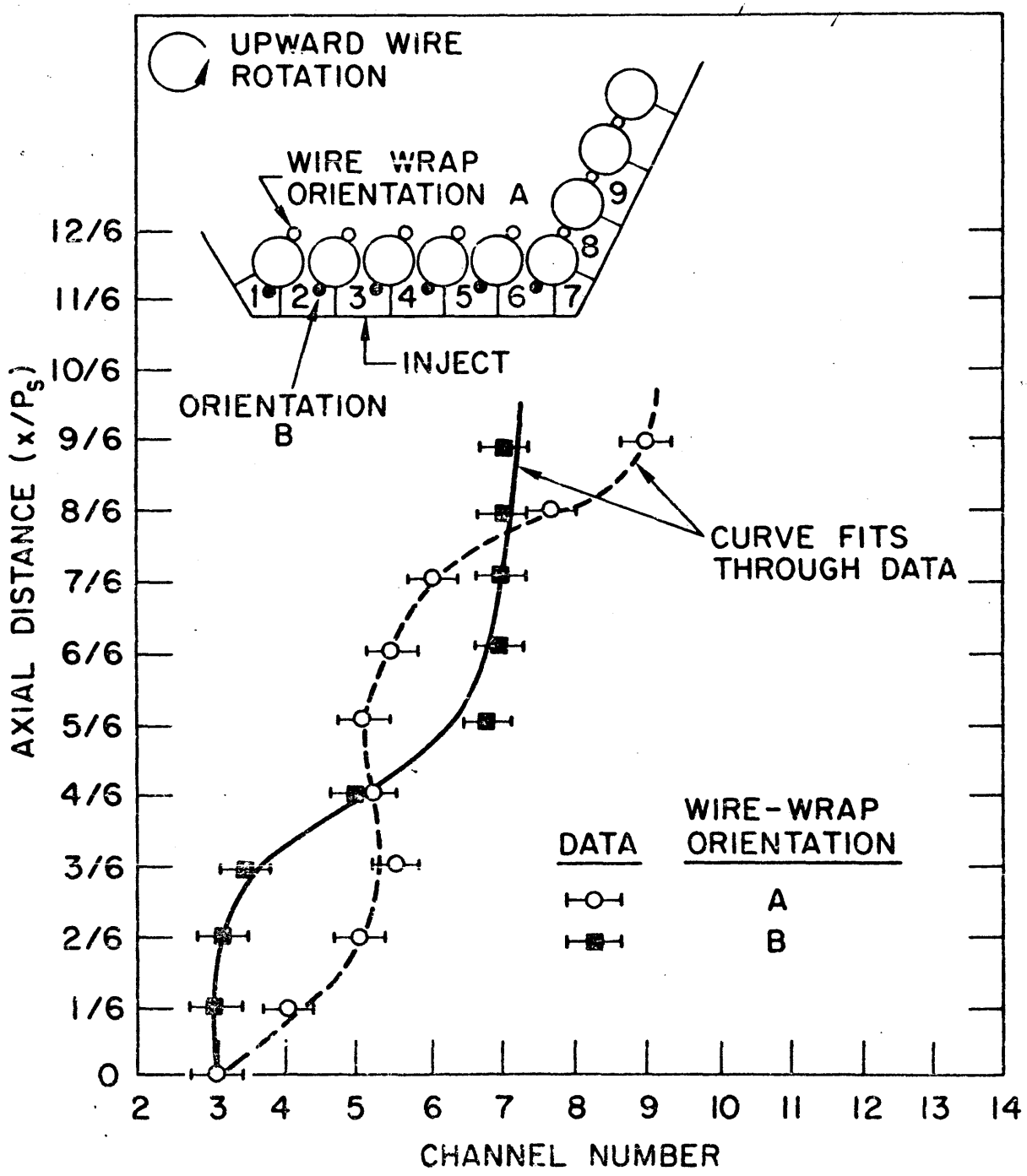
UPWARD WIRE ROTATION
WIRE WRAP ORIENTATION A
1
2
3
4
5
6
7
8
9
INJECT
ORIENTATION B
CURVE FITS THROUGH DATA
DATA
WIRE-WRAP ORIENTATION
A
B
AXIAL DISTANCE (x/Ps)
12/6
11/6
10/6
9/6
8/6
7/6
6/6
5/6
4/6
3/6
2/6
1/6
0
2
3
4
5
6
7
8
9
10
11
12
13
14
CHANNEL NUMBER

FIG. 21

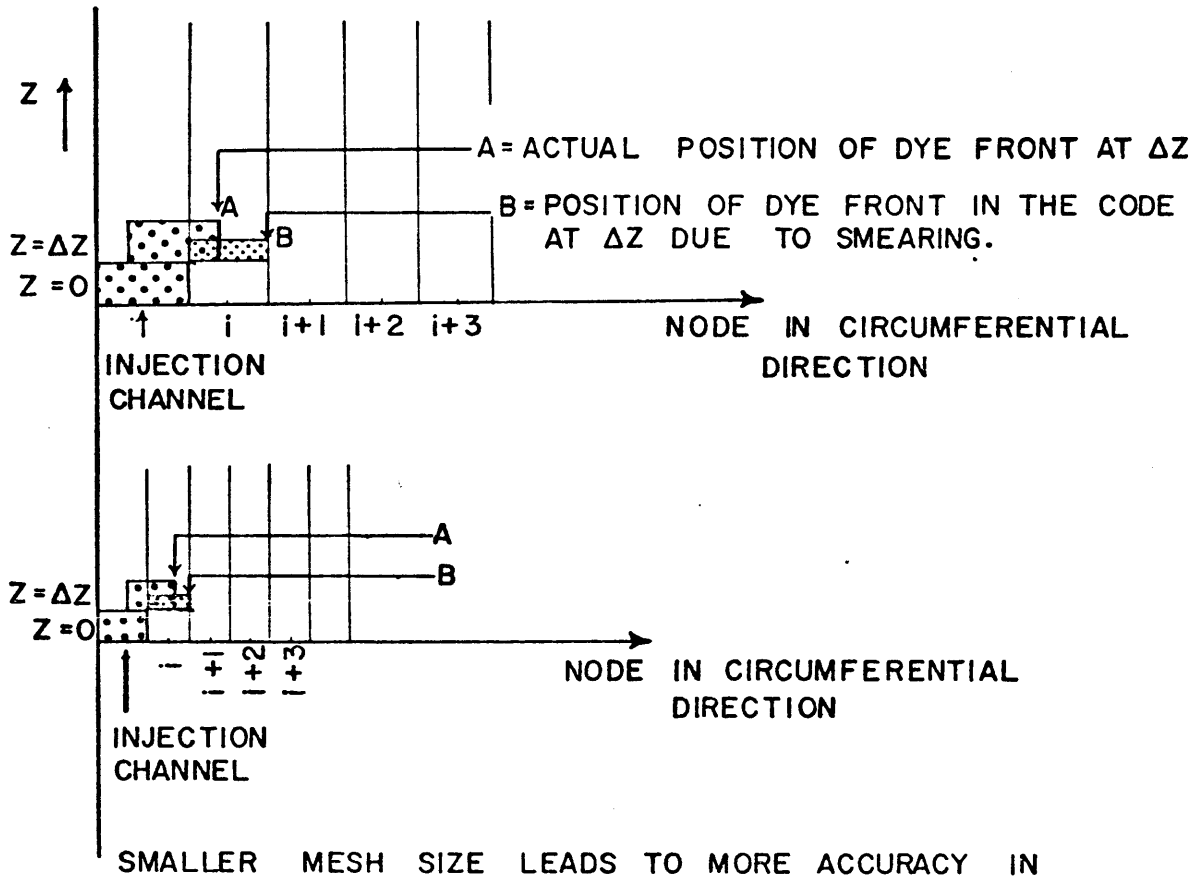
Z
A = ACTUAL POSITION OF DYE FRONT AT ΔZ
B = POSITION OF DYE FRONT IN THE CODE AT ΔZ DUE TO SMEARING.
A
B
Z=ΔZ
Z=0
i
i+1
i+2
i+3
NODE IN CIRCUMFERENTIAL DIRECTION
INJECTION CHANNEL
A
B
Z=ΔZ
Z=0
NODE IN CIRCUMFERENTIAL DIRECTION
INJECTION CHANNEL
SMALLER MESH SIZE LEADS TO MORE ACCURACY IN DETERMINING LOCATION OF DYE FRONT

FIG. 22

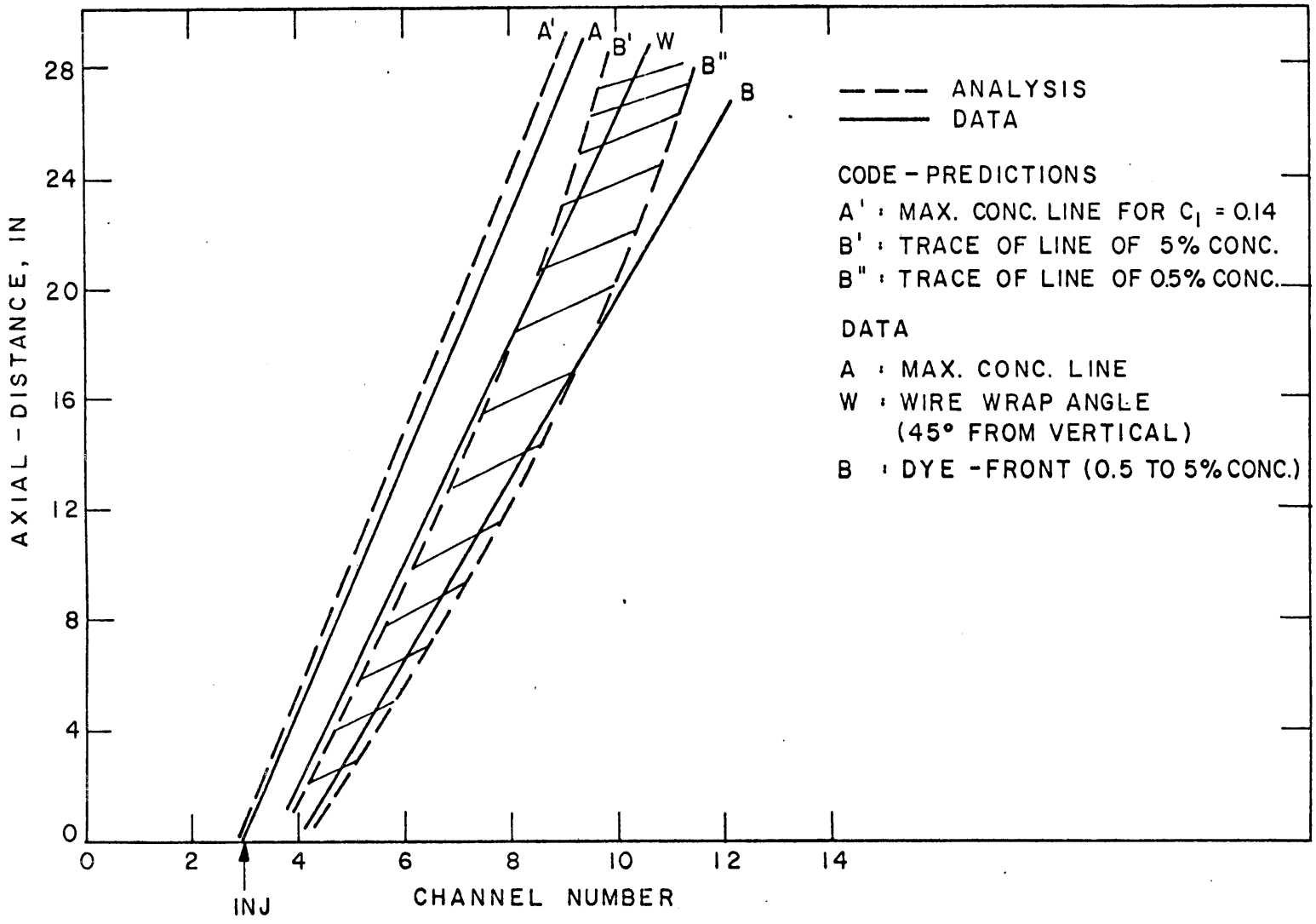
A'
A
B'
W
B"
B
28
24
20
16
12
8
4
0
AXIAL - DISTANCE, IN
0
2
4
6
8
10
12
14
INJ
CHANNEL NUMBER
ANALYSIS
DATA
CODE - PREDICTIONS
A' : MAX. CONC. LINE FOR C_1 = 0.14
B' : TRACE OF LINE OF 5% CONC.
B" : TRACE OF LINE OF 0.5% CONC.
DATA
A : MAX. CONC. LINE
W : WIRE WRAP ANGLE
(45° FROM VERTICAL)
B : DYE - FRONT (0.5 TO 5% CONC.)

FIG. 23

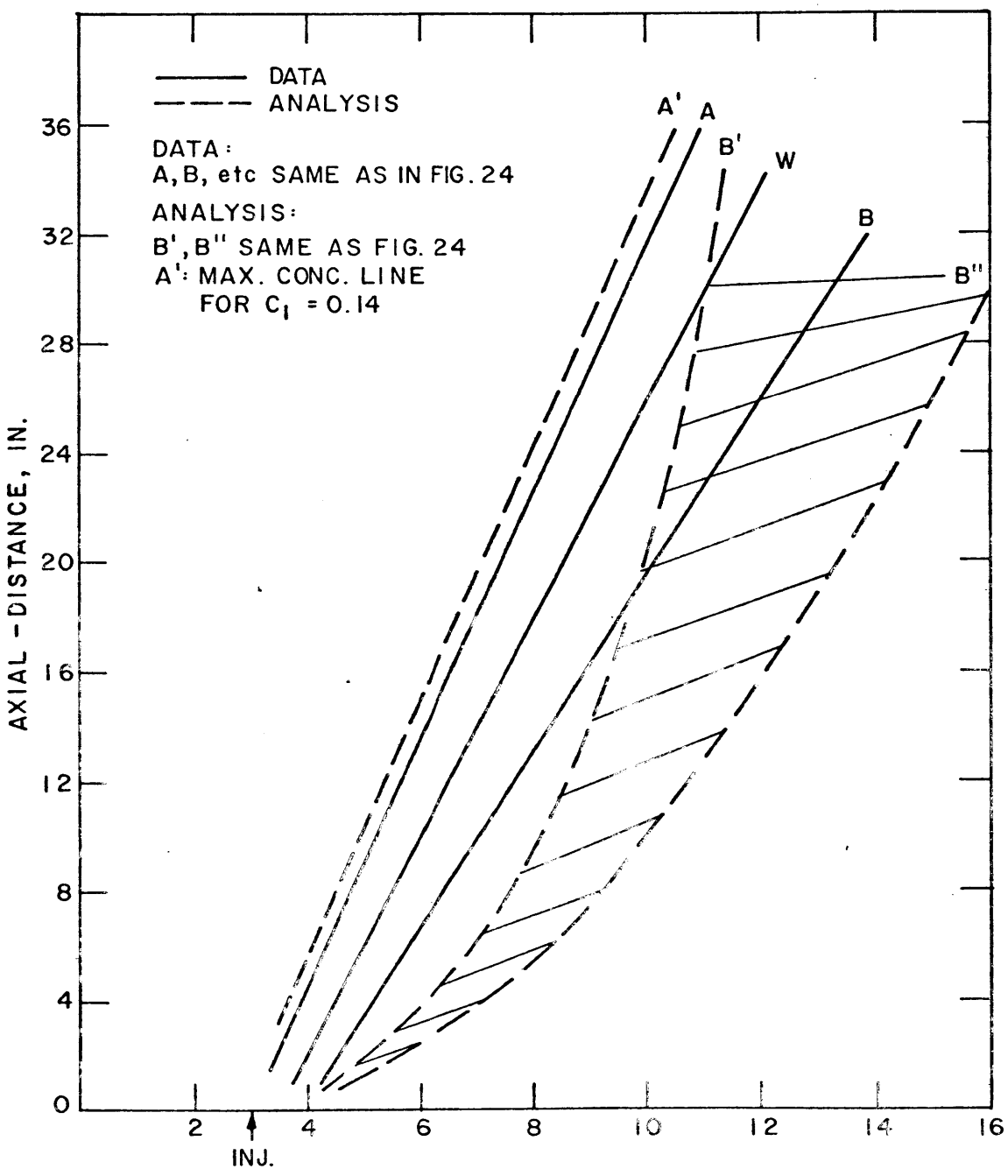
DATA
ANALYSIS
DATA:
A, B, etc SAME AS IN FIG. 24
ANALYSIS:
B', B'' SAME AS FIG. 24
A': MAX. CONC. LINE
FOR C_1 = 0.14
A'
A
B'
W
B
B''
AXIAL - DISTANCE, IN.
0
4
8
12
16
20
24
28
32
36
2
4
6
8
10
12
14
16
INJ.

FIG. 24

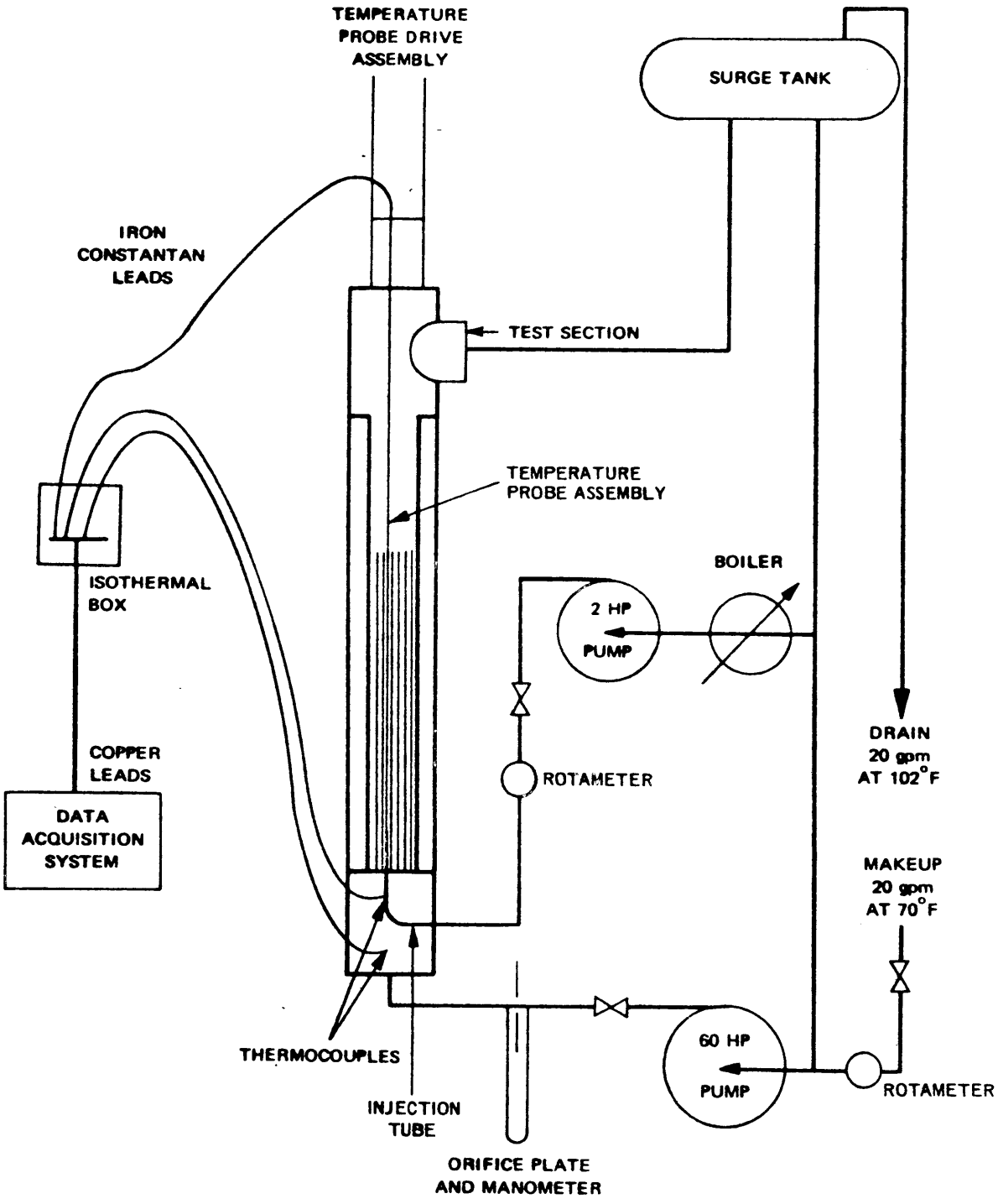
TEMPERATURE
PROBE DRIVE
ASSEMBLY
SURGE TANK
IRON
CONSTANTAN
LEADS
TEST SECTION
TEMPERATURE
PROBE ASSEMBLY
BOILER
ISOTHERMAL
BOX
2 HP
PUMP
DRAIN
20 gpm
AT 102°F
COPPER
LEADS
ROTAMETER
DATA
ACQUISITION
SYSTEM
MAKEUP
20 gpm
AT 70°F
60 HP
PUMP
ROTAMETER
THERMOCOUPLES
INJECTION
TUBE
ORIFICE PLATE
AND MANOMETER

FIG. 25

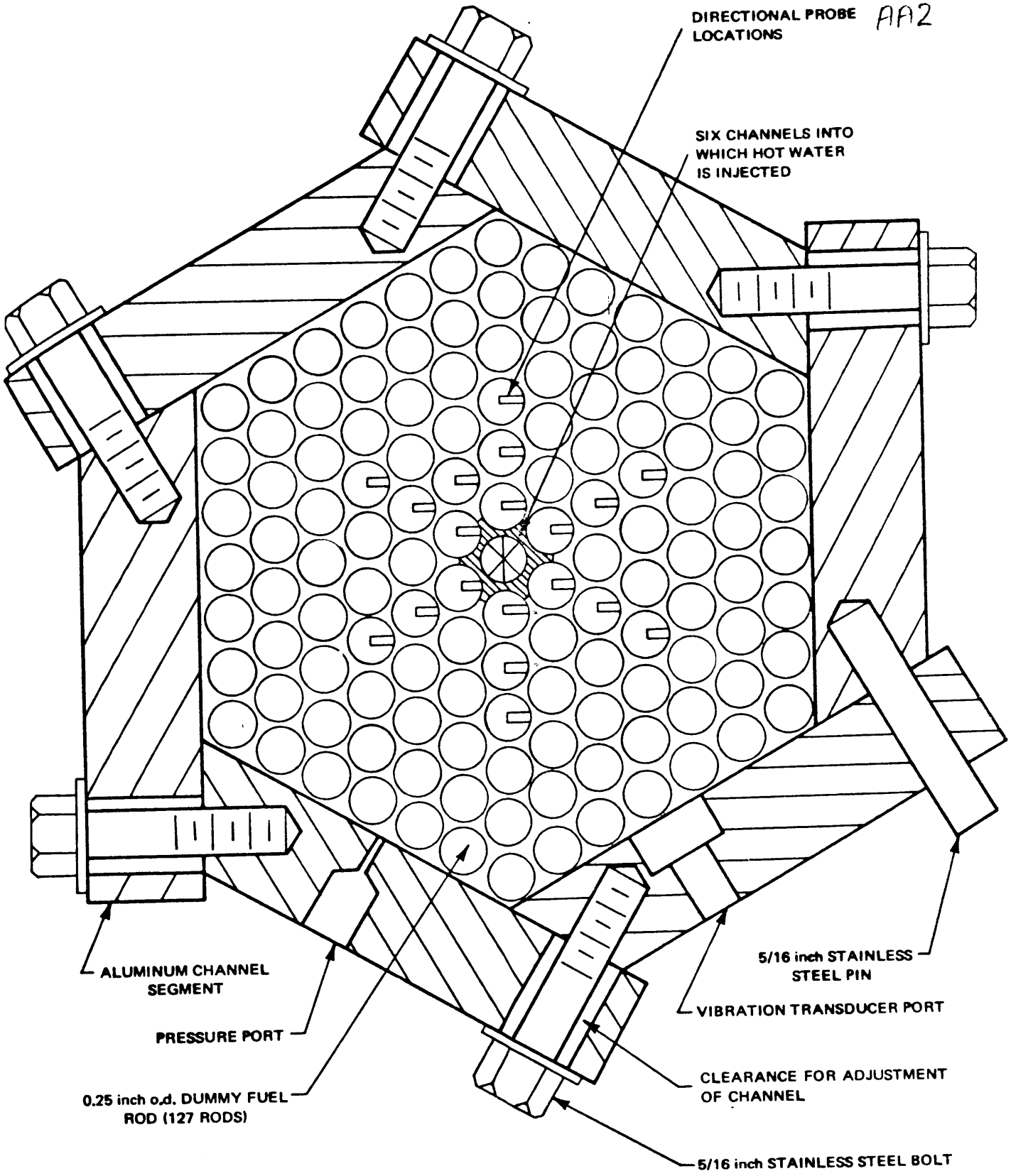
DIRECTIONAL PROBE LOCATIONS
AA2
SIX CHANNELS INTO WHICH HOT WATER IS INJECTED
ALUMINUM CHANNEL SEGMENT
PRESSURE PORT
0.25 inch o.d. DUMMY FUEL ROD (127 RODS)
5/16 inch STAINLESS STEEL PIN
VIBRATION TRANSDUCER PORT
CLEARANCE FOR ADJUSTMENT OF CHANNEL
5/16 inch STAINLESS STEEL BOLT

FIG. 26

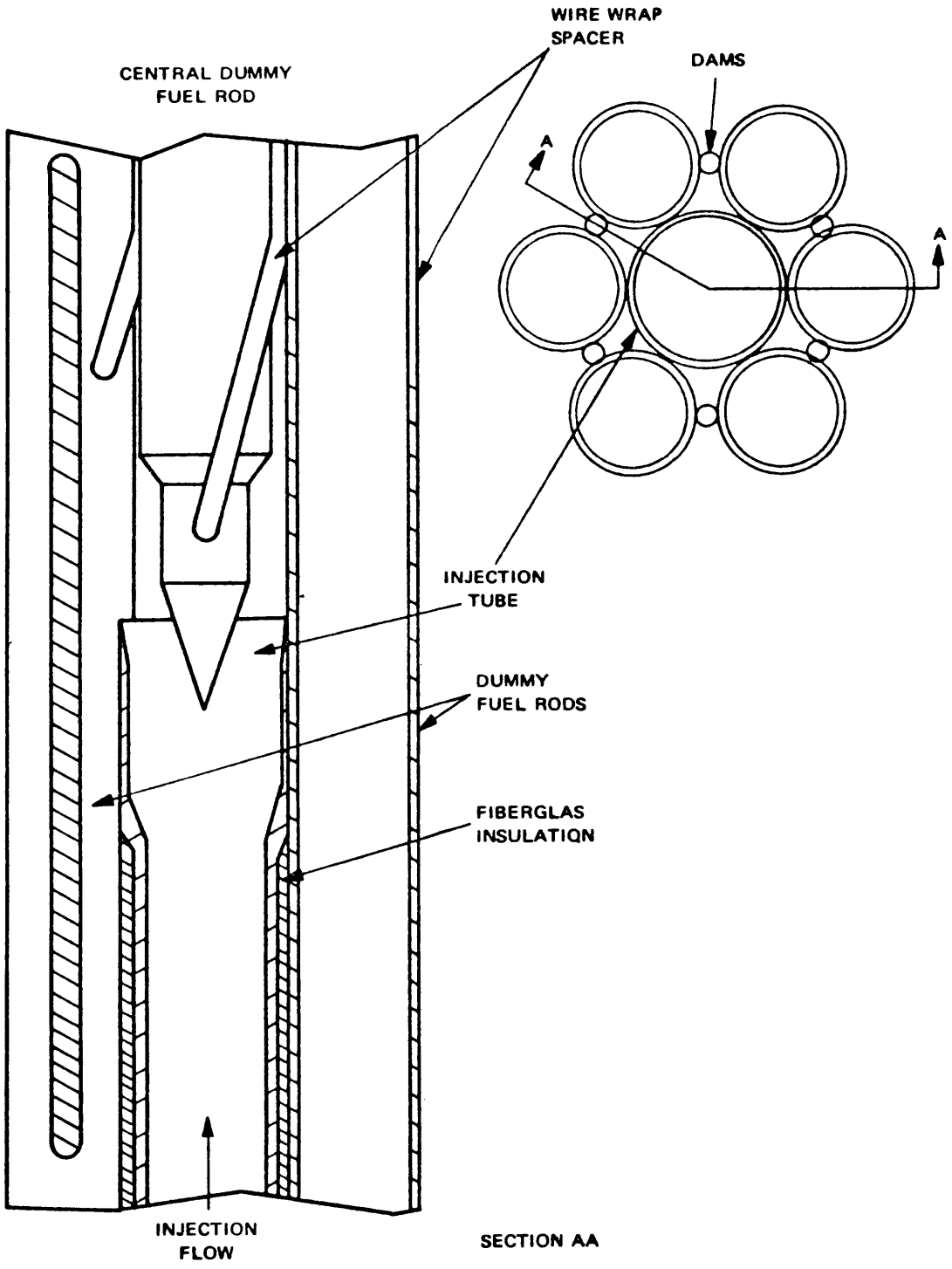
WIRE WRAP
SPACER
DAMS
CENTRAL DUMMY
FUEL ROD
A
A
INJECTION
TUBE
DUMMY
FUEL RODS
FIBERGLAS
INSULATION
INJECTION
FLOW
SECTION AA

FIG. 27

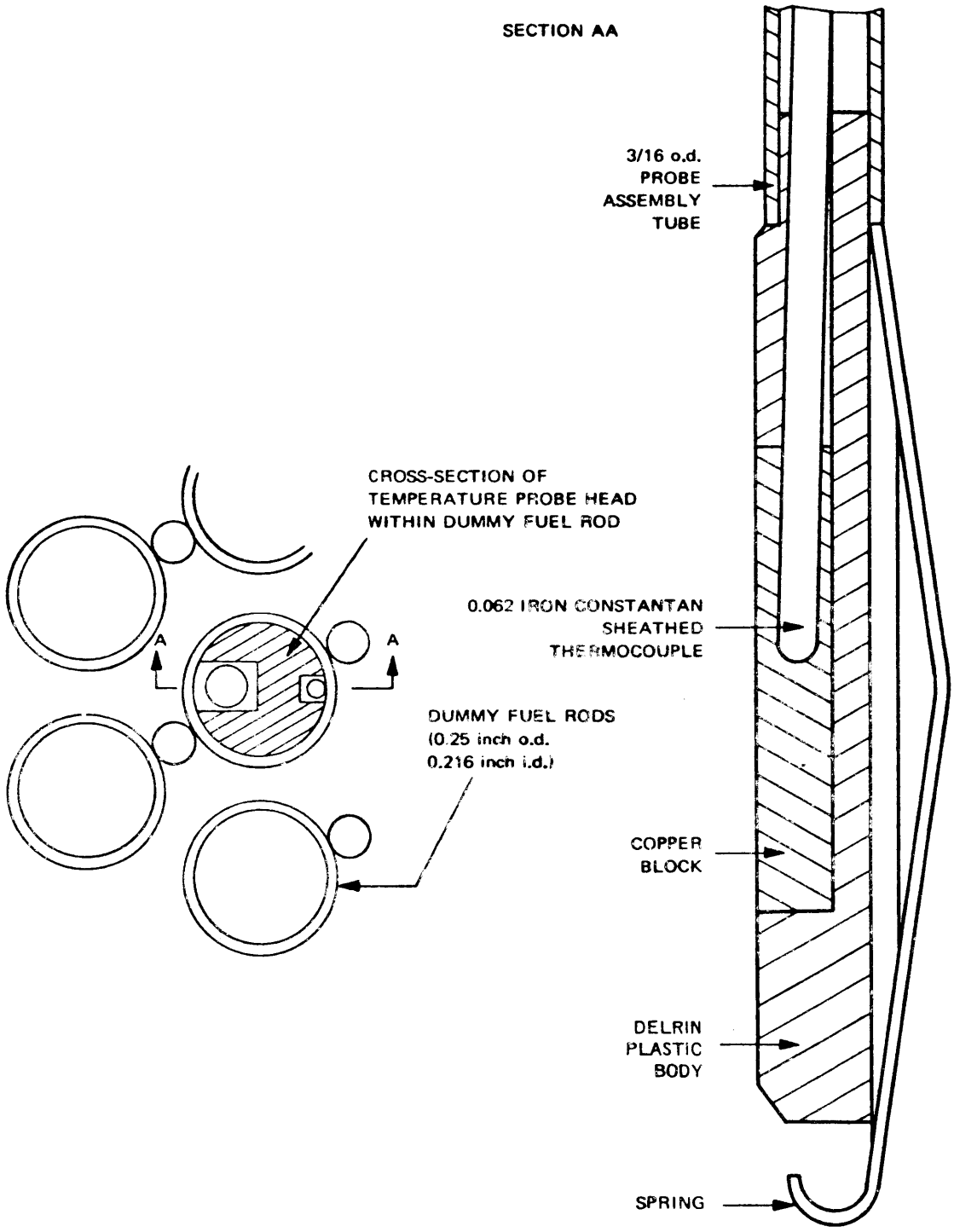
SECTION AA
3/16 o.d.
PROBE
ASSEMBLY
TUBE
CROSS-SECTION OF
TEMPERATURE PROBE HEAD
WITHIN DUMMY FUEL ROD
A
A
0.062 IRON CONSTANTAN
SHEATHED
THERMOCOUPLE
DUMMY FUEL RODS
(0.25 inch o.d.
0.216 inch i.d.)
COPPER
BLOCK
DELRIN
PLASTIC
BODY
SPRING

FIG. 28

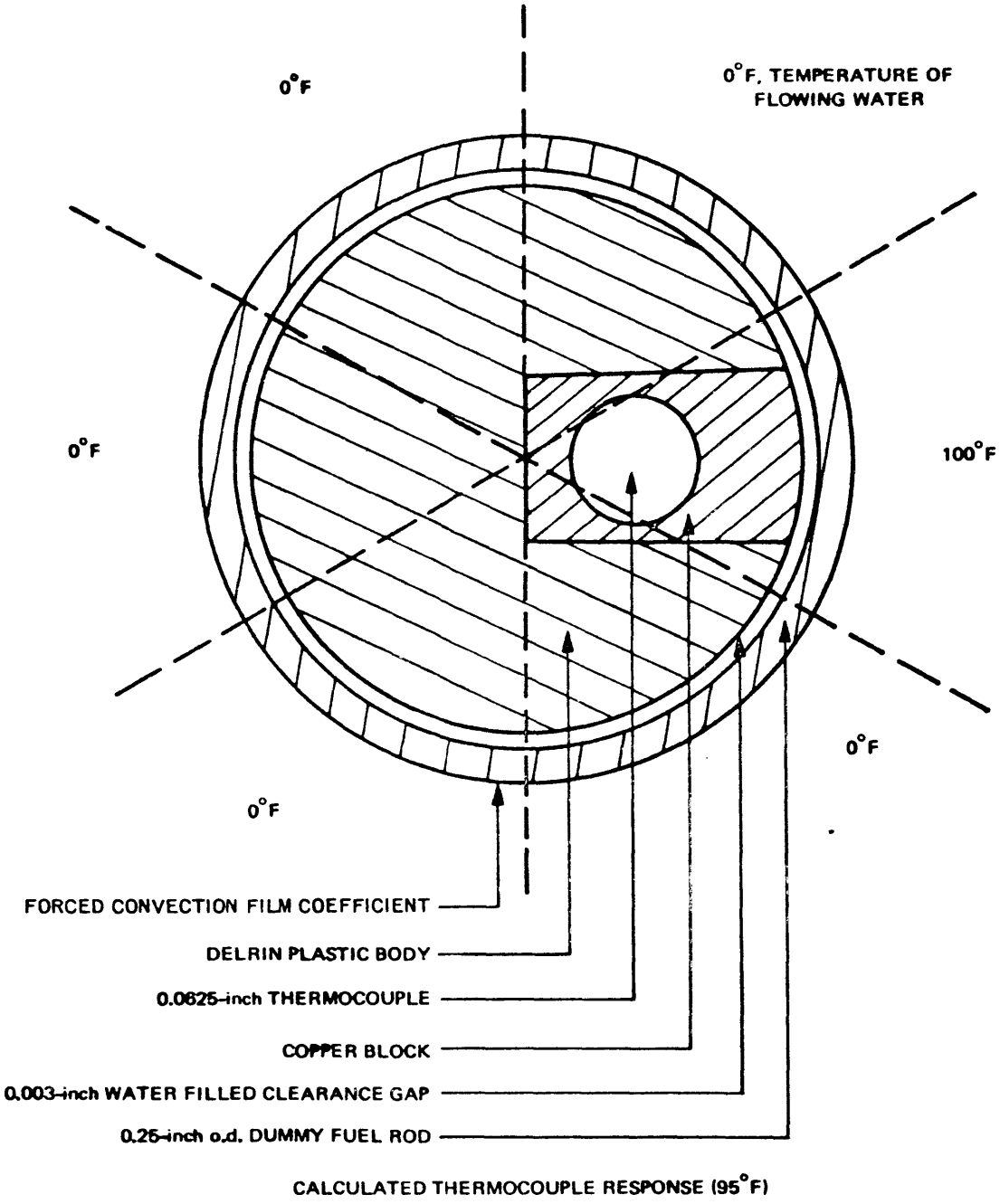
0°F
0°F, TEMPERATURE OF FLOWING WATER
0°F
100°F
0°F
0°F
FORCED CONVECTION FILM COEFFICIENT
DELRIN PLASTIC BODY
0.0625-inch THERMOCOUPLE
COPPER BLOCK
0.003-inch WATER FILLED CLEARANCE GAP
0.25-inch o.d. DUMMY FUEL ROD
CALCULATED THERMOCOUPLE RESPONSE (95°F)

FIG. 29

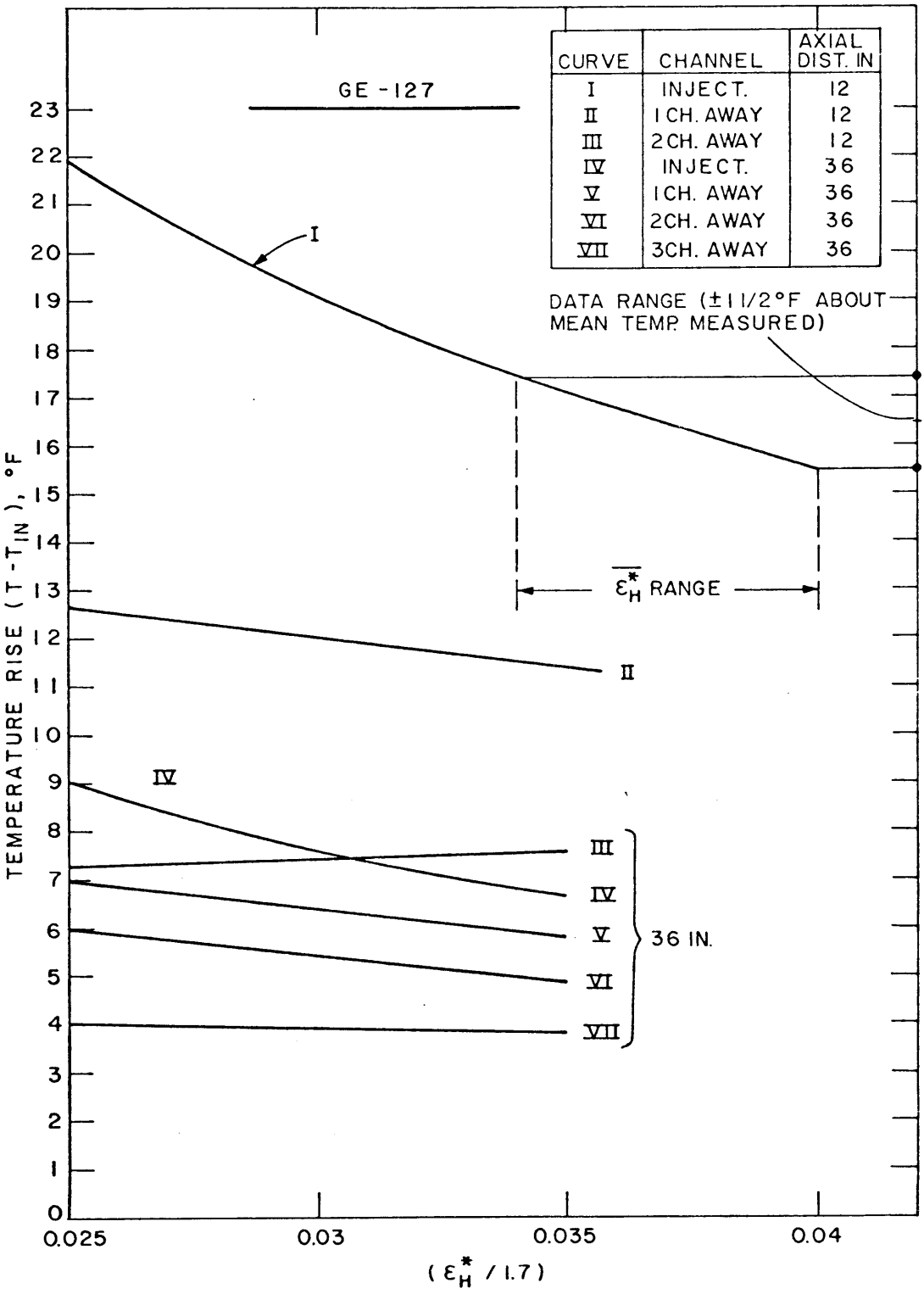
GE -127
CURVE | CHANNEL | AXIAL DIST. IN
I | INJECT. | 12
II | 1 CH. AWAY | 12
III | 2 CH. AWAY | 12
IV | INJECT. | 36
V | 1 CH. AWAY | 36
VI | 2 CH. AWAY | 36
VII | 3 CH. AWAY | 36
DATA RANGE (±1 1/2°F ABOUT MEAN TEMP. MEASURED)
$\overline{\varepsilon_H^*}$ RANGE
36 IN.
TEMPERATURE RISE (T - T_{IN}), °F
$(\varepsilon_H^* / 1.7)$
0.025
0.03
0.035
0.04

FIG. 30

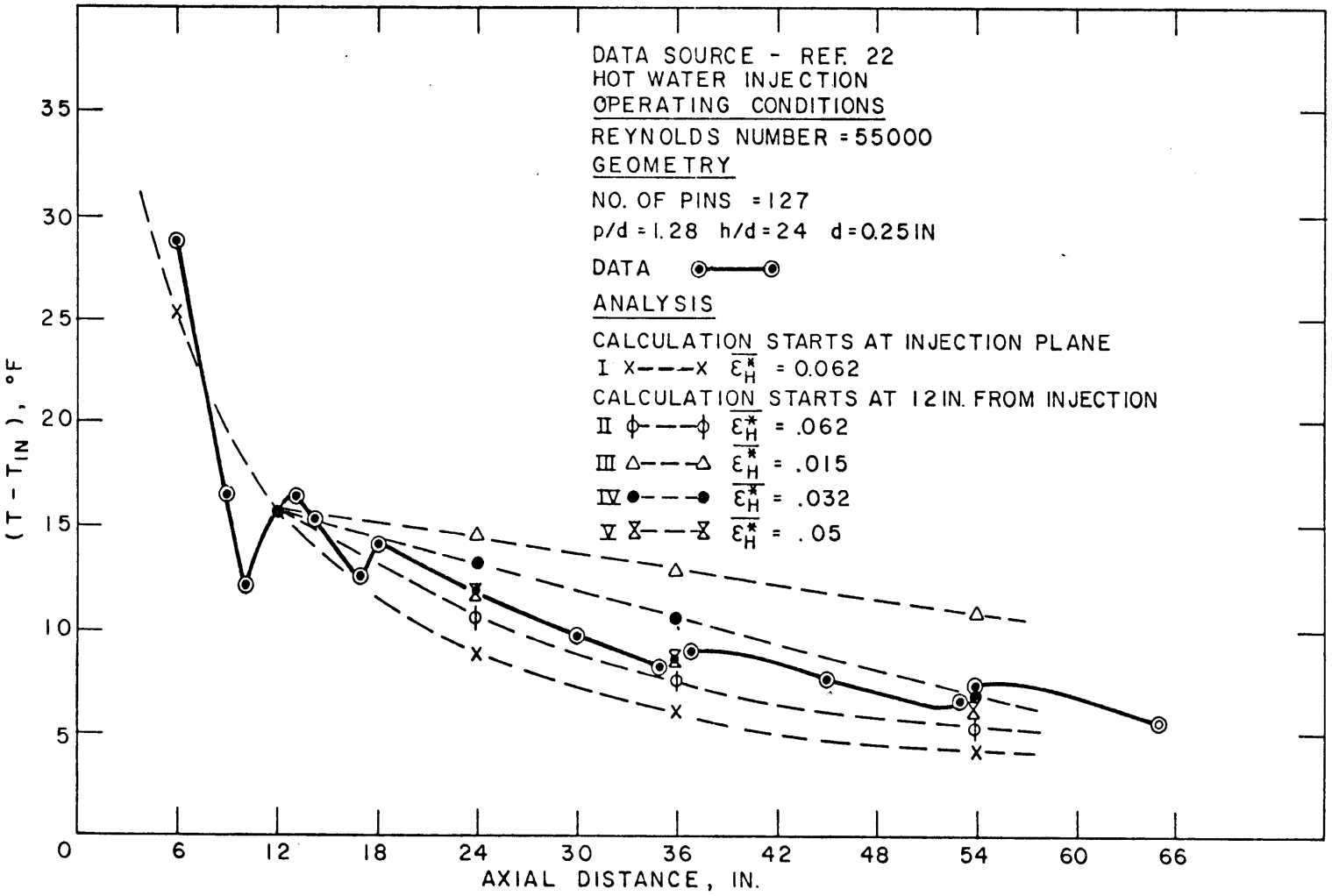
DATA SOURCE - REF. 22
HOT WATER INJECTION
OPERATING CONDITIONS
REYNOLDS NUMBER = 55000
GEOMETRY
NO. OF PINS = 127
p/d = 1.28 h/d = 24 d = 0.25 IN
DATA
ANALYSIS
CALCULATION STARTS AT INJECTION PLANE
I $\overline{\varepsilon_H^*}$ = 0.062
CALCULATION STARTS AT 12 IN. FROM INJECTION
II $\overline{\varepsilon_H^*}$ = .062
III $\overline{\varepsilon_H^*}$ = .015
IV $\overline{\varepsilon_H^*}$ = .032
V $\overline{\varepsilon_H^*}$ = .05
$(T - T_{IN})$, °F
AXIAL DISTANCE, IN.
0
5
10
15
20
25
30
35
6
12
18
24
30
36
42
48
54
60
66

FIG. 31

12 IN. BELOW FINNED REGION

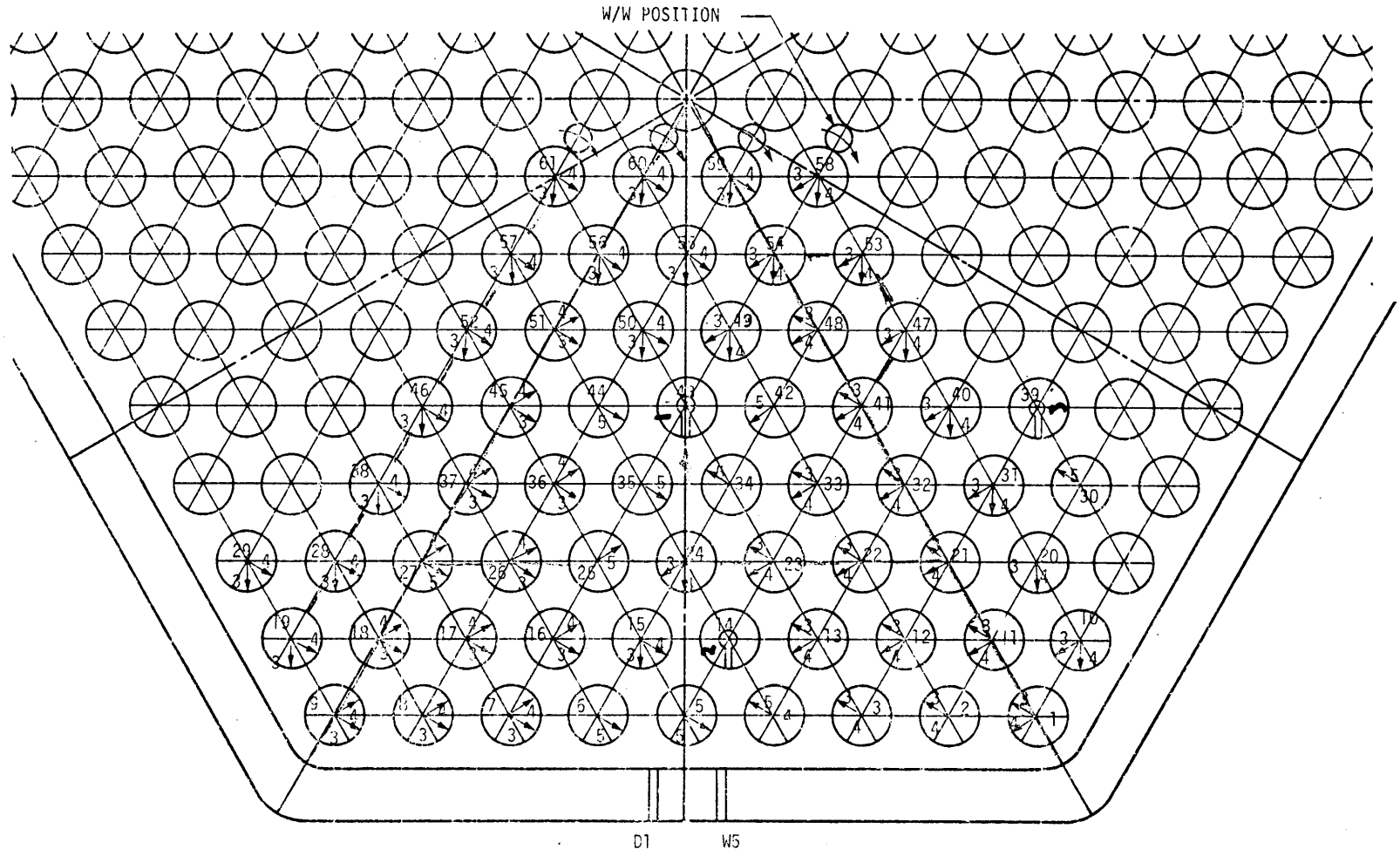

FIG. 32

RUN 19 430 gpm

Inj P43 6 IN. DOWNSTREAM

C_{inj} = 2165 ppm $\sum_n C_n \frac{\dot{m}_n}{\dot{m}_{in}}$ = 1991 ppm

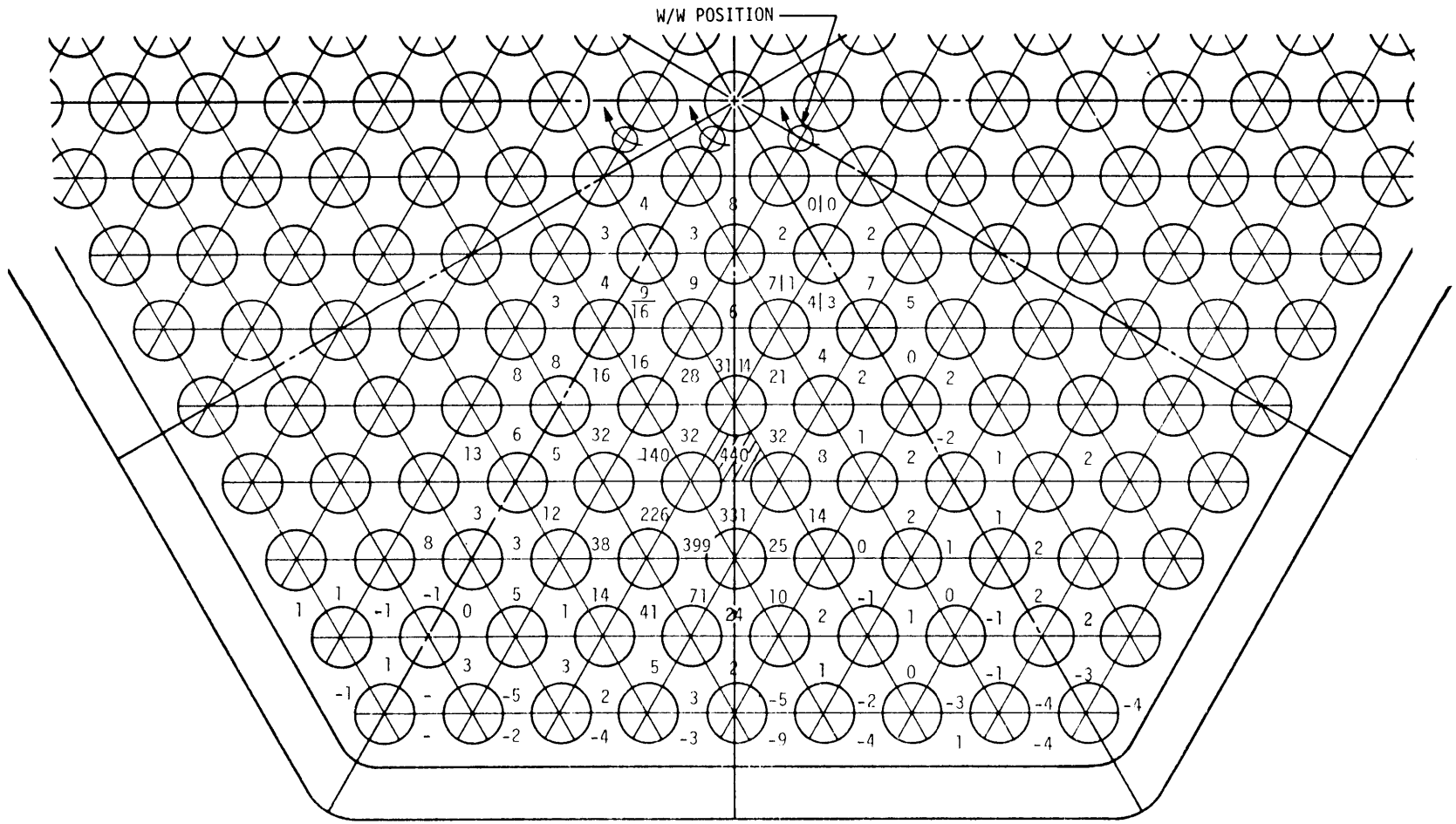

FIG. 33a

RUN 19 430 gpm

Inj P43 12 IN. DOWNSTREAM

C_{inj} = 2165 ppm $\sum_{n}^{C_n} \frac{\dot{m}_n}{\dot{m}_{in}}$ = 2206 ppm

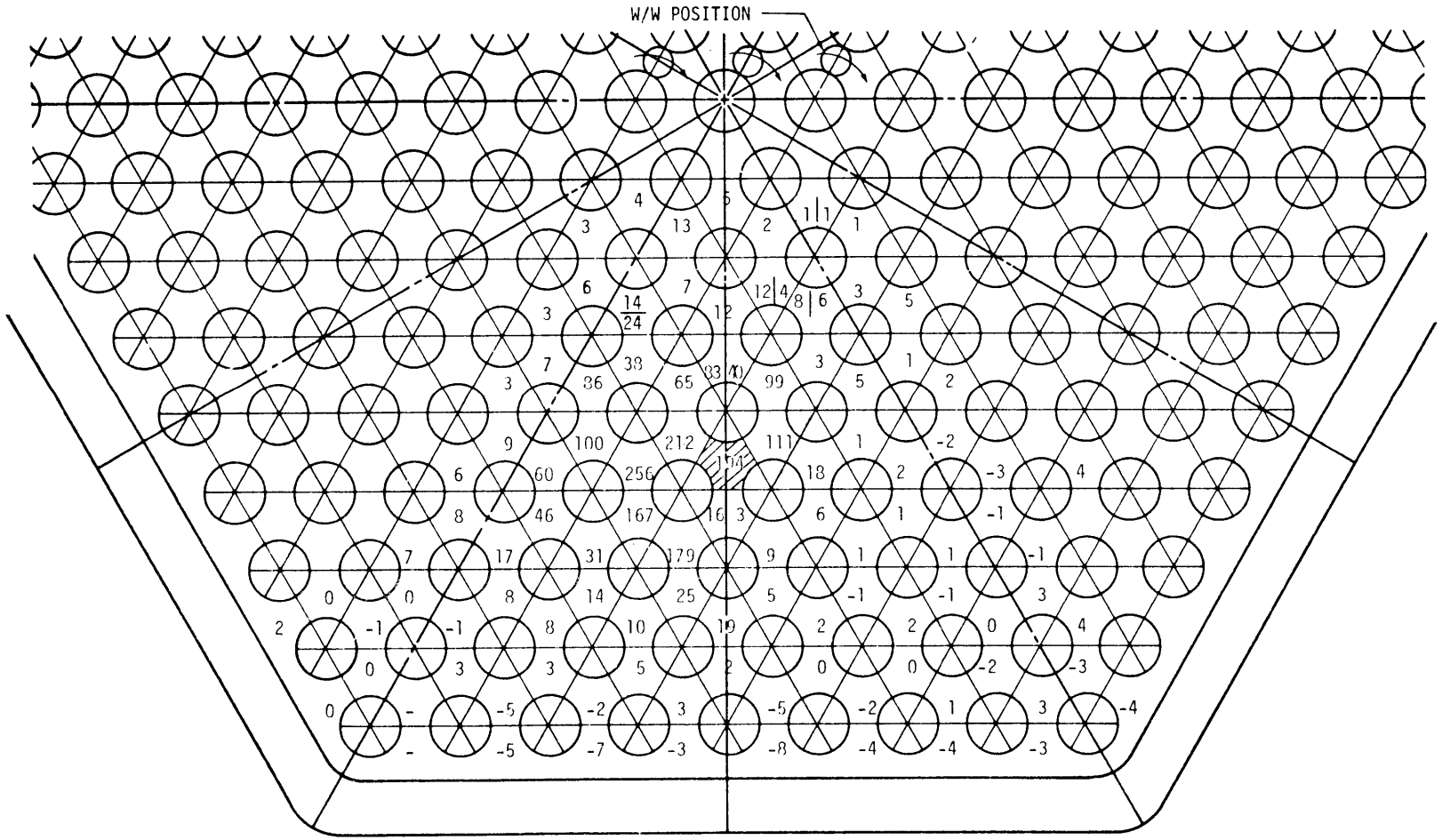

FIG. 33b

RUN 19 430 gpm

Inj P43 24 IN. DOWNSTREAM

C_{inj} = 2165 ppm $\sum_n C_n \frac{\dot{m}_n}{\dot{m}_{in}}$ = 2288 ppm

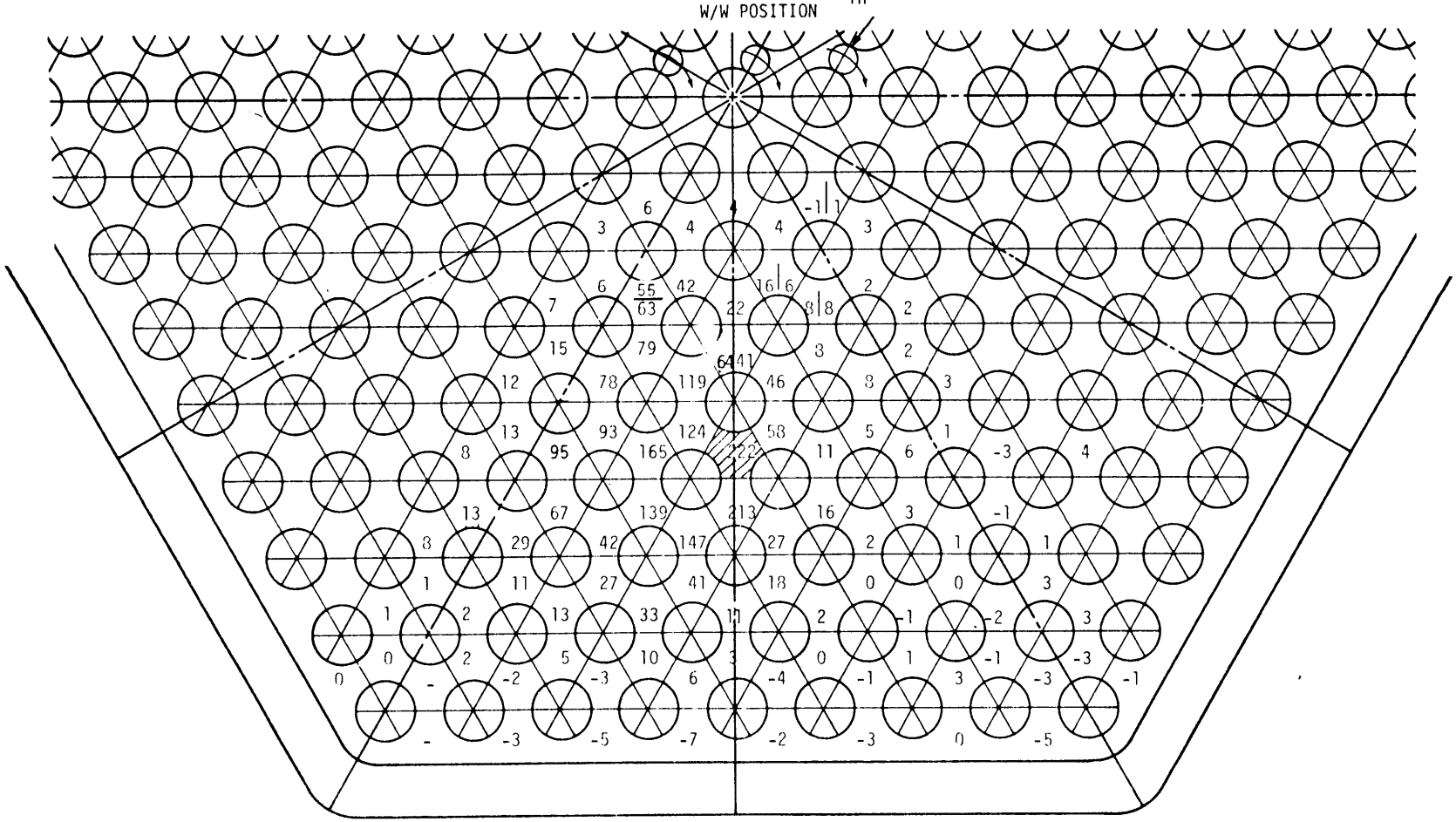

FIG. 33c

RUN 19 430 gpm

Inj P43 36 IN. DOWNSTREAM

C_{inj} = 2165 ppm $\sum_n C_n \frac{\dot{m}_n}{\dot{m}_{in}}$ = 2370 ppm

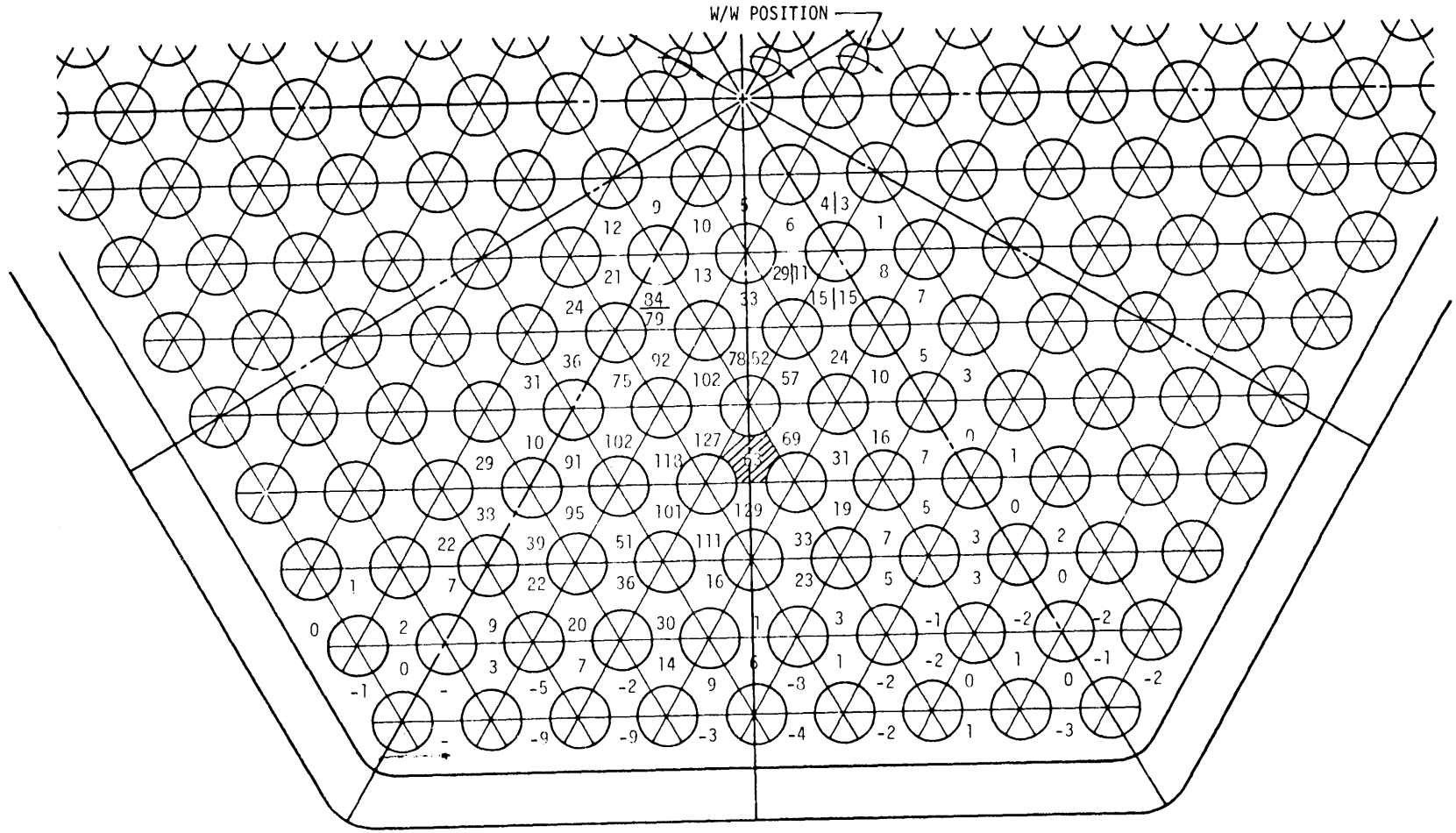

FIG. 33d

RUN 2 430 gpm

Inj LOCATION C 6 IN. DOWNSTREAM

C_{inj} = 1802 ppm $\sum_n C_n \frac{\dot{m}_n}{\dot{m}_{in}}$ = 3246 ppm

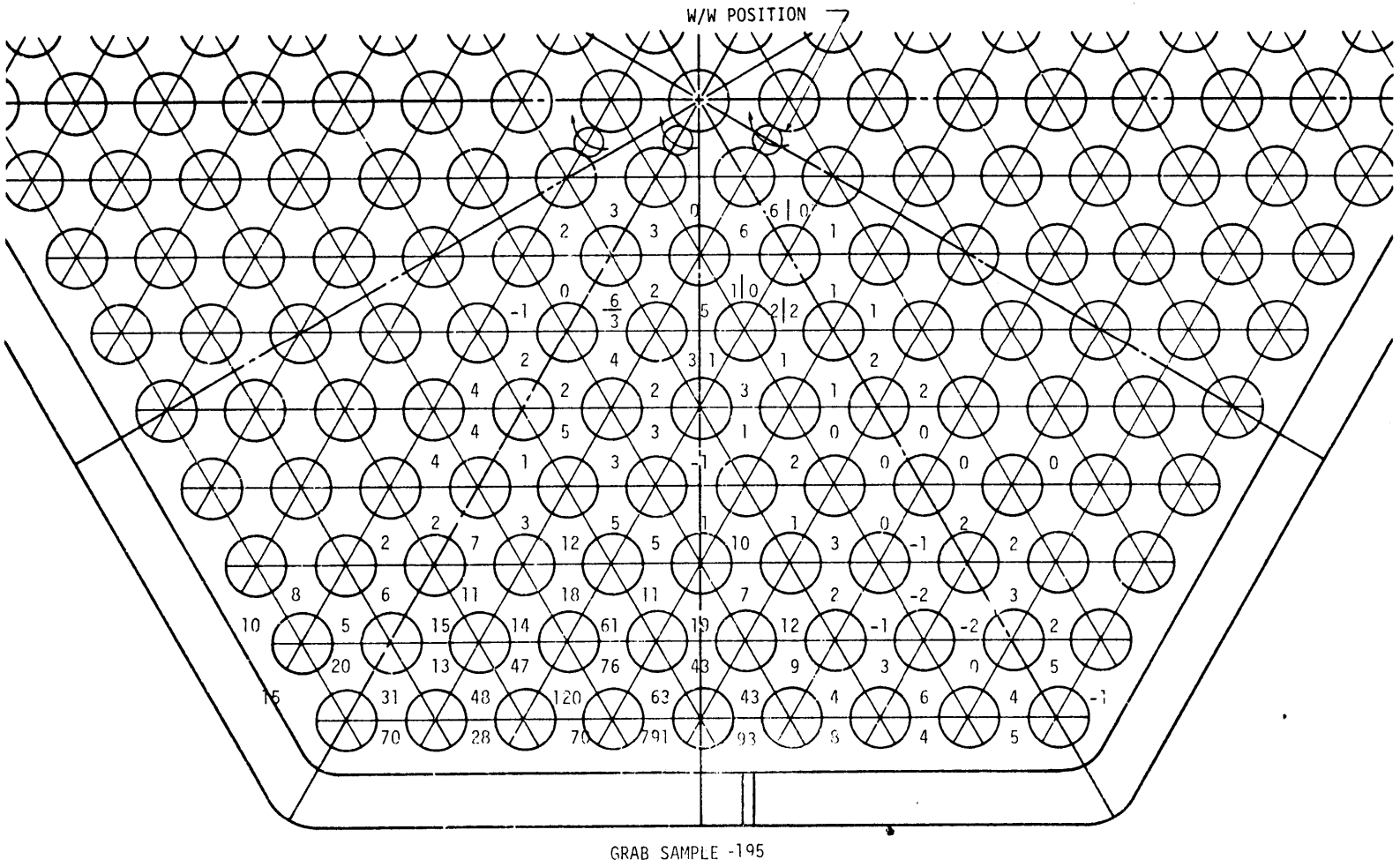

FIG. 34a

RUN 2 430 gpm

Inj LOCATION C 12 IN. DOWNSTREAM

$$C_{inj} = \text{~~4745 ppm~~ } 1802 \sum_n C_n \frac{\dot{m}_n}{\dot{m}_{in}} = 4790 \text{ ppm}$$

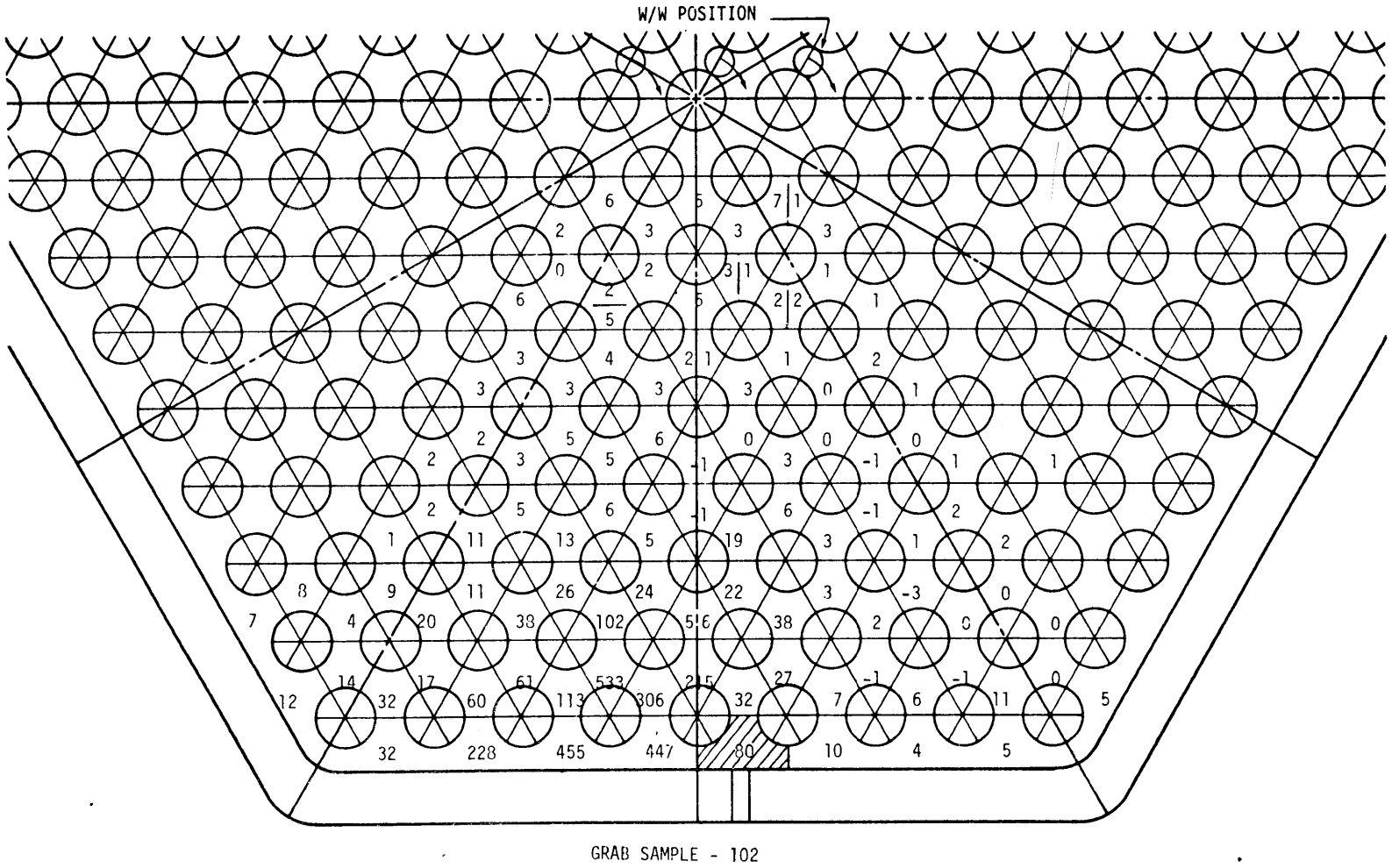

FIG. 34b

RUN 2 430 gpm

Inj LOCATION C 24 IN. DOWNSTREAM

C_{inj} = ~~4145~~ ppm $\sum_n C_n \frac{\dot{m}_n}{\dot{m}_{in}}$ = 3833 ppm

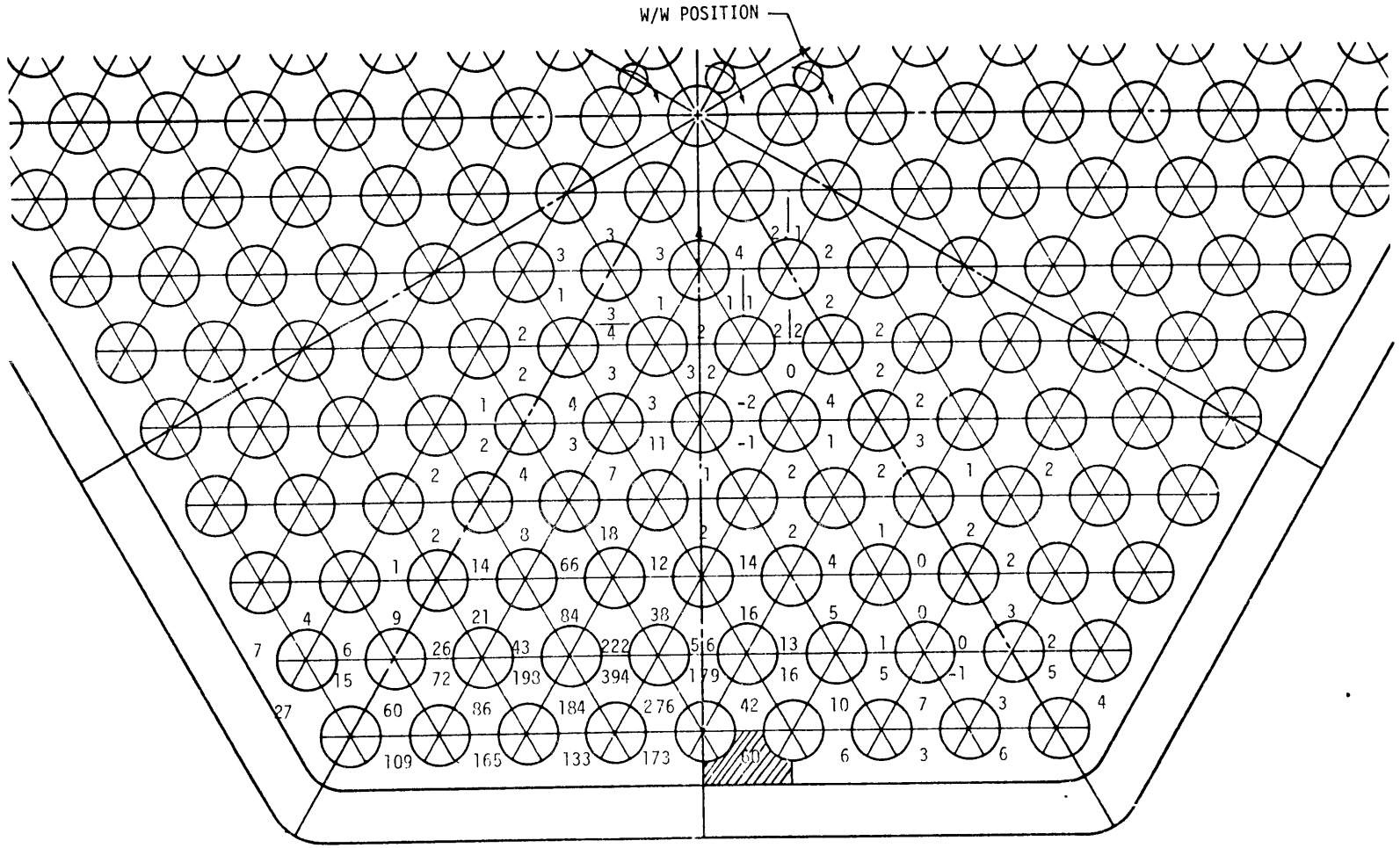

FIG. 34c

RUN 2 430 gpm

Inj LOCATION C 36 IN. DOWNSTREAM

C_{inj} = 4145 ppm $\sum_n C_n \frac{\dot{m}_n}{\dot{m}_{in}}$ = 4987 ppm

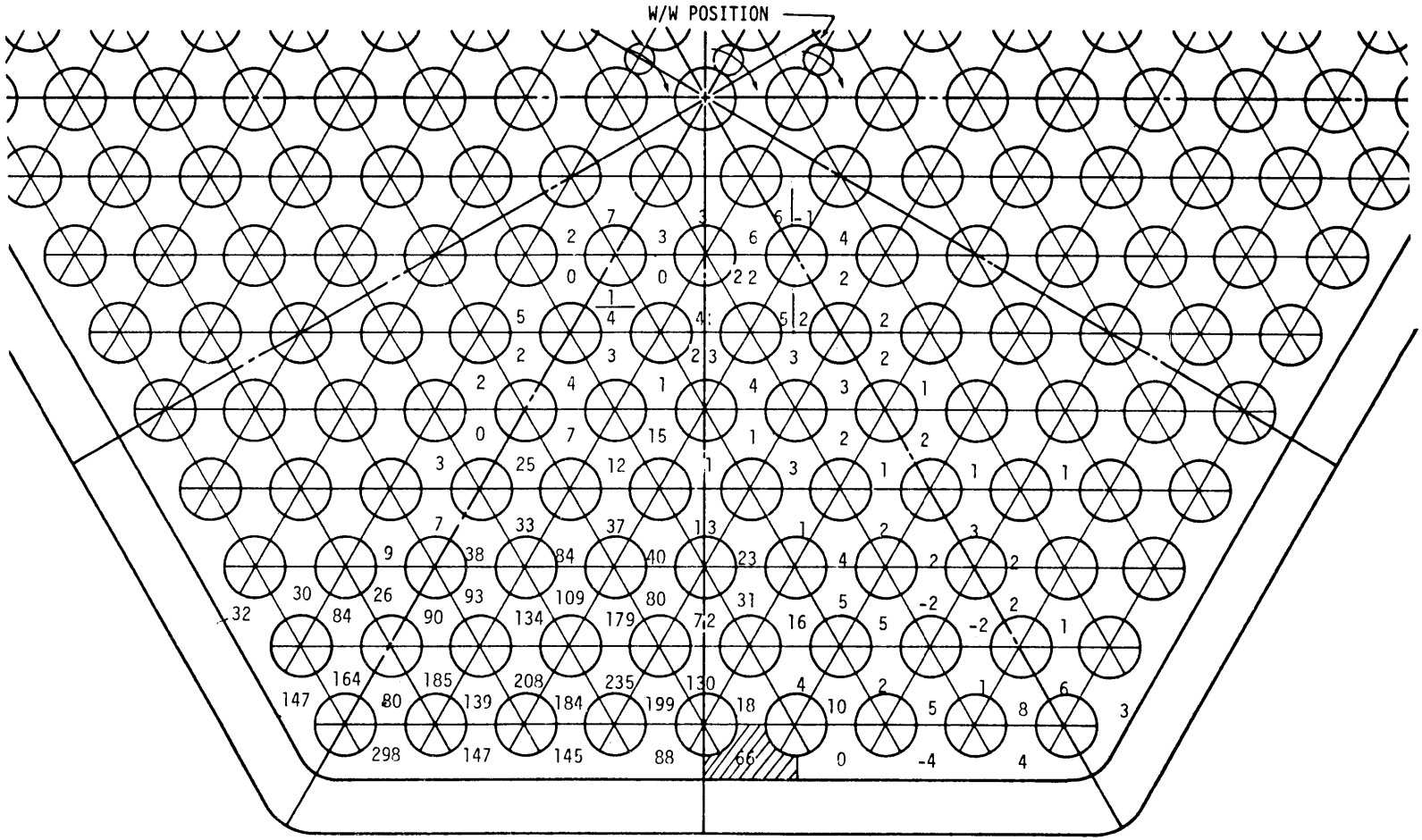

FIG. 34d

DATA - SOURCE - REF. 23
SALT - INJECTION EXPT.
OPERATING CONDITIONS
Re = 30000
GEOMETRY
NO. OF PINS = 217
p/d = 1.24 h/d = 52 d = 0.23 IN
RUN 14 (HEDL)
RESULTS AT EXIT (36 IN)
( ) DATA
( ) ANALYSIS

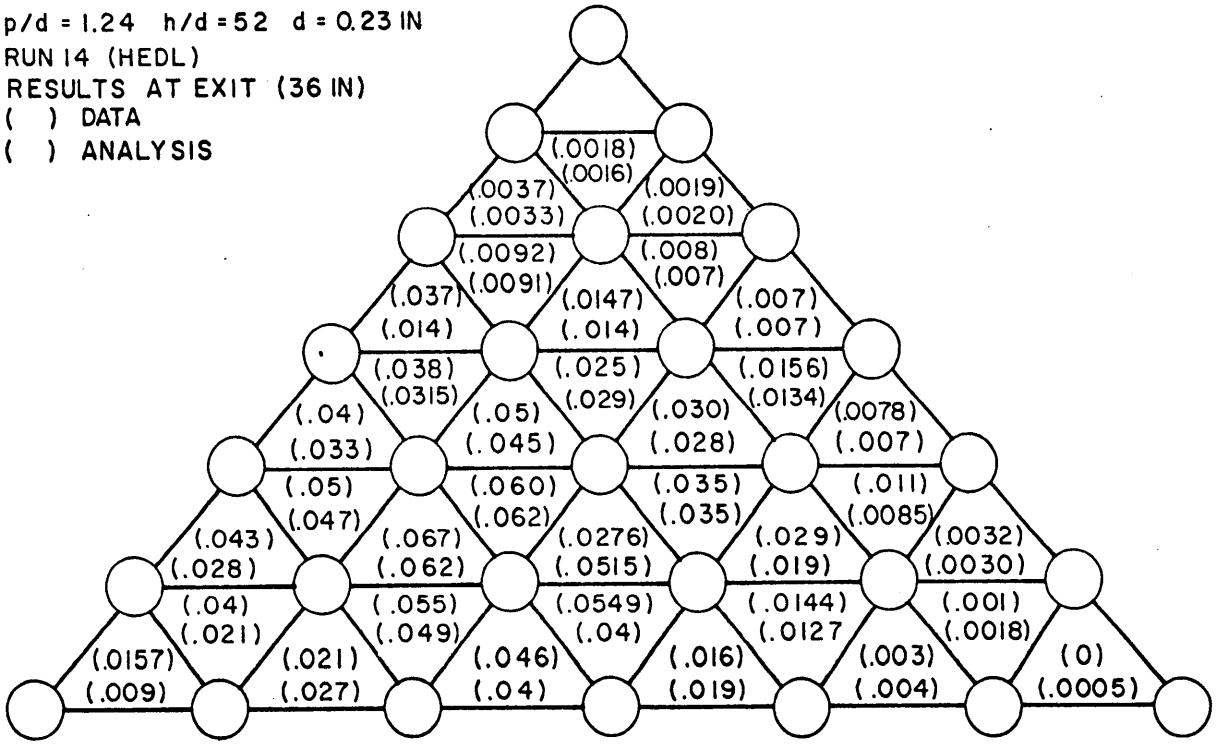

FIG. 35

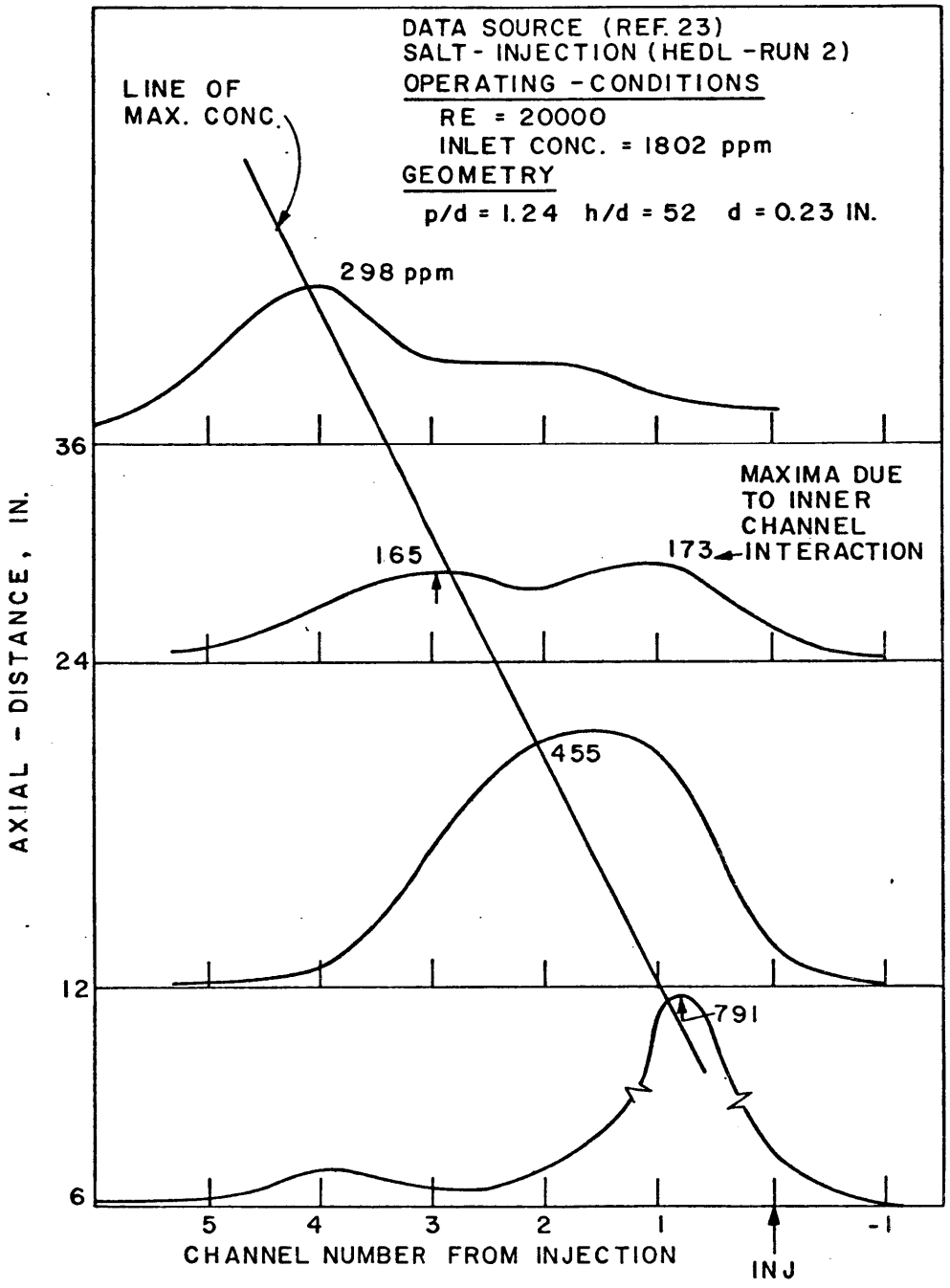
DATA SOURCE (REF. 23)
SALT - INJECTION (HEDL - RUN 2)
OPERATING - CONDITIONS
RE = 20000
INLET CONC. = 1802 ppm
GEOMETRY
p/d = 1.24 h/d = 52 d = 0.23 IN.
LINE OF MAX. CONC.
298 ppm
MAXIMA DUE TO INNER CHANNEL INTERACTION
165
173
455
791
AXIAL - DISTANCE, IN.
36
24
12
6
5
4
3
2
1
-1
CHANNEL NUMBER FROM INJECTION
INJ

FIG. 36a

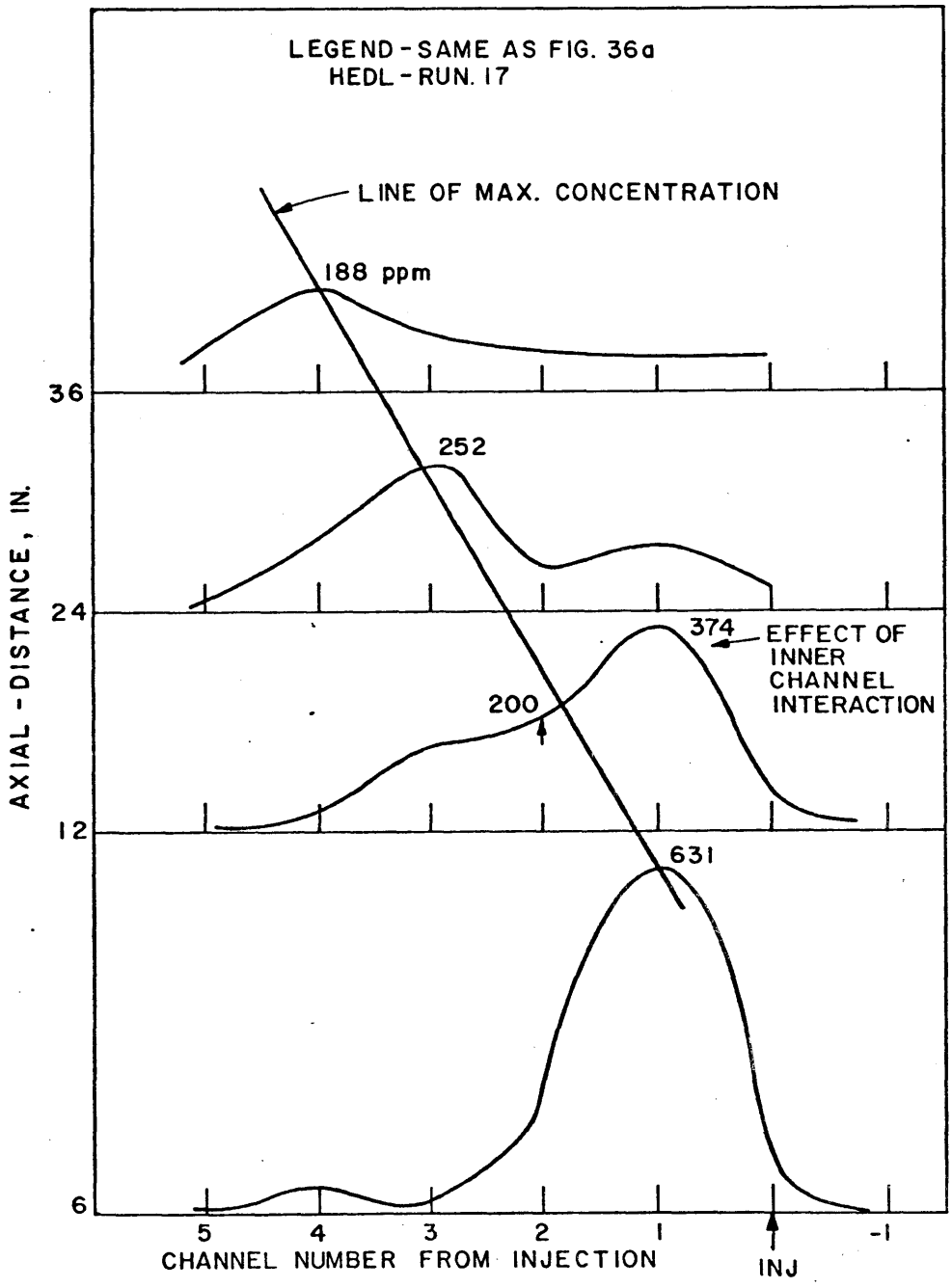
LEGEND - SAME AS FIG. 36a
HEDL - RUN. 17
LINE OF MAX. CONCENTRATION
188 ppm
252
374
EFFECT OF INNER CHANNEL INTERACTION
200
631
AXIAL - DISTANCE, IN.
36
24
12
6
5
4
3
2
1
-1
CHANNEL NUMBER FROM INJECTION
INJ

FIG. 36b

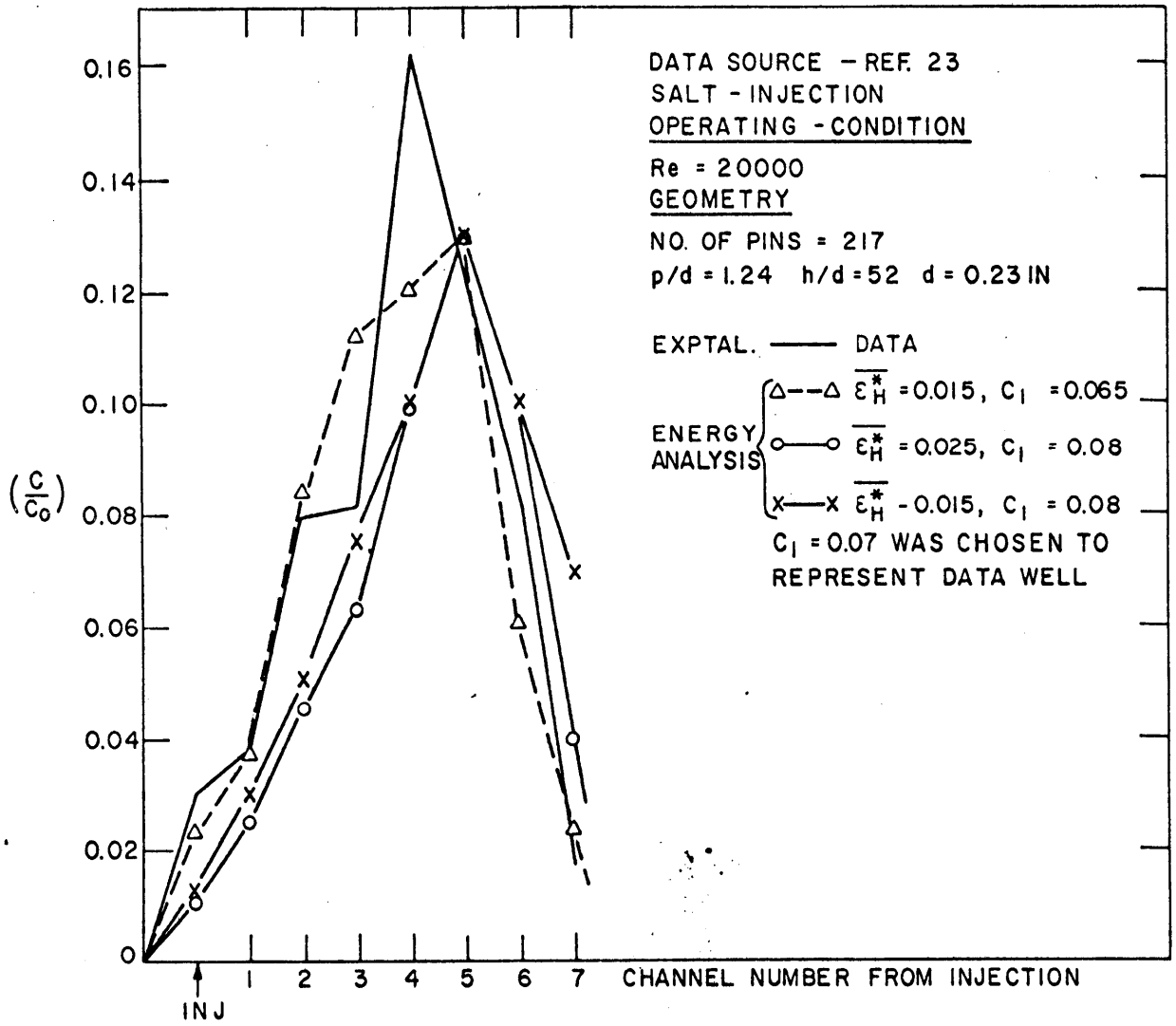
DATA SOURCE – REF. 23
SALT - INJECTION
OPERATING - CONDITION
Re = 20000
GEOMETRY
NO. OF PINS = 217
p/d = 1.24 h/d = 52 d = 0.23 IN
EXPTAL. —— DATA
ENERGY ANALYSIS
$\overline{\varepsilon_H^*}$ = 0.015, C_1 = 0.065
$\overline{\varepsilon_H^*}$ = 0.025, C_1 = 0.08
$\overline{\varepsilon_H^*}$ - 0.015, C_1 = 0.08
C_1 = 0.07 WAS CHOSEN TO REPRESENT DATA WELL
$\left(\frac{C}{C_0}\right)$
0.16
0.14
0.12
0.10
0.08
0.06
0.04
0.02
0
INJ
1 2 3 4 5 6 7
CHANNEL NUMBER FROM INJECTION

FIG. 37

8. References

1. E.Khan, W. Rohsenow, A.A. Sonin, N.E. Todreas, "A Simplified Method for Predicting Temperature Distribution in Wire Wrapped Fuel Rod Assemblies", COO-2245-5, M.I.T. 1973.
2. E. Khan and N. Todreas, "A Review of Recent Analytical and Experimental Studies Applicable to LMFBR Fuel and Blanket Assembly Design", M.I.T. DSR-Report No. COO-2245-4TR, Depts. of Mechanical and Nuclear Engineering, Sept. 1973.
3. R. Vijuk (Ward), Personal Communications with E. Khan
4. Y.B. Chen, K. Ip and N. E. Todreas, "Velocity Measurement in Edge Subchannels of Wire Wrapped LMFBR Fuel Assemblies", COO-2245-11TR, M.I.T., Sept. 1974.
5. C.L. Wheeler, D.S. Rose, J. Smith, "An Experimental Study of Axial and Cross Flow Velocity in a 7-pin Wire Wrap Bundle", BNWL-1804, Feb. 1974.
6. J.J. Lorenz and T. Ginsberg, "Results and Analysis of 7-pin Wire Wrap Mixing Tests", TRANS ANS Vol. 15, No. 2, Nov. 1972.
7. E. Novendstern, "Turbulent Flow Pressure Drop Model for Fuel Rod Assemblies, Utilizing a Helical Wire-Wrap Spacer System", Nuclear Engineering And Design, Vol. 22, No. 1, Aug. 1972.
8. J. Skok, "Mixing of the Fluid due to Helicoidal Wires of Fuel Pins in a Triangular Array", Progress in Heat and Mass Transfer, vol. 7, 1973.
9. M. Fontana, R.E. MacPherson, P.A. Gnadt, J.L. Wantland, L.F. Parsly, TRANS ANS 15(1):409 June 1972.

10. W.T. Sha, "Benchmark Temperature Mapping of FTR Fuel Assemblies Using the THI-3D Computer Code", ANL-Ct-73-07, April 1973.

11. E. Novendstern, "Mixing Model for Wire-Wrap Fuel Assemblies", TRANS ANS Vol. 15, No. 2, Nov. 1972.

12. D.R. Pedersen, R.D. Pierce, R.E. Wilson, C.J. Roop "Crossflow Mixing in a 91-Element Bundle", ANL/RAS 74-2, Feb. 1974.

13. Y. Okamoto, N. Akuno, K. Emon, M. Tamida, "Hydraulic Tests on FBR Fuel Sub-Assemblies", JAPFNR-24 1971.

14. T.R. Bump and H.O. Monson,"Flow Characteristeristics of the EBR-II Core Type Subassembly", ANL-6549 (Feb. 1969).

15. H. Hoffman and E. Baumgärtner, "Experimental Investigations of the Thermodynamic Behavior of Fast Breeder Reactor Fuel Elements with Different Space Types",Fuel and Fuel Elements for Fast Reactors, Vol.1, IAEA Vienna, 1974.

16. W. Baumann and H. Hoffman, "Coolant Cross-Mixing of Sodium Flowing in Line Through Multi rod Bundles with Different Space Arrangements", Int. Seminar on Heat Transfer in Liquid Metals, Tragir, 1971.

17. H. Hoffman, "Experimentelle Untersuchunger Zur Kühlmittelqueruermischung und zum Druckabfall in Stabbündeln mit wendelförmigen Abstandshalten", KFK 1843 Dec. 1973.

18. J.J. Lorenz, D.R. Pedersen, R.D. Pierce,"Peripheral-Flow Visualisation Studies in a 91-Element Bundle", ANL/RAS 73-14 (June 1973).

19. J.J. Lorenz, T. Ginsberg and R.A. MOrris, "Experimental Mixing Studies and Velocity Measurements with a Simulated 91-Element LMFBR Fuel Assembly", ANL-CT-74-09, March 1974.

20. A.W. Graves and I. Catton, "An Explicit Method for Predicting the Thermal Performance of FBR Wire Wrapped Fuel Rod Assemblies", TRANS ANS 15, 404, 1972.

21. E. Khan, "Analytical Methods Development", Quarterly Progress Report, COO-2245-8, March, 1974.

22. D.P. Hines, L.R. Boyd, V.R. Marian, "In-Core-Boiling or Over-Temperature Detector Development", General Electric NEDC-13650 April 1971.

23. R.E. Collingham, W.L. Thorne andJ.D. McCormack, "217 Pin Wire Wrapped Bundle Coolant Mixing Test", HEDL-TME 71-146 Nov. 1971.

24. T. Eaton, Quarterly Progress Report, COO-2245-8, M.I.T. March 1974.

25. Quarterly Progress Report, COO-2245-9, M.I.T. July 1974.

26. W.T. Sha and R.C. Schmitt, "Calibration of Mixing Constant Used in the THI-3D Computer Program", Internal Memorandum ANL. May 1974.

27. A. Hanson, Quarterly Progress Report, COO-2245-2, March 1973.

28. R.E. Henry, "A Subassembly Interchannel Mixing Program (SIMPLE)" TRANS ANS, Vol. 15, No. 2, Nov. 1972.

29. S. Yagi and D. Kunii, "Studies on Heat Transfer Near Wall Surface in Packed Beds", AICHE Journal Vol. 6, No.1, p. 97.

30. A.W. Graves, Personal Communications with E. Khan.